NUMERICAL COMPUTATION OF SCHWARZ-CHRISTOFFEL TRANSFORMATIONS AND SLIT MAPS FOR MULTIPLY CONNECTED DOMAINS

A Dissertation by

Everett Kropf

Bachelor of Arts, Wichita State University, 2007

Master of Science, Wichita State University, 2009

Submitted to the Department of Mathematics, Statistics and Physics
and the faculty of the Graduate School of
Wichita State University
in partial fulfillment of
the requirements for the degree of
Doctor of Philosophy

May 2012

NUMERICAL COMPUTATION OF SCHWARZ-CHRISTOFFEL TRANSFORMATIONS AND SLIT MAPS FOR MULTIPLY CONNECTED DOMAINS

The following faculty members have examined the final copy of this dissertation for form and content, and recommend that it be accepted in partial fulfillment of the requirement for the degree of Doctor of Philosophy with a major in Applied Mathematics.

Thomas DeLillo, Committee Chair

Alan Elcrat, Committee Member

Victor Isakov, Committee Member

Tianshi Lu, Committee Member

Ikramuddin Ahmed, Committee Member

Accepted for the College of Liberal Arts and Sciences

William Bischoff, Dean

Accepted for the Graduate School

J. David McDonald, Dean

ABSTRACT

Two methods for the numerical conformal mapping of domains with $m < \infty$ separated circular holes to domains with m polygonal holes are presented; bounded and unbounded domains are both considered. The methods are based on extensions of the classical Schwarz-Christoffel transformation to finitely connected domains. The first method uses a truncated infinite product expressed in terms of reflections through circles, and is found to have a computational time which increases geometrically with the number of levels of reflection used. The second method uses the boundary behavior of the map to construct a linear system which gives the coefficients of a Laurent series expansion for the map. The second method has a computational time which is polynomial with the number of terms of the truncated series. Both methods require the solution of a non-linear system of equations which gives the correct parameters for the desired map. The solution to the non-linear system is achieved by a numerical continuation (homotopy) method. An application is given. Maps from the circle domains to the canonical slit domains are also computed using similar techniques.

TABLE OF CONTENTS

TABLE OF CONTENTS (continued)

Chapter **Page**

LIST OF TABLES

Table **Page**

LIST OF FIGURES

Figure **Page**

LIST OF FIGURES (continued)

Figure **Page**

LIST OF FIGURES (continued)

Figure **Page**

CHAPTER 1

INTRODUCTION

For over 100 years conformal mapping has been a topic of theoretical interest and a useful tool for solving boundary value problems of potential theory in the plane. With the development of computers, many numerical methods have been proposed for approximating conformal maps. The book by Henrici [26] provides an introduction to this field. The survey paper by Wegmann [39] and the book on Schwarz-Christoffel mapping by Driscoll and Trefethen [22] review more recent work especially relevant to numerical computations. In spite of the ability of today's computers to solve many fully three dimensional problems, there is a continuing interest in these inherently two dimensional methods of function theory due to the power of the techniques and the clarity of the understanding that they bring to many important applications.

In the last several years there have been a number of advances in methods for multiply connected domains; see, for example, [5, 39]. In particular the Schwarz-Christoffel transformation for domains with polygonal boundaries has been extended to multiply connected domains in [13, 17, 18] by the use of reflection arguments, in [8, 9] using the closely related Schottky-Klein prime function, and in [2] in terms of Green's function and the harmonic measure functions of a conformally equivalent Jordan domain. The results in [13, 17, 18] and [8, 9] were the topic of a recent article in SIAM News [6]. Those methods use multiply connected domains with circular boundaries as their computational domains and involve infinite products. Explicit formulas for conformal maps can be derived using the same techniques [11, 15]. Canonical slit maps can be used to represent Green's functions for the Dirichlet, Neumann, and mixed boundary value problems for the Laplace equation in multiply connected domains; see [12]. One advantage of using circle domains is the possibility of using fast computational methods based on Fourier/Laurent expansions centered at the circles.

This dissertation extends the recent work by presenting a method for the numerical computation of the multiply connected Schwarz-Christoffel maps given in [18, 13], as well as the computation of some canonical slit maps. In addition a new method is presented for computing both multiply connected slit domains as well as the unbounded Schwarz-Christoffel maps. Some of the results of this thesis have appeared in [16], [19], and [20], along with additional details and computations. Chapter 2 reviews recent work on multiply connected maps given in terms of reflections. Chapter 3 discusses the numerical methods used to implement the maps in Chapters 2 and 4. A more efficient method to compute maps discussed in Chapter 2 is developed in Chapter 4. In Chapter 5 an application involving the computation of the resistance of thin polygonal resistors with multiple polygonal holes is given.

CHAPTER 2

MAPS BY INFINITE REFLECTION

In this chapter recent work on multiply connected conformal maps formulated in terms of infinite products of reflections is reviewed. Specifically we discuss various types of canonical slit domains, and bounded and unbounded Schwarz-Christoffel transformations. The maps under discussion all have as a domain a (bounded or unbounded) region $\mathbb{D}$ of connectivity $1 < m < \infty$, whose boundary components consist of m non-intersecting circles. The maps are denoted by $w = f(z)$, where w is in the region $\mathbb{P}$, the image of $z \in \mathbb{D}$ under one of these maps. The boundary circles of $\mathbb{D}$ are denoted, for $j = 1, \ldots, m$, by C_j, and the centers and radii of these boundary circles are denoted by c_j and r_j respectively. All of the maps below are normalized such that C_1 is the unit circle centered at the origin, *i.e.*, $c_1 = 0$ and $r_1 = 1$. In the unbounded case, circles $C_1, \ldots, C_m$ are mutually exterior with $\infty \in \mathbb{P}$. In the bounded case, circles $C_2, \ldots, C_m$ are in the interior of C_1 and are otherwise mutually exterior. The images of the boundary components of $\mathbb{D}$ under these maps will be denoted by $\Gamma_j = f(C_j)$.

2.1 Reflections: notation and facts

The maps derived in the following sections are based on analytic extensions of the mapping function by Schwarz reflection across arcs of boundary circles in $\mathbb{D}$ and the reflections across corresponding sides of slits or sides of polygons as appropriate in $\mathbb{P}$. The reflection process is then repeated across the arcs of reflected circles and slits or polygon sides an infinite number of times until the entire plane of the circle domain (minus some limit set) is covered. Complete mathematical details of the reflection process in $\mathbb{D}$ can be found in [18], and will only be summarized here.

First recall that in the complex plane the *reflection* of a point z through a circle C

with center c and radius r is given by

$$z^* = \rho_C(z) := c + \frac{r^2}{\overline{z} - \overline{c}},$$

i.e., z and z^* are symmetric points with respect to the circle C. If $z \in C$ then $z^* = z$, so that trivially $\rho_C(C) = C$. Given any two mutually exclusive circles C_τ, C_λ, the reflection of C_τ through C_λ is denoted $C_{\lambda\tau} = \rho_\lambda(C_\tau) := \rho_{C_\lambda}(C_\tau)$.

Lemma 2.1. *[18, Prop. 1]*

$$\rho_\lambda(\rho_\tau(z)) = \rho_{\lambda\tau}(\rho_\lambda(z)). \tag{2.1}$$

Proof. Recall that Möbius transformations preserve reflections in circles and straight lines, so let C_λ be the real axis, where reflection is just complex conjugation. Then

$$\rho_\lambda(\rho_\tau(z)) = \overline{\rho_\tau(z)} = \rho_{\lambda\tau}(\overline{z}) = \rho_{\lambda\tau}(\rho_\lambda(z)). \qquad \square$$

Note that the order in which reflections are carried out is important, *i.e.*, in general $\rho_\lambda(\rho_\tau(z)) \neq \rho_\tau(\rho_\lambda(z))$.

Definition 2.2. The set of multi-indices ν of length $|\nu| = n > 0$ is denoted

$$\sigma_n = \{\nu_1\nu_2\cdots\nu_n : 1 \leq \nu_i \leq m \text{ for } i = 1, \ldots, n; \text{ and } \nu_i \neq \nu_{i+1} \text{ for } i = 1, \ldots, n-1\},$$

with $\sigma_0 := \phi$. (If $\nu \in \sigma_0$, then we write for convenience $\nu j = j$.) Also

$$\sigma_n(j) = \{\nu \in \sigma_n : \nu_n \neq j\},$$

denotes sequences in σ_n whose last factor never equals j.

An arbitrary reflected circle is denoted by C_ν with a multi-index ν labeling the sequence of reflections. Consider for example an unbounded circle domain with $m = 3$. For $|\nu| = 3$, three levels of reflection, the set of multi-indices would be

$$\sigma_3 = \{121, 123, 131, 132, 212, 213, 231, 232, 312, 313, 321, 323\}$$

with

$$\sigma_3(1) = \{123, 132, 212, 213, 232, 312, 313, 323\}\,.$$

The reflections of circles C_2 and C_3 through circle C_1 are $C_{12} = \rho_1(C_2)$ and $C_{13} = \rho_1(C_3)$ respectively. The reflection process is continued with, for instance, the circle C_1 reflected through C_{12} for $C_{121} = \rho_{12}(C_1) = \rho_{12}(\rho_1(C_1)) = \rho_1(\rho_2(C_1))$ by an application of (2.1), and C_{13} reflected through C_{12} for $C_{123} = \rho_{12}(C_{13}) = \rho_{12}(\rho_1(C_3)) = \rho_1(\rho_2(C_3))$, etc. See Figure 2.1. Some care is required to reconstruct the original sequence of reflections from the index ν, as illustrated by C_{123}. However note that in general, $C_\nu = C_{\nu_1\nu_2\cdots\nu_n}$ is in the interior of C_{ν_1} and arises from a sequence of reflections of C_{ν_n}.

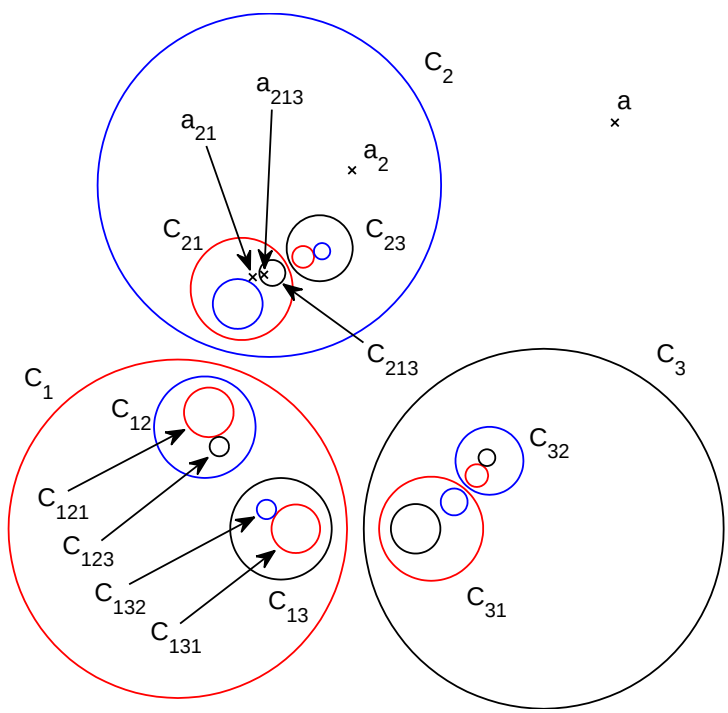

Figure 2.1: An example of reflected circles to a level of $|\nu| = 3$. The point $a_{213} = \rho_{213}(\rho_{21}(\rho_2(a)))$ is also shown.

Use of the radii and centers of the reflected circles, as well as the reflections of the centers of the boundary circles of $\mathbb{D}$, will be required. The radius of a reflected circle $C_{\nu j}$

will be denoted $r_{\nu j}$, and let $c_{\nu j}$ be the center of such a circle. To make a distinction between centers of reflected circles and reflections of the centers of the $C_j \in \partial\mathbb{D}$, set $s_j = c_j$ so that $s_{\nu j}$ represents the latter. It is clear that $s_{\nu j} \neq c_{\nu j}$ for $\nu \in \sigma_n(j)$, $n > 0$.

Repeated use of (2.1) shows that reflection through any circle C_ν can be factored into a sequence of reflections solely through the $C_j \in \partial\mathbb{D}$, which greatly simplifies the numerical computation of these reflections. This factoring is expressed in the following form of [18, Lemma 1].

Lemma 2.3. *For* $\nu = \nu_1\nu_2\cdots\nu_n \in \sigma_n(j)$,

$$C_{\nu j} = \rho_{\nu_1}(\rho_{\nu_2}(\cdots(\rho_{\nu_n}(C_j))\cdots)), \text{ and}$$

$$s_{\nu j} = \rho_{\nu_1}(\rho_{\nu_2}(\cdots(\rho_{\nu_n}(s_j))\cdots)).$$

The proof of [18, Lemma 1] uses (2.1) and an induction argument, which will not be given here, to show that, *e.g.*, $C_{\nu j} = \rho_{\nu_1}(C_{\nu_2\cdots\nu_n j})$. Repeated application of this to ν_2 through ν_n gives the Lemma.

In this vein, for any $a \in \mathbb{D}$, let $a_\nu := \rho_{\nu_1}(\rho_{\nu_2}(\cdots(\rho_{\nu_n}(a))\cdots))$. Then given for example a point a_{213}, one may reconstruct the original sequence of reflections, by the use of (2.1),

$$\begin{aligned} a_{213} &= \rho_2(\rho_1(\rho_3(a))) = \rho_2(\rho_{13}(\rho_1(a))) \\ &= \rho_{213}(\rho_2(\rho_1(a))) = \rho_{213}(\rho_{21}(\rho_2(a))). \end{aligned}$$

This is a reflected through C_2, which is then reflected through C_{21}, and this result is then reflected through $C_{213} = \rho_{21}(C_{23})$. See Figure 2.1.

Based on Lemma 2.3, a routine was developed in MATLAB which performs the reflections of centers of boundary circles and points on these circles to some specified level $|\nu| = n$. Only reflections across the original circles are computed. For instance, $a_{123} = \rho_{123}(a_{12})$ is computed as $a_{123} = \rho_1(\rho_2(\rho_3(a)))$. The code stores an expanding array of integers, $j \in \{1, \ldots, m\}$, for each reflection such that ρ_j is the most recent reflection. For the next level of reflections, ρ_j is then skipped, since $\rho_j(\rho_j(a)) = a$. It should be noted that for a given $|\nu| = n > 0$, the set σ_n has $|\sigma_n| = m(m-1)^{n-1}$ elements. This exponential increase in size is a principle difficulty in computing maps in terms of these reflections. A listing of

a simplified version of the reflection code is given in [19, Algor. 2.2, p. 198], and is given for convenience as Algorithm A.1 in Appendix A.

In order to state convergence results for infinite products given in the Sections below, the following definitions and lemma are needed.

Definition 2.4. The *separation parameter* of an unbounded, m-connected, $m > 1$, circular domain $\mathbb{D}$, is

$$\Delta := \max_{\substack{j,p;\, j\neq p \\ 1\leq j,p\leq m}} \frac{r_j + r_p}{|c_j + c_p|}. \tag{2.2}$$

In the case that $\mathbb{D}$ is a bounded domain, we first reflect across C_1 to create an unbounded domain with boundary components $C_1, C_{12}, \ldots, C_{1m}$. The separation parameter for the bounded domain is then calculated at this first level of reflection, and definition 2.4 becomes

Definition 2.5. The *separation parameter* of a bounded, m-connected, $m > 1$, circular domain $\mathbb{D}$ is

$$\Delta := \max_{\substack{\nu,\mu;\, \nu\neq\mu \\ \nu,\mu\in\{1\}\cup\{12,\ldots,1m\}}} \frac{r_\nu + r_\mu}{|c_\nu + c_\mu|}. \tag{2.3}$$

The rate at which the radii of the reflected circles shrink will be of interest, so an inequality from [26, p. 505] is given.

Lemma 2.6.

$$\sum_{\nu\in\sigma_{n+1}} r_\nu^2 \leq \Delta^{4n} \sum_{j=1}^{m} r_j^2. \tag{2.4}$$

2.2 Maps to canonical multiply connected slit domains

The purpose of this section is to catalog a list of canonical slit domains for use mainly as an easy source of orthogonal grids when plotting the Schwarz-Christoffel maps below.

Formulas for unbounded multiply connected radial and circular slit maps based on infinite products of reflections were introduced in [15]. Variations on these for bounded domains were given in [19]. A thorough discussion on slit domains as canonical domains can be found in [31]. In general only sketches of the proofs for the formulas of these maps will be given here; complete details are given in the the referenced papers.

In all cases, formulas for the maps f are derived by extending them through repeated use of Schwarz reflections to a globally defined $\hat{f}$ on $\mathbb{C} \setminus \{\text{limit points}\}$. Although $\hat{f}$ is many valued, it is shown that $\hat{f}'/\hat{f}$ is single valued. A singularity function S is defined as the uniform limit of a sequence of functions S_N, each the sum of singular parts of expansions around singularities of $\hat{f}'/\hat{f}$, where it is then shown by a use of the argument principle that $S = f'/f$. The desired maps are then given by $f(z) = \exp(\int S(z))$. Examples are given.

2.2.1 Slit maps from unbounded circular domains

Radial slit map

Consider now the derivation of a formula for the map f from an unbounded, m-connected circle domain $\mathbb{D}$ to an unbounded domain $\mathbb{P}$ with m radial slits with respect to the origin, that is the boundary circles $C_j \in \partial\mathbb{D}$ map to the radial slits $f(C_j) = \Gamma_j \in \partial\mathbb{P}$. The map satisfies $f(a) = 0$, for some point $a \in \mathbb{D} \setminus \{\partial\mathbb{D} \cup \infty\}$, and $f(\infty) = \infty$. See Figure 2.2. This map was first given in [15]. The derivation is sketched in brief here; full details may be found in the given reference.

Theorem 2.7. *Let $\mathbb{P}$ be an unbounded m-connected radial slit region with $0, \infty \in \mathbb{P}$, and $\mathbb{D}$ a conformally equivalent circular domain with $a, \infty \in \mathbb{D}$. Furthermore suppose $\mathbb{D}$ satisfies the separation property $\Delta < (m-1)^{-1/4}$ for $m > 1$. Then $\mathbb{D}$ is mapped conformally onto $\mathbb{P}$ by f with $f(a) = 0$ and $f(\infty) = \infty$ if and only if*

$$f(z) = A(z-a) \prod_{j=1}^{m} \prod_{\substack{n=0 \\ \nu \in \sigma_n(j)}}^{\infty} \frac{z - a_{\nu j}}{z - s_{\nu j}} \tag{2.5}$$

for some constant A.

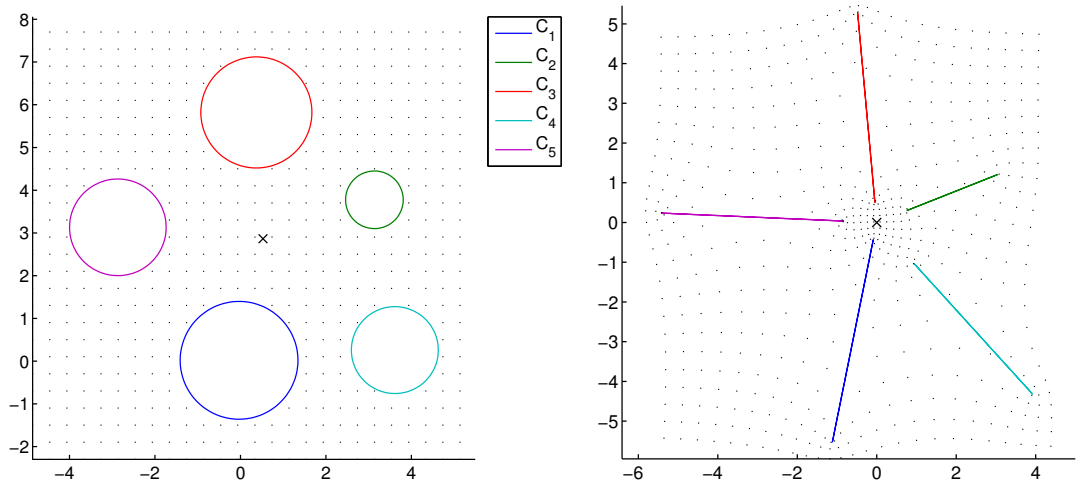

Figure 2.2: Example of a map to an unbounded radial slit domain.

Proof. Only a sketch of this proof is given here; full details may be found in [15].

Let f be the map under consideration and extend it to a globally defined, many valued function $\hat{f}$ on $\mathbb{C}^* \setminus \{\text{limit points}\}$ by repeated use of the reflection principle. When a point z is reflected across the arc of a circle C_j which maps to one side of a radial slit, the corresponding reflection for $w = \hat{f}(z)$ is across the radial slit $\Gamma_j = f(C_j)$. Reflections across these slits leave 0 fixed, so the zeros of $\hat{f}$ are given by a and all of its reflections. Reflection of infinity across a circle C_j takes infinity to the circle center $c_j = s_j$; the corresponding reflection across the slit Γ_j leaves infinity fixed. The reflection of this s_j across any circle reflected inside of C_j corresponds to the reflection of infinity across one of the slits, which also leaves infinity fixed, thus the poles of $\hat{f}$ are given by ∞ and the centers of the circles in $\partial\mathbb{D}$ and their reflections. Although $\hat{f}$ is a global many valued function, the expression $\hat{f}'/\hat{f}$ is single valued, since reflections across radial slits amount to a rotation. Let $A = e^{i\phi}$ be this rotation and observe $(Af(z))'/(Af(z)) = f'(z)/f(z)$.

Using the singular parts of the globally defined $f'(z)/f(z)$ at the nth level of reflection, define a function

$$B_n(z) := \sum_{j=1}^{m} \sum_{\nu \in \sigma_n(j)} \left(\frac{1}{z - a_{\nu j}} - \frac{1}{z - s_{\nu j}} \right) = \sum_{j=1}^{m} \sum_{\nu \in \sigma_n(j)} \frac{a_{\nu j} - s_{\nu j}}{(z - a_{\nu j})(z - s_{\nu j})}$$

and the function

$$S_N(z) := \frac{1}{z-a} + \sum_{n=0}^{N} B_n(z) \tag{2.6}$$

which is analytic on $\overline{\mathbb{D}} \setminus \{a\}$. We now show this series converges uniformly. Let

$$\delta = \delta_{\mathbb{D}} := \inf_{z\in\Delta} \{|z-a_\nu|, |z-s_\nu| : \nu \in \sigma_n, n = 1, 2, 3, \ldots\},$$

and note that $\delta > 0$ since a_ν and s_ν are in the compliment of $\overline{\mathbb{D}}$. Recall that $|\sigma_n| = m(m-1)^{n-1}$ and observe $|a_{\nu j} - s_{\nu j}| < 2r_{\nu j}$. Then

$$|B_n(z)| \leq \sum_{j=1}^{m} \sum_{\nu\in\sigma_n(j)} \frac{|a_{\nu j} - s_{\nu j}|}{|z-a_{\nu j}||z-s_{\nu j}|} \leq \frac{2}{\delta^2} \sum_{j=1}^{m} \sum_{\nu\in\sigma_n(j)} r_{\nu j}.$$

Using the Cauchy-Schwarz inequality and Lemma 2.6,

$$\begin{aligned}
\frac{2}{\delta^2} \sum_{j=1}^{m} \sum_{\nu\in\sigma_n(j)} r_{\nu j} &\leq \frac{2}{\delta^2} \left(\sum_{\nu\in\sigma_n(j)} \sum_{j=1}^{m} r_{\nu j}^2 \right)^{1/2} \left(\sum_{\nu\in\sigma_n(j)} \sum_{j=1}^{m} 1 \right)^{1/2} \\
&\leq \frac{2}{\delta^2} \Delta^{2n} \left(\sum_{j=1}^{m} r_j^2 \right)^{1/2} \sqrt{m}(m-1)^{n/2} \\
&\leq C\Delta^{2n}(m-1)^{n/2}.
\end{aligned}$$

The series S_N thus converges absolutely if $\Delta^2\sqrt{m-1} < 1$ by the Weierstrass M-test, and, since this is true for any point $z \in \overline{\mathbb{D}} \setminus \{a\}$, the convergence is uniform. Denote the limit of this series, called the *singularity function*, by

$$S(z) := \lim_{N\to\infty} S_N(z), \tag{2.7}$$

and note that since it is the uniform limit of a sequence of analytic functions, $S(z)$ is analytic as well. Note this implies the estimate $|S(z) - S_N(z)| = O\left((\Delta^2\sqrt{m-1})^{N+1}\right)$.

The argument principle, along with Lemmas 2.8 and 2.9 below, is used to show that $S(z) = f'(z)/f(z)$. Since f'/f is the logarithmic derivative of f, we have, for some constant A,

$$f(z) = A \exp\left(\int S(z)\, dz \right) = A(z-a) \prod_{j=1}^{m} \prod_{\substack{n=0 \\ \nu\in\sigma_n(j)}}^{\infty} \frac{z-a_{\nu j}}{z-s_{\nu j}}. \qquad \square$$

The boundary condition for the map is used in the proof of Theorem 2.7 in [14], and is also referenced in Chapter 4. The following two lemmas give this condition for f'/f and S.

Lemma 2.8. *The circles in $\partial\mathbb{D}$ are mapped to radial slits by f if and only if*

$$\mathrm{Re}\left\{(z-c_j)\frac{f'(z)}{f(z)}\right\} = 0 \quad \textit{for} \quad z \in C_j,\ j = 1, \ldots, m.$$

Proof. Parametrize $z \in C_j$ by $z = c_j + r_j e^{i\theta}$. Since f maps to radial slits, it must be that $\arg f(z) = \text{const.}$, thus

$$0 = \frac{d}{d\theta}\arg f(z) = \frac{d}{d\theta}\,\mathrm{Im}\left\{\log f(c_j + r_j e^{i\theta})\right\} = \mathrm{Im}\left\{i r_j e^{i\theta}\frac{f'}{f}\right\} = \mathrm{Re}\left\{r_j e^{i\theta}\frac{f'}{f}\right\}. \qquad \square$$

The proof of Lemma 2.9 uses the following fact. Let $w = re^{i\theta}$ and $w^* = \frac{1}{r}e^{i\theta}$ for $r > 0$ (w and w^* are symmetric points with respect to the unit circle). Then

$$\begin{aligned}
\frac{w}{w-1} + \frac{w^*}{w^*-1} &= \frac{re^{i\theta}}{re^{i\theta}-1} + \frac{e^{i\theta}}{e^{i\theta}-r} \\
&= \frac{re^{i\theta}(re^{-i\theta}-1)}{r^2-2r\cos\theta+1} + \frac{e^{i\theta}(e^{-i\theta}-r)}{r^2-2r\cos\theta+1} \\
&= \frac{r^2-2re^{i\theta}+1}{r^2-2r\cos\theta+1} \\
&= \frac{r^2-2r\cos\theta-i2r\sin\theta+1}{r^2-2r\cos\theta+1}
\end{aligned}$$

shows that

$$\mathrm{Re}\left\{\frac{w}{w-1} + \frac{w^*}{w^*-1}\right\} = 1. \tag{2.8}$$

Lemma 2.9. *If $m > 1$ and $\Delta < (m-1)^{-1/4}$, then*

$$\mathrm{Re}\left\{(z-c_j)S_N(z)\right\} = O\left((\Delta^2\sqrt{m-1})^N\right)$$

for all $z \in \mathbb{C}_j$. That is,

$$\mathrm{Re}\left\{(z-c_j)S(z)\right\} = 0.$$

Proof. Given $z \in C_j$, group terms in S_N related by reflection across C_j:

$$S_N(z) = -\frac{1}{z-s_j} + \left(\frac{1}{z-a} + \frac{1}{z-a_j}\right) + \cdots$$
$$+ \left(\frac{1}{z-a_\nu} + \frac{1}{z-a_{j\nu}}\right) - \left(\frac{1}{z-s_\nu} + \frac{1}{z-s_{j\nu}}\right) + \cdots$$

Multiplying by $z - c_j$ allows writing

$$\begin{aligned}
&(z-c_j)S_N(z) = \\
&\quad -1 + \frac{(z-s_j)/(a-s_j)}{(z-s_j)/(a-s_j)-1} + \frac{(z-s_j)/(a_j-s_j)}{(z-s_j)/(a_j-s_j)-1} \\
&\quad + \sum_{p=1}^{m}\sum_{n=1}^{N-1}\sum_{\substack{\nu\in\sigma_n(p)\\ \nu p,\nu_1\neq j}} \left(\frac{(z-s_j)/(a_{\nu p}-s_j)}{(z-s_j)/(a_{\nu p}-s_j)-1} + \frac{(z-s_j)/(a_{j\nu p})-s_j)}{(z-s_j)/(a_{j\nu p}-s_j)-1}\right) \\
&\quad - \sum_{p=1}^{m}\sum_{n=1}^{N-1}\sum_{\substack{\nu\in\sigma_n(p)\\ \nu p,\nu_1\neq j}} \left(\frac{(z-s_j)/(s_{\nu p}-s_j)}{(z-s_j)/(s_{\nu p}-s_j)-1} + \frac{(z-s_j)/(s_{j\nu p}-s_j)}{(z-s_j)/(s_{j\nu p}-s_j)-1}\right) \\
&\quad + (z-s_j)\sum_{\substack{p=1\\ p\neq j}}^{m}\sum_{k=1}^{m}\sum_{p\nu\in\sigma_N(k)} \left(\frac{a_{p\nu k}-s_{p\nu k}}{(z-a_{p\nu k})(z-s_{p\nu k})}\right).
\end{aligned} \tag{2.9}$$

Set $w = (z-s_j)/(a_{\nu p}-s_j)$; it is easy to show that $w^* = 1/\overline{w} = (z-s_j)/(a_{j\nu p}-s_j)$. Indeed, define $r_a = |a_{\nu p}-s_j|$ and write $a_{\nu p} = s_j + r_a e^{i\theta_a}$. Reflecting $a_{\nu p}$ across circle C_j gives

$$\rho_j(a_{\nu p}) = s_j + \frac{r_j^2}{\bar{a}_{\nu p}-\bar{s}_j} = s_j + \frac{r_j^2}{r_a}e^{i\theta_a} = a_{j\nu p},$$

where one then has

$$\frac{z-s_j}{a_{\nu p}-s_j} = \frac{r_j}{r_a}e^{i(\theta-\theta_a)} \quad \text{and} \quad \frac{z-s_j}{a_{j\nu p}-s_j} = \frac{r_a}{r_j}e^{i(\theta-\theta_a)}.$$

Taking the real part of (2.9) and applying equation (2.8) shows that

$$\mathrm{Re}\left\{(z-s_j)S_N(z)\right\} = \mathrm{Re}\left\{(z-s_j)\sum_{\substack{p=1\\ p\neq j}}^{m}\sum_{k=1}^{m}\sum_{p\nu\in\sigma_N(k)}\left(\frac{a_{p\nu k}-s_{p\nu k}}{(z-a_{p\nu k})(z-s_{p\nu k})}\right)\right\}.$$

The estimate for the remaining terms are given by Lemma 2.6, in a manner similar to that found in the proof of Theorem 2.7. □

Circular slit map

Now consider the map from an unbounded domain $\mathbb{D}$ to a conformally equivalent circular slit domain; the circular slits are arcs of circles with the origin as center and various radii. This map was given in [15]; see Figure 2.3 for an example.

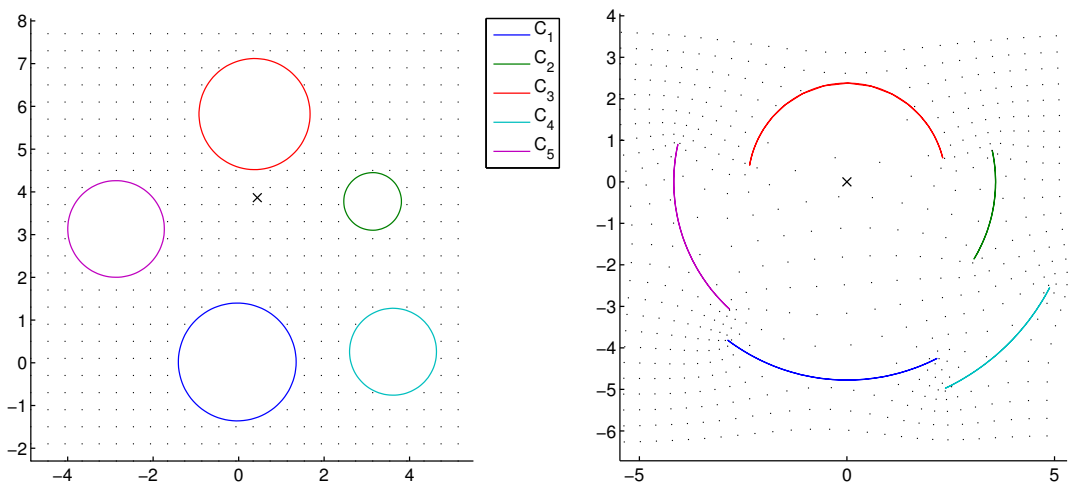

Figure 2.3: An example of an unbounded circular slit map.

As above this function is constructed by repeated use of the reflection principle. Even though details of the proof of the map stated in Theorem 2.10 below will not be given, a discussion the extension of f to $\hat{f}$ will be instructive in understanding the zeros and poles of the function.

Again let a be such that $f(a) = 0$ with a simple pole at infinity, *i.e.*, $f(\infty) = \infty$. The reflection of a across circle C_j to a_j is related to the reflection of 0 across the circle arc Γ_j, that is $\hat{f}(a_j) = \infty$. A reflection of a_j across any circle C_p, $p \neq j$, relates to the reflection of ∞ across the circle arc Γ_p, $p \neq j$, to the origin. It follows that any sequence of reflections, odd in number, of a_j will be a zero of $\hat{f}$, and an even number of reflections of a_j will be a simple pole. The center of any C_j is the reflection of infinity, and infinity reflected across a Γ_j is the origin. It follows that a sequence of reflections odd in number of s_j will be a pole of $\hat{f}$, and an even number of reflections of s_j will be a zero. As a notational convenience, let

ν_e denote reflection multi-indices of even length, that is $|\nu_e| = 2n$ for some integer n, and let ν_o denote multi-indices of odd length, $|\nu_o| = 2n+1$.

Theorem 2.10. *Let $\mathbb{P}$ be an unbounded m-connected circular slit region with $0, \infty \in \mathbb{P}$, and $\mathbb{D}$ a conformally equivalent circular domain with $a, \infty \in \mathbb{D}$. Furthermore suppose $\mathbb{D}$ satisfies the separation property $\Delta < (m-1)^{-1/4}$ for $m > 1$. Then $\mathbb{D}$ is mapped conformally onto $\mathbb{P}$ by f with $f(a) = 0$ and $f(\infty) = \infty$ if and only if*

$$f(z) = A(z-a)\prod_{j=1}^{m}\prod_{\substack{n=0\\ \nu\in\sigma_n(j)\\ |\nu_e|=2n\\ |\nu_o|=2n+1}}^{\infty}\frac{(z-a_{\nu_o j})(z-s_{\nu_e j})}{(z-a_{\nu_e j})(z-s_{\nu_o j})} \tag{2.10}$$

for some constant A.

Proof of this theorem will not be given here.

Maps to domains with mixed radial and circular slits

Here the circular and radial slits are combined, that is, we map from an unbounded circle domain $\mathbb{D}$ to a domain $\mathbb{P}$ where a circle C_j goes to either a circular or a radial slit Γ_j. This map was also given in [15]; see Figure 2.4 for an example.

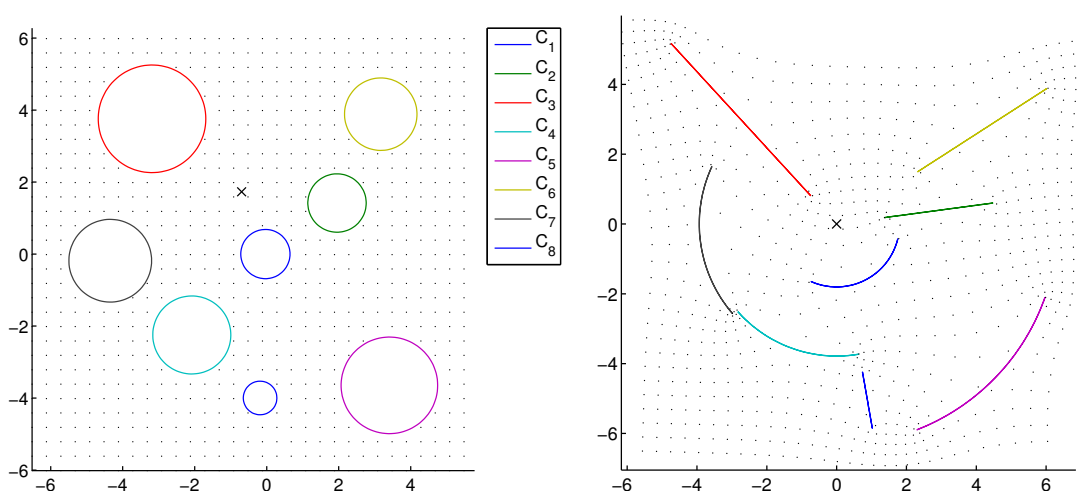

Figure 2.4: An example of an unbounded combined slit map.

Consider a point $a \in \mathbb{D}$ such that $f(a) = 0$ and the normalization $f(z)/z = O(1)$ as $z \to \infty$. Reflections through radial slits will keep 0 and ∞ fixed, and reflections through circular slits will swap 0 and ∞. Let a_{ν_e} denote a sequence of reflections, an even number of which are reflections of a through circles which map to circular slits, and let ∞_{ν_o} denote a sequence of reflections, an odd number of which are reflections of ∞ through circles which map to circular slits; these will be the simple zeros of the map. Similarly, a_{ν_o} and ∞_{ν_e} will be the simple poles.

Theorem 2.11. *Let $\mathbb{P}$ be an unbounded ($0, \infty \in \mathbb{P}$) m-connected region with m_r radial slits and m_c circular slits such that $m_r + m_c = m$, and $\mathbb{D}$ a conformally equivalent circular domain with $a, \infty \in \mathbb{D}$. Furthermore suppose $\mathbb{D}$ satisfies the separation property $\Delta < (m-1)^{-1/4}$ for $m > 1$. Then $\mathbb{D}$ is mapped conformally onto $\mathbb{P}$ by f with $f(a) = 0$ and $f(\infty) = \infty$ if and only if*

$$f(z) = A(z-a) \prod_{j=1}^{m} \prod_{\substack{n=0 \\ \nu \in \sigma_n(j) \\ |\nu_e| = 2n \\ |\nu_o| = 2n+1}}^{\infty} \frac{(z - a_{\nu_e})(z - \infty_{\nu_o})}{(z - a_{\nu_o})(z - \infty_{\nu_e})} \tag{2.11}$$

for some constant A.

2.2.2 Slit maps from bounded circular domains

Half-plane radial slits

Here the bounded circle domain $\mathbb{D}$ is mapped to a half-plane with the origin on the boundary and radial slits with respect to the origin. This map was given in [19]; see Figure 2.5 for an example.

Consider distinct points a and b on one of the boundary circles such that $f(a) = \infty$ and $f(b) = 0$. Reflections across the radial slits will leave 0 and ∞ fixed, thus reflections b_ν of b will be simple zeros and reflections a_ν of a will be simple poles.

Theorem 2.12. *Let $\mathbb{P}$ be an unbounded, m-connected radial slit upper half-plane and $\mathbb{D}$ a conformally equivalent bounded circular domain with $a, b \in C_1$. Further, suppose $\mathbb{D}$ satisfies*

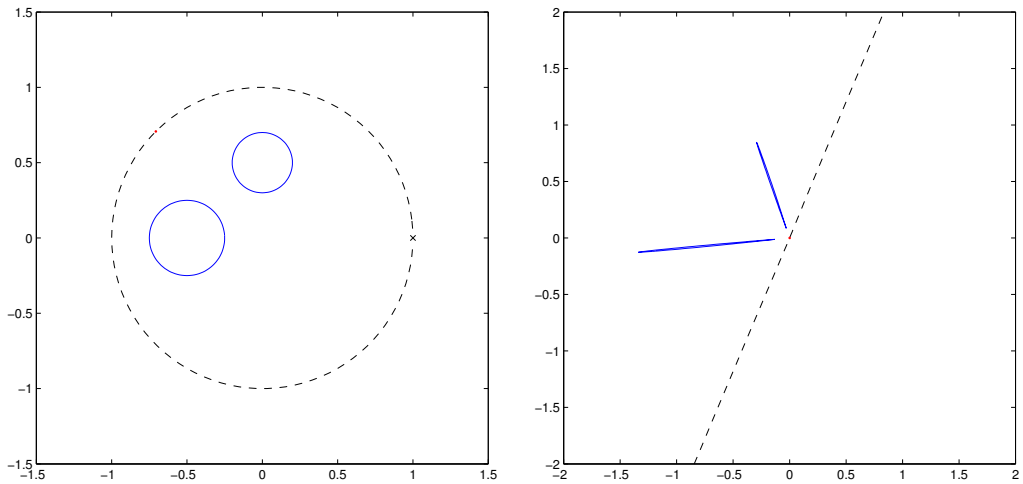

Figure 2.5: An example of the bounded half-plane map. This was done with $N = 4$ levels of reflection.

the separation property $\Delta < m^{-1/4}$ *for* $m > 1$. *Then* $\mathbb{D}$ *is mapped conformally onto* $\mathbb{P}$ *by* f *with* $f(a) = 0$ *and* $f(b) = \infty$ *if and only if*

$$f(z) = A \prod_{\substack{n=0 \\ \nu \in \sigma_n}}^{\infty} \frac{z - a_\nu}{z - b_\nu} \tag{2.12}$$

for some constant A.

Bounded radial and circular slits

As discussed in [19], the map from the bounded circle domain $\mathbb{D}$ to the bounded domain $\mathbb{P}$, where by a normalization Γ_1 is the unit circle and $\Gamma_2, \ldots, \Gamma_m$ are radial or circular slits, has the same form as the unbounded case, equation (2.11). See Figure 2.6.

Annulus with radial slits

Here a map from a bounded circle domain $\mathbb{D}$ to an annulus with radial slits is briefly discussed.

The construction of this map was motivated by a similar map given in Nehari [31, Chap. VII, eq. (8)]. There the map from an arbitrary multiply connected domain to a circular slit ring, with boundary component j going to the outer circle and boundary component i

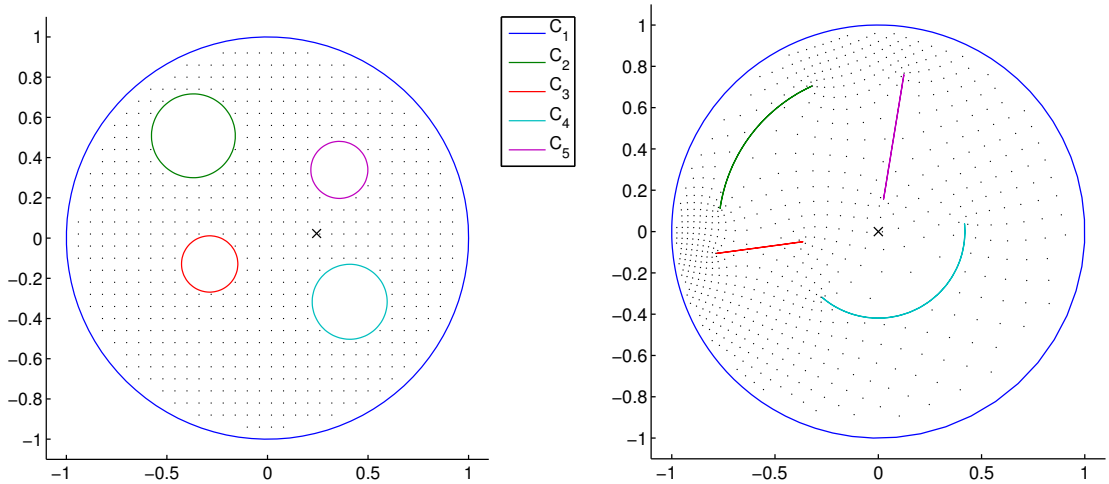

Figure 2.6: An example of the bounded, mixed radial and circular slit map.

going to the inner circle, is shown to be the ratio of the maps R_j and R_i to circular slit disks taking side j and side i, respectively, to the boundary of the disk (and a to the origin). The map is denoted

$$S_{ji}(z) = \frac{R_j(z;a)}{R_i(z;a)}.$$

In this case since we are mapping from circle domains, the maps can be represented explicitly by infinite product formulas. Two specified circles C_j and C_i can be mapped to the outer and inner annulus boundaries and the remaining boundaries map to radial slits. Specifically, given j, i, the map to the radial slit annulus is given by

$$f_{ji}(z) = \frac{f_j(z)}{f_i(z)},$$

where here $f_j(z)$ denotes the map from the circle domain to the disk with one circular slit and $m-2$ radial slits, such that C_j maps to the outer circle, $C_i, i \neq j$, maps to a circular slit, and the other circles map to the radial slits. The function $f_i(z)$ just exchanges the roles of C_i and C_j. The ratio clearly maps the circles C_j and C_i to boundaries of constant radius and maps the other circles to radial slits. For instance, in Figure 2.7, if inner circles are $j = 2$ and $i = 3$, then the map to the radial slit annulus would be $f_{23}(z)$ and would map the outer circle C_1 to the radial slit.

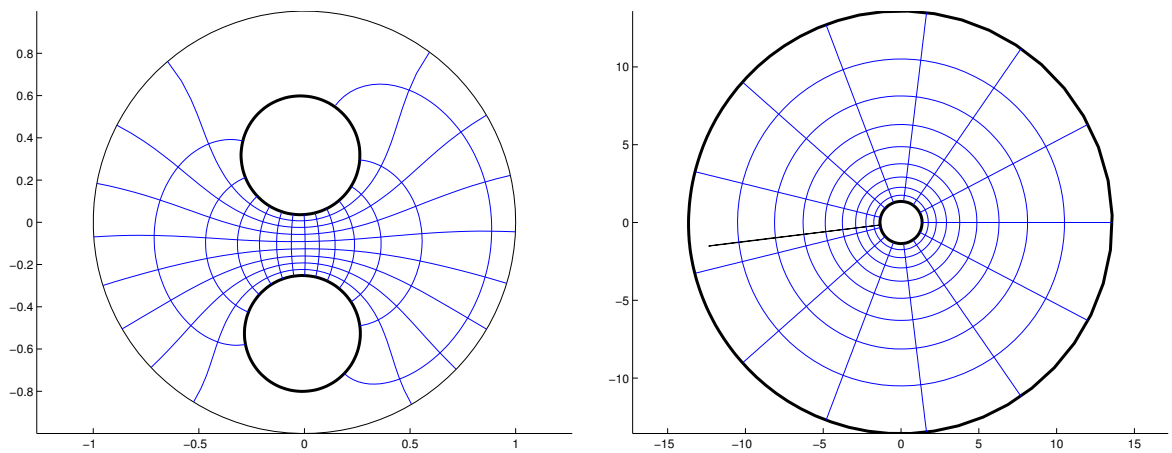

Figure 2.7: Example of a slit annulus map.

2.3 The Schwarz-Christoffel map for multiply connected domains

Here we recall formulas given in [18, 13] for multiply connected Schwarz-Christoffel (MCSC) maps, *i.e.*, conformal maps from an m-connected (un)bounded circle domain $\mathbb{D}$ with component boundary circles $C_1, \ldots, C_m$ to an m-connected (un)bounded polygonal domain $\mathbb{P}$ with component boundary polygons $\Gamma_1, \ldots, \Gamma_m$.

For $j \in \{1, \ldots, m\}$ let K_j be the number of vertices on the jth polygon Γ_j. Let $w_{k,j}$ denote the kth vertex on Γ_j. The maps will satisfy $f(z_{k,j}) = w_{k,j}$ where $z_{k,j} = c_j + r_j e^{i\theta_{k,j}}$ is the kth *prevertex* on circle C_j. (The notation $\Gamma_j = f(C_j)$ will also be used for images of the circle boundaries.) Polygonal boundaries are given a counterclockwise orientation, and the vertices are numbered in order according to this orientation. The interior angles of the polygons at the vertices are denoted $\pi\alpha_{k,j}$ with $0 < \alpha_{k,j} \leq 2$. The formulas below use the turning angle $\pi\beta_{k,j}$ of the tangent vector on the polygonal boundaries at the vertices. The interior angle and the turning angle satisfy the relation $\alpha_{k,j} + \beta_{k,j} = 1$. Also

$$\sum_{k=1}^{K_j} \beta_{k,j} = 2 \quad \text{for all} \quad j \in \{1, \ldots, m\}$$

with the exception of Γ_1 in the bounded case where we use the convention

$$\sum_{k=1}^{K_1} \beta_{k,1} = -2.$$

The derivation of the maps below are similar to the slit maps above. The map f is extended by repeated Schwarz reflection to a global, many valued function $\hat{f}$ on $\mathbb{C} \setminus \{\text{limit points}\}$. It is shown that $\hat{f}''/\hat{f}'$ is single valued. A singularity function S is constructed and it is shown that $S = f''/f'$. Thus the maps are of the form $f(z) = \int \exp(\int S(z))$.

2.3.1 Unbounded case

The map for the unbounded domain was given in [18]. For examples of this map see Figures 2.8 and 2.9.

Theorem 2.13. *Let $\mathbb{P}$ be an unbounded m-connected polygonal region with $\infty \in \mathbb{P}$, and $\mathbb{D}$ a conformally equivalent circular domain. Further, suppose $\mathbb{P}$ satisfies the separation property $\Delta < (m-1)^{-1/4}$ for $m > 1$. Then $\mathbb{D}$ is mapped conformally onto $\mathbb{P}$ by a function of the form $Af(z) + B$ where*

$$f(z) = \int^z \prod_{j=1}^{m} \prod_{k=1}^{K_j} \prod_{\substack{n=0 \\ \nu \in \sigma_n(j)}}^{\infty} \left(\frac{\zeta - z_{k,\nu j}}{\zeta - s_{\nu j}} \right)^{\beta_{k,j}} d\zeta \tag{2.13}$$

for constants A and B. Here $-1 < \beta_{k,j} < 1$ and $\sum_{k=1}^{K_j} \beta_{k,j} = 2$.

Although the proof of this theorem will not be given here, the proof of the convergence of the singularity function $S(z) = (d/dz) \log f'(z) = f''(z)/f'(z)$ will be shown since a numerical error estimate based on the proof of this theorem will be discussed in Section 3.6.

In a fashion similar to that given in Section 2.2.1 we define a function using the singular parts of the pre-Schwarzian $f''(z)/f'(z)$,

$$B_n(z) := \sum_{\nu \in \sigma_n(j)} \sum_{j=1}^{m} \left(\sum_{k=1}^{K_j} \frac{\beta_{k,j}}{z - z_{k,\nu j}} - \frac{\beta_{k,j}}{z - s_{\nu j}} \right) = \sum_{\nu \in \sigma_n(j)} \sum_{j=1}^{m} \sum_{k=1}^{K_j} \frac{\beta_{k,j}(z_{k,\nu j} - s_{\nu j})}{(z - z_{k,\nu j})(z - s_{\nu j})}$$

and the function

$$S_N(z) := \sum_{n=0}^{N} B_n(z) = \sum_{j=1}^{m} \sum_{\substack{n=0 \\ \nu \in \sigma_n(j)}}^{N} \left(\sum_{k=1}^{K_j} \frac{\beta_{k,j}}{z - z_{k,\nu j}} - \frac{\beta_{k,j}}{z - s_{\nu j}} \right). \tag{2.14}$$

The singularity function is then defined, using $\sum \beta_{k,j} = 2$,

$$S(z) := \lim_{N \to \infty} S_N(z) = \sum_{j=1}^{m} \sum_{\substack{n=0 \\ \nu \in \sigma_n(j)}}^{\infty} \left[\left(\sum_{k=1}^{K_j} \frac{\beta_{k,j}}{z - z_{k,\nu j}} \right) - \frac{2}{z - s_{\nu j}} \right]. \tag{2.15}$$

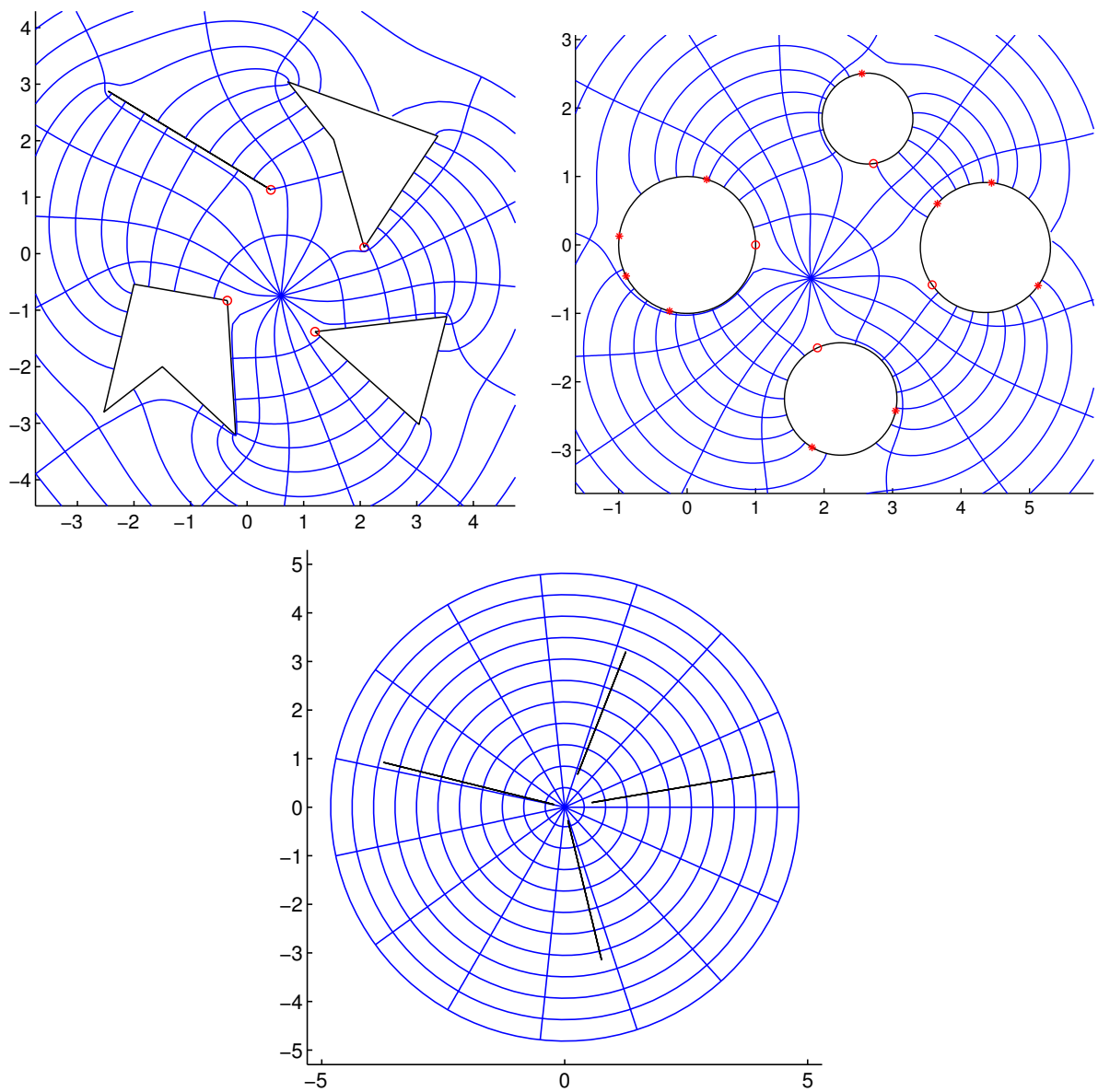

Figure 2.8: An example of an unbounded MCSC map with $m = 4$. Here $\Delta \approx 0.6321 < (4-1)^{-1/4} \approx 0.7598$. Also shown is the orthogonal grid from the conformally equivalent slit domain; see Section 3.8.

Lemma 2.14. *Suppose for connectivity $m > 1$ that $\mathbb{D}$ satisfies $\Delta < (m-1)^{-1/4}$, then $S_N(z)$ converges to $S(z)$ uniformly on closed subsets of $\overline{\mathbb{D}} \setminus \{z_{k,j} : j = 1, \ldots, m;\ k = 1, \ldots, K_j\}$ by the estimate*

$$|S(z) - S_N(z)| = O\left((\Delta^2\sqrt{m-1})^{N+1}\right).$$

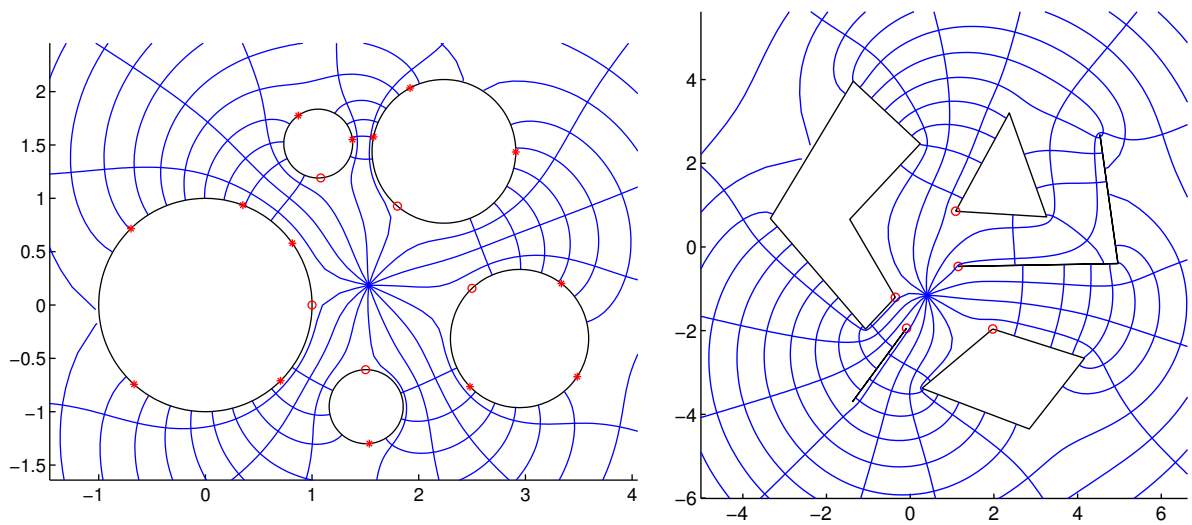

Figure 2.9: An example of an unbounded MCSC map with $m = 5$. The separation condition is violated since $\Delta \approx 0.8438 > (5-1)^{-1/4} \approx 0.7071$.

Proof. Let G be a closed subset of $\overline{\mathbb{D}} \setminus \{z_{k,j} : j = 1, \ldots, m;\ k = 1, \ldots, K_j\}$ such that $z \in G$ and $n > 0$ a level of reflection. Define $\delta = \inf_{z \in G}\{|z - z_{k,\nu}|, |z - s_\nu| : k = 1, \ldots, K_j;\ j = 1, \ldots, m;\ \nu \in \sigma_n\}$ and $K_{\max} := \max_j K_j$. Recall that $-1 < \beta_{k,j} < 1$ and note $|z_{k,\nu j} - s_{\nu j}| < 2r_{\nu j}$. Then

$$|B_n(z)| \leq \sum_{\nu \in \sigma_n(j)} \sum_{j=1}^{m} \sum_{k=1}^{K_j} \frac{|\beta_{k,j}||(z_{k,\nu j} - s_{\nu j})|}{|(z - z_{k,\nu j})||(z - s_{\nu j})|} \leq \frac{2}{\delta^2} \sum_{\nu \in \sigma_n(j)} \sum_{j=1}^{m} \sum_{k=1}^{K_j} r_{\nu j}.$$

Using the Cauchy-Schwarz inequality and Lemma 2.6,

$$\begin{aligned}
\frac{2}{\delta^2} \sum_{\nu \in \sigma_n(j)} \sum_{j=1}^{m} \sum_{k=1}^{K_j} r_{\nu j} &\leq \frac{2K_{\max}}{\delta^2} \sum_{\nu \in \sigma_n(j)} \sum_{j=1}^{m} r_{\nu j} \\
&\leq \frac{2K_{\max}}{\delta^2} \left(\sum_{\nu \in \sigma_n(j)} \sum_{j=1}^{m} r_{\nu j}^2 \right)^{1/2} \left(\sum_{\nu \in \sigma_n(j)} \sum_{j=1}^{m} 1 \right)^{1/2} \\
&\leq \frac{2K_{\max}}{\delta^2} \Delta^{2j} \left(\sum_{j=1}^{m} r_{\nu j}^2 \right)^{1/2} \sqrt{m}(m-1)^{j/2} \\
&\leq C\Delta^{2j}(m-1)^{j/2},
\end{aligned}$$

thus the series S_N converges absolutely if $\Delta^2\sqrt{m-1} < 1$. $\square$

It should be noted that the residues of $S_N(z)$ add out in pairs which makes

$$\lim_{N\to\infty} \int^z S_N(\zeta)\, d\zeta = \int^z S(\zeta)\, d\zeta$$

a single valued analytic function on $\overline{\mathbb{D}}$ minus the prevertex points.

In Chapter 4 we derive a method for calculating equation (2.13) which does not make use of the reflections. We will have need of the boundary conditions of this map, stated in terms of the singularity function. To emphasize that in fact $f''(z)/f'(z) = S(z)$, the boundary condition will be given here in terms of both the pre-Schwarzian and the singularity function.

Lemma 2.15.

$$\mathrm{Re}\left\{(z-c_j)\frac{f''(z)}{f'(z)}\right\} = -1 \quad \textit{for} \quad z = c_j + r_j e^{i\theta} \in C_j \setminus \{z_{k,j} : k = 1, \ldots, K_j\}.$$

Proof. The tangent angle of the boundary C_j is constant on each of the arcs between prevertices, that is

$$\arg\left\{\frac{d}{d\theta} f(c_j + r_j e^{i\theta})\right\} = \mathrm{Im}\left\{\log\left(ir_j e^{i\theta} f'(z)\right)\right\} = \text{const.}$$

Thus

$$\begin{aligned}\frac{d}{d\theta}\,&\mathrm{Im}\left\{\,\log(f'(z)) + \log\left(ir_j e^{i\theta}\right)\,\right\} \\ &= \mathrm{Im}\left\{ir_j e^{i\theta}\frac{f''(z)}{f'(z)} + i\right\} = \mathrm{Re}\left\{(z-c_j)\frac{f''(z)}{f'(z)} + 1\right\} = 0.\end{aligned}$$ $\square$

Lemma 2.16. *If $\Delta < (m-1)^{-1/4}$, then, for $z \in C_j \setminus \{z_{k,j} : k = 1, \ldots, K_j\}$,*

$$\mathrm{Re}\left\{(z-c_j)S(z)\right\} = -1.$$

Proof of Lemma 2.16 is not given here; for details see [18].

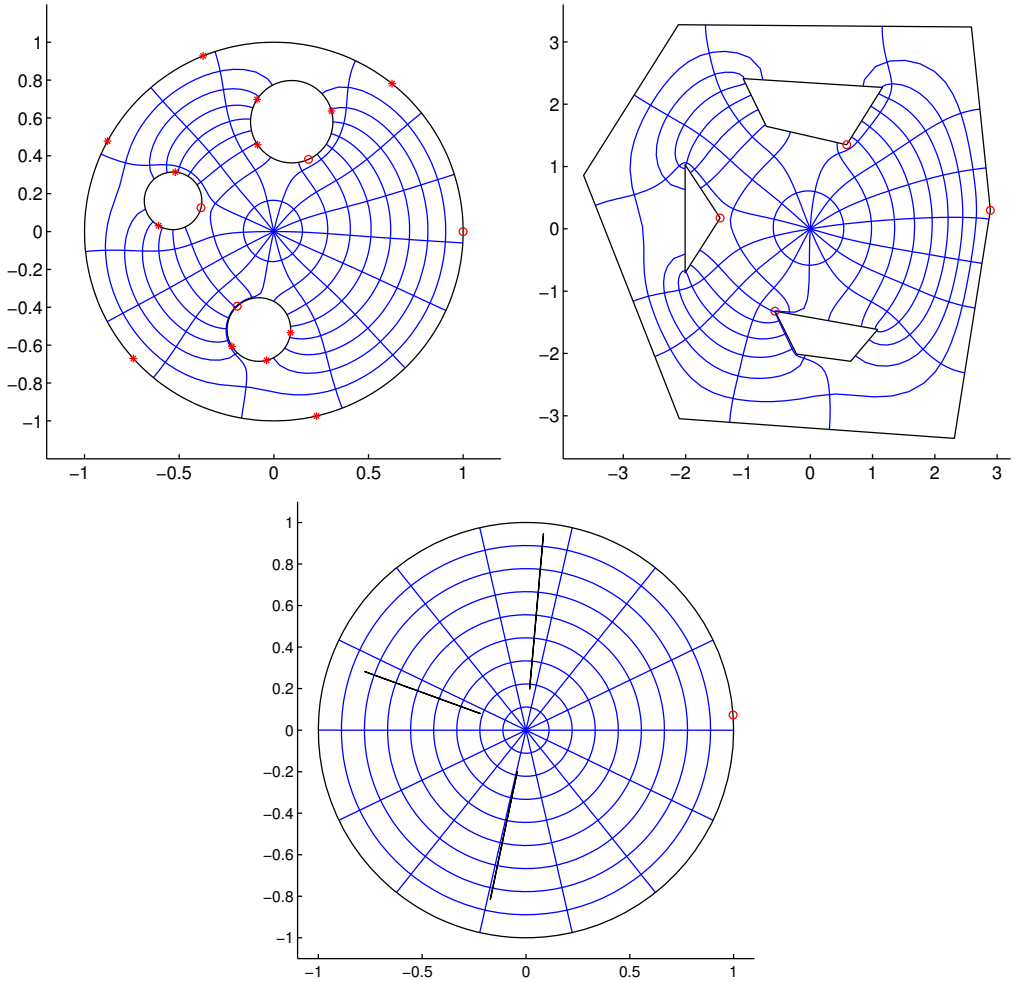

Figure 2.10: An example of a bounded MCSC map with connectivity $m = 4$. Note that the separation condition is violated in this example, that is $\Delta \approx 0.8775 > (4-1)^{-1/4} \approx 0.7598$. Also shown is the orthogonal grid from the conformally equivalent slit domain; see Section 3.8.

2.3.2 Bounded case

The map for the bounded case was given in [13]. See Figures 2.10 and 2.11 for examples of this map.

Theorem 2.17. *Let $\mathbb{P}$ be a bounded m-connected polygonal region, and $\mathbb{D}$ a conformally equivalent circular domain. Further, suppose $\mathbb{D}$ satisfies the separation property $\Delta < (m-1)^{-1/4}$ for $m > 1$. Then $\mathbb{D}$ is mapped conformally onto $\mathbb{P}$ by a function of the form $Af(z)+B$*

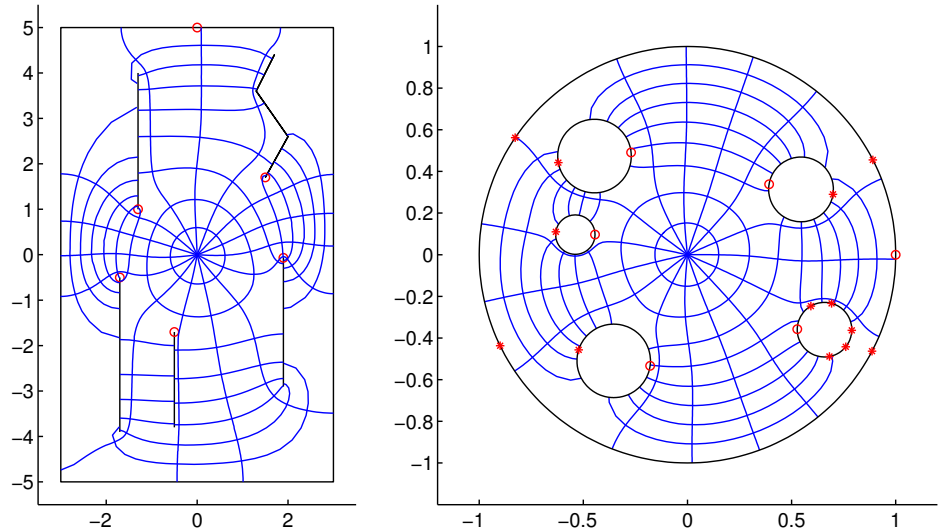

Figure 2.11: An example of a bounded MCSC map with connectivity $m = 6$. The separation condition is violated in this example, that is $\Delta \approx 0.9017 > (6-1)^{-1/4} \approx 0.6687$.

where

$$f(z) = \int^z \prod_{j=1}^{m} \prod_{k=1}^{K_j} \prod_{\substack{n=0 \\ \nu \in \sigma_n(j)}}^{\infty} (\zeta - z_{k,\nu j})^{\beta_{k,j}} \, d\zeta, \tag{2.16}$$

for constants A and B. Here $-1 < \beta_{k,j} < 1$ with $\sum_{k=1}^{K_j} \beta_{k,j} = 2$ for $1 < j \leq m$ and $\sum_{k=1}^{K_1} \beta_{k,1} = -2$.

Again the proof of this theorem will not be given here, but we note that the singularity function

$$S(z) = \frac{d}{dz} \log\left(f'(z)\right) = \sum_{j=1}^{m} \sum_{\substack{n=0 \\ \nu \in \sigma_n(j)}}^{\infty} \sum_{k=1}^{K_j} \frac{\beta_{k,j}}{z - z_{k,\nu j}} \tag{2.17}$$

satisfies an estimate in the term related to the nth level of reflection similar to that given in the proof of Lemma 2.14, that is

$$\sum_{j=2}^{m} \sum_{\nu \in \sigma_n(j)} \left(\sum_{k=1}^{K_j} \left| \frac{\beta_{k,j}(z_{k,\nu j} - s_{\nu j})}{(z - z_{\nu j})(z - s_{\nu j})} \right| + \sum_{k=1}^{K_1} \left| \frac{\beta_{k,j1}(z_{k,\nu j1} - s_{\nu j1})}{(z - z_{\nu j1})(z - s_{\nu j1})} \right| \right)$$
$$\leq \frac{2K_{\max}}{\delta^2} \sum_{j=1}^{m} \sum_{\nu \in \sigma_n(j)} r_{\nu j}. \tag{2.18}$$

Note that in the bounded case, when working with truncated forms of $f'(z)$ or $S(z)$, we must pair one extra level reflection of points on C_1 with reflections at some level $n > 0$. This extra level of reflection plays a role similar to that of the terms involving the centers of reflected circles in the unbounded case, that is, these terms ensure the residues of $S_N(z)$ add out in pairs which makes $\lim_{N\to\infty} \int^z S_N(\zeta)\, d\zeta = \int^z S(\zeta)\, d\zeta$ a single valued analytic function on $\overline{\mathbb{D}}$ minus the prevertex points.

CHAPTER 3

NUMERICAL METHODS

The focus of this Chapter is on the numerical methods involved computing the multiply connected Schwarz Christoffel maps. For computation, the infinite products in the formulas for the bounded and unbounded MCSC maps, equations (2.13) and (2.16), are truncated to N levels of reflection,

$$p_u(z) := \prod_{j=1}^{m} \prod_{k=1}^{K_j} \prod_{\substack{n=0 \\ \nu\in\sigma_n(j)}}^{N} \left(\frac{z - z_{k,\nu j}}{z - s_{\nu j}}\right)^{\beta_{k,j}} \approx \prod_{j=1}^{m} \prod_{k=1}^{K_j} \prod_{\substack{n=0 \\ \nu\in\sigma_n(j)}}^{\infty} \left(\frac{z - z_{k,\nu j}}{z - s_{\nu j}}\right)^{\beta_{k,j}} \tag{3.1}$$

and

$$p_b(z) := \prod_{k=1}^{K_1} (z - z_{k,1})^{\beta_{k,1}} \prod_{j=2}^{m} \prod_{\substack{n=0 \\ \nu\in\sigma_n(j)}}^{N} \left(\prod_{k=1}^{K_1} (z - z_{k,\nu j1})^{\beta_{k,1}} \prod_{k=1}^{K_j} (z - z_{k,\nu j})^{\beta_{k,j}}\right). \tag{3.2}$$

Following the remark at the end of Section 2.3.2, note that p_b must include an extra level of reflection for C_1.

3.1 The parameter problem

The Schwarz-Christoffel transformations (2.13) and (2.16) above give the form of the mapping functions f for polygonal domains $\mathbb{P}$. It is required, in order to apply these formulas to the computation of the mapping function, to find the prevertices $z_{k,j}$ such that $f(z_{k,j}) = w_{k,j}$, along with the centers c_j and radii r_j of the conformally equivalent circle domain. Recall that K_j for $j = 1, \ldots, m$ represents the number of vertices on each Γ_j in $\partial\mathbb{P}$. Parametrize the prevertices by $z_{k,j} = c_j + r_j e^{i\theta_{k,j}}$ for $k = 1, \ldots, K_j$ with

$$\theta_{1,j} < \theta_{2,j} < \ldots < \theta_{K_j,j}. \tag{3.3}$$

The unknown centers, radii, and prevertex angles amount to a total of

$$K_1 + \cdots + K_m + 3m$$

unknown real parameters. Finding these quantities for a given polygonal domain is known as the *parameter problem*.

In order to solve the parameter problem we will apply the normalization conditions for conformal maps of multiply connected domains and enforce conditions, based on the geometry of the polygonal domains, to set up complete systems of independent nonlinear equations for these unknown parameters. The choice of the geometric conditions is not unique, as will be demonstrated. The construction of the nonlinear system for the unbounded case will be slightly different than the bounded case.

3.1.1 Unbounded case

The nonlinear equations for this case were first given in [14] and will be restated here. By the theory given in [26, 31], given $\mathbb{P}$ and the normalization condition $f(z) = z + O(1/z)$ for $z \to \infty$, there is a unique circle domain $\mathbb{D}$ such that f uniquely maps $\mathbb{D}$ onto $\mathbb{P}$. Since this normalization is difficult to impose, it is relaxed to

$$f(z) = Cz + D + O(1/z), \quad z \to \infty,$$

and constants C and D are determined implicitly. To do this set $c_1 = 0$, $r_1 = 1$, and $\theta_{1,1} = 0$. Define

$$A = \frac{w_{2,1} - w_{1,1}}{\int_{z_{1,1}}^{z_{2,1}} p_u(\zeta)\, d\zeta}$$

and then write

$$f(z) = A \int_{z_{1,1}}^{z} p_u(\zeta)\, d\zeta + B,$$

with $B = w_{1,1} = f(z_{1,1})$. This normalization takes care of four of the real parameters, leaving

$$(K_1 - 1) + K_2 + \cdots + K_m + (3m - 3) = K_1 + \cdots + K_m + 3m - 4$$

real parameters to be determined.

Here and below expressions such as $f(z_{k+1,j}) - f(z_{k,j})$ or similarly $f(z_{1,j}) - f(z_{1,1})$ are used as a short-hand for numerical integration over a path in domain connecting two

prevertices. For example

$$f(z_{k+1,j}) - f(z_{k,j}) := A \int_{z_{k,j}}^{z_{k+1,j}} p_u(\zeta)\, d\zeta$$

or

$$f(z_{1,j}) - f(z_{1,1}) := A \int_{z_{1,1}}^{z_{1,j}} p_u(\zeta)\, d\zeta.$$

The nonlinear conditions are now derived from the geometry of the polygonal domain. To ensure the correct side lengths of the polygons, define the *side length conditions*

$$|f(z_{k+1,j}) - f(z_{k,j})| = |w_{k+1,j} - w_{k,j}|,$$

for $j = 1, \ldots, m$ and $k = 1, \ldots, K_j$, with $z_{K_j+1,j} := z_{1,j}$ and $w_{K_j+1,j} := w_{1,j}$. This is a total of $K_1 + \ldots + K_m$ equations, but the definition of A above fixes the first side length of Γ_1 by scaling, which removes one from this count. The positions of polygons Γ_2 through Γ_m in relation to Γ_1 (the position of the first polygon Γ_1 is fixed by the normalization) are determined by the *position conditions*

$$f(z_{1,j}) - f(z_{1,1}) = w_{1,j} - w_{1,1}$$

for $j = 2, \ldots, m$ which gives $2(m-1)$ real equations. Finally the orientations of polygons Γ_2 through Γ_m are determined by the *orientation conditions*

$$\arg(f(z_{2,j}) - f(z_{1,j})) = \arg(w_{2,j} - w_{1,j})$$

for $j = 2, \ldots, m$ (again the orientation of Γ_1 is determined by the normalization), which gives $(m-1)$ real equations. The three conditions amount to a system of $K_1 + \cdots + K_m + 3m - 4$ equations, equal to the number of undetermined parameters.

3.1.2 Bounded case

In order to guarantee uniqueness of the mapping function in the bounded case, the map is normalized by fixing one boundary point, $f(1) = w_{1,1}$, and one interior point, $f(z_0) = w_0$. (The map can also be normalized by fixing three vertices on the outer boundary, but this has not yet been implemented.)

As above set

$$A = \frac{w_{2,1} - w_{1,1}}{\int_{z_{1,1}}^{z_{2,1}} p_b(z)\, dz},$$

and write

$$f(z) = A \int_{z_{1,1}}^{z} p_b(\zeta)\, d\zeta + B,$$

with $f(z_{1,1}) = B = w_{1,1}$. We again require that $c_1 = 0$ and $r_1 = 1$, and note that fixing $f(1) = w_{1,1}$ is equivalent to setting $\theta_{1,1} = 0$. This amounts to fixing four of the real parameters, so once again there are $K_1 + \cdots + K_m + 3m - 4$ real unknown parameters to determine.

The remaining parameters are determined as follows. As in the unbounded case define the *side length conditions*,

$$|f(z_{k+1,j}) - f(z_{k,j})| = |w_{k+1,j} - w_{k,j}|,$$

for $j = 1, \ldots, m$ and $k = 1, \ldots, K_j$. This gives $K_1 + \cdots + K_m$ real equations, but, as above, the calculation of A removes one from this count. In addition the last side lengths of the first two polygons, Γ_1 and Γ_2, are left off. The side length conditions then add up to $K_1 + \cdots + K_m - 3$ real equations. The positions of Γ_1 through Γ_m with respect to the fixed point w_0 are given by the *position conditions*,

$$f(z_{1,j}) - f(z_0) = w_{1,j} - w_0,$$

for $j = 1, \ldots, m$. This is $2m$ real equations. Finally, the orientations of Γ_2 through Γ_m (the orientation of Γ_1 is determined by the calculation of A) are given by the $(m-1)$ real equations, the *orientation conditions*,

$$\arg(f(z_{2,j}) - f(z_{1,j})) = \arg(w_{2,j} - w_{1,j}),$$

for $j = 2, \ldots, m$. Once again the side length, position, and orientation conditions give $K_1 + \cdots + K_m + 3m - 4$ real equations, exactly as needed.

3.2 Transformation to unconstrained variables

The constraint (3.3) is difficult to enforce directly on the $\theta_{k,j}$, and its violation can cause the nonlinear solver to fail to converge to a good solution. Therefore, as in [34, 3, 22, 36], a transformation to a set of unconstrained variables is made which guarantees (3.3). This change was not implemented in the initial attempt to compute multiply connected Schwarz-Christoffel maps in [14] and it severely limited the robustness of the algorithm. With this change the method is extremely robust and rarely fails, with very little care needed in the selection of an initial guess. Fortunately it does not seem to be necessary, in practice, to constrain the circles from overlapping by enforcing $\Delta < 1$. This would be a difficult set of conditions to apply.

The unconstrained variables, $\mathrm{Re}\{c_j\}$, $\mathrm{Im}\{c_j\}$, and $\log(r_j)$ will be used in place of the centers and radii in the nonlinear equation solver. For the $\theta_{k,j}$, which will be denoted for the moment by θ_k for brevity, a transformation similar to [3, eq. (21)] is used.

On any of the boundary circles in the computational domain with K prevertices, the problem is to find the angles of these prevertices with respect to the circle center. The angles, of course, must meet the constraint

$$\sum_{k=1}^{K}(\theta_{k+1} - \theta_k) = 2\pi,$$

where we will use the convention $\theta_{K+1} = \theta_1 + 2\pi$. Defining

$$\phi_k := \theta_{k+1} - \theta_k \quad \text{for } k = 1, \ldots, K,$$

the unconstrained angle variables for a given circle are then

$$\psi_k := \log \frac{\phi_{k+1}}{\phi_1} \quad \text{for } k = 1, \ldots, K-1 \tag{3.4}$$

(with $\psi_{k,j}$ temporarily represented by ψ_k). In order to invert this transformation, note that

$$1 + \sum_{j=1}^{K-1} e^{\psi_j} = 1 + \frac{\phi_2}{\phi_1} + \cdots + \frac{\phi_K}{\phi_1} = \frac{2\pi}{\phi_1}$$

and

$$1+\sum_{j=1}^{k-2} e^{\psi_j} = 1+\frac{\phi_2}{\phi_1}+\cdots+\frac{\phi_{k-1}}{\phi_1} = \frac{\theta_2-\theta_1}{\phi_1}+\frac{\theta_3-\theta_2}{\phi_1}+\cdots+\frac{\theta_k-\theta_{k-1}}{\phi_1} = \frac{\theta_k-\theta_1}{\phi_1},$$

so that

$$2\pi\frac{1+\sum_{j=1}^{k-2} e^{\psi_j}}{1+\sum_{j=1}^{K-1} e^{\psi_j}} = 2\pi\frac{(\theta_k-\theta_1)/\phi_1}{2\pi/\phi_1} = \theta_k-\theta_1.$$

Assume that θ_1 is known for the circle in question. Then any angle θ_k, for $k=2,\ldots,K$, is given by

$$\theta_k = \theta_1 + 2\pi\frac{1+\sum_{j=1}^{k-2} e^{\psi_j}}{1+\sum_{j=1}^{K-1} e^{\psi_j}}. \tag{3.5}$$

Thus the transformation (3.4) gives K_1-1 unconstrained parameters,

$$\psi_{1,1}, \psi_{2,1}, \ldots, \psi_{K_1-1,1},$$

on C_1 (recall $\theta_{1,1}$ is fixed at zero). On each of the other circles with K_j prevertices, $j=2,\ldots,m$, the angle of the first prevertex, $\theta_{1,j}$, is allowed to be unconstrained (this angle is easily re-normalized to 2π), for exactly K_j unconstrained, parameters

$$\theta_{1,j}, \psi_{1,j}, \psi_{2,j}, \ldots, \psi_{K_j-1,j}.$$

The remaining angles on all circles, $\theta_{2,j},\ldots,\theta_{K_j,j}$ for $j=1,\ldots,m$, are then recovered by (3.5) and (3.3) is automatically satisfied.

3.3 Solving the non-linear system

The system of non-linear equations given in Section 3.1 in terms of the transformed variables from Section 3.2 can be expressed as a non-linear system,

$$F(X)=0, \tag{3.6}$$

where $F:\mathbb{R}^n\to\mathbb{R}^n$, with $n=K_1+\cdots+K_m+3m-4$. To solve this system, the continuation algorithm CONTUP from [1, Program 3] is used, as in [14].

3.3.1 Numerical continuation

A brief description of this method is now given. It is assumed that F is smooth enough; that is, F has enough derivatives to facilitate the required analysis. Let G be a trivial map $G : \mathbb{R}^n \to \mathbb{R}^n$ with known zeros. Let $X_0, X_1 \in \mathbb{R}^n$ be such that $G(X_0) = 0$ and $F(X_1) = 0$. Define the homotopy function

$$H(X, \lambda) = \lambda F(X) + (1 - \lambda)G(X)$$

for $\lambda \in [0, 1]$. Note then that

$$H^{-1}(0) = \ker H = \{(X, \lambda) : H(X, \lambda) = 0\} \subset \mathbb{R}^{n+1}.$$

A curve $c(s) \in \ker H$, *i.e.*,

$$c : \mathbb{R} \to \ker H,$$

is then determined such that $c(s_0) = (X_0, 0)$ and $c(s_1) = (X_1, 1)$ for some $s_0 < s_1 \in \mathbb{R}$. The idea then is to simply trace the curve $c(s)$, via a predictor-corrector method, from $s = s_0$ to s_1, at which point we have a solution to (3.6). The existence of this curve is discussed in [1] and will not be repeated here. Uniqueness of the solution is guaranteed by the uniqueness of the conformally equivalent circle domain.

For the implementation of the algorithm in this case, let $X_0 \in \mathbb{R}^n$ be an initial guess for the unknown parameters representing the circle domain, and set $F_0 = F(X_0)$. Define $G(X) = F(X) - F_0$ so that the homotopy function is then given by

$$H(X, \lambda) = (1 - \lambda)G(X) + \lambda F(X) = F(X) + (\lambda - 1)F_0.$$

A finite difference approximation to the Jacobian is used in tracing the curve $c(s)$. The condition number of the Jacobian has been generally found to be of order 10. A much larger condition number indicates in the author's experience an incorrect formulation of the nonlinear equations leading to non-convergence, or convergence to an incorrect solution, that is, a solution to an incomplete set of conditions. In such cases, a plot of an orthogonal grid for the corresponding mapping function is usually obviously incorrect.

3.3.2 Comparison to other solvers

Numerical continuation was chosen for use during the development of the numerics since the method is by design not sensitive to the accuracy of the initial guess. It seems a worthwhile question to ask how other nonlinear equation solvers, specifically those built into MATLAB, handle the parameter problem. The discussion in this section closely follows that of [20].

Since conformally equivalent domains can have inherently large geometric distortions, it is not clear how one would in general make an initial guess for the map parameters which might be close to a solution. We settle on a reasonable geometry for the circle domain for a given polygonal domain. For example, an easy-to-generate initial guess for the polygonal domain and associated circle domain shown in Figure 3.1 is given in Figure 3.2.

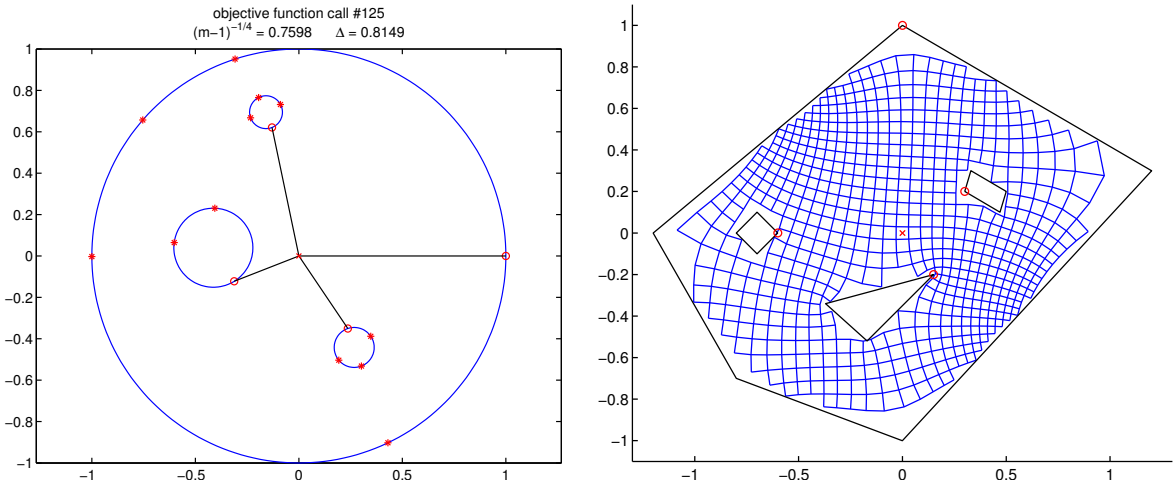

Figure 3.1: An example with $m = 4$ used to test the different nonlinear solvers.

We tested the solvers in MATLAB's Optimization Toolbox [29] which could be applied to this problem. These were `fsolve`, `lsqnonlin`, `fminunc`, and `fminsearch`. The `fsolve` function was tested with the trust-region-dogleg (t-r-d), trust-region-reflective (t-r-r), and Levenberg-Marquardt (l-m) algorithms. The function `lsqnonlin` was tested with the (t-r-r) and (l-m) algorithms. Since we did not supply the numerical gradient for our system

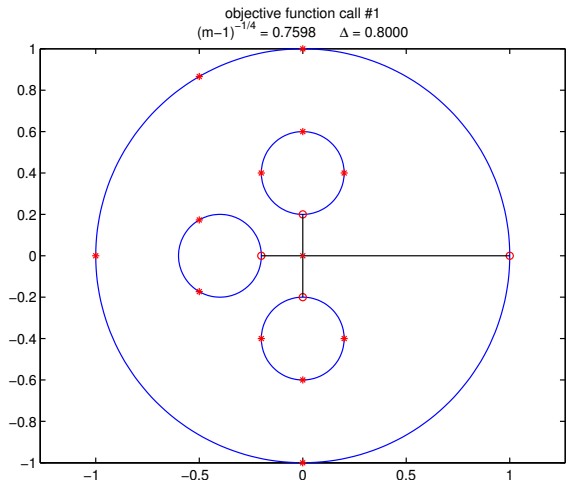

Figure 3.2: Initial guess for Figure 3.1 used with the nonlinear solvers in Table 3.1.

of equations, we tried the `fminunc` function with the BFGS quasi-Newton algorithm only. Finally `fminsearch` was tried which uses the Nelder-Mead simplex algorithm. Results of these comparisons are shown in Table 3.1; the infinity norm of the objective function (the system of equations for the parameter problem) and the time in seconds each solver took to find this solution are shown.[1] Note that `fminunc` and `fminsearch` were not tried with connectivity above $m = 3$, since these functions failed to find a solution in the simplest case.

There is also the question of the sensitivity of the MATLAB solvers to the initial guess. As a first attempt to address this question, we make the initial guess shown in Figure 3.3 to solve the problem shown in in Figure 3.1. Numerical continuation handled this new initial guess with no problem, but only the the Levenberg-Marquardt algorithm as used in `fsolve` and `lsqnonlin` was able to find a solution; all other attempts failed. The successful results are shown in Table 3.2.

Interestingly, a slight change in the previous poor initial guess, see Figure 3.4, results in a starting point at which the Levenberg-Marquardt algorithm fails for both `fsolve` and `lsqnonlin`. However using the 'trust-region-reflect' algorithm in either of these functions allows finding a solution; see Table 3.3.

[1] The solution time is obviously machine-dependent and is only given here for a sense of the relative speed of each algorithm.

Table 3.1: Different nonlinear solvers with an initial guess which was not near the solution. The last two solvers in this table were not successful for $m = 3$, and thus were not used for higher values of m. The infinity norm of the objective function and the time in seconds each solver took to find this solution are shown. Only the Figure 3.1 for $m = 4$ is shown. The other domains just add or delete an inner polygon. Note the increase in timings with m.

	$m = 3$		$m = 4$		$m = 5$	
Solver	$\|F\|_\infty$	secs	$\|F\|_\infty$	secs	$\|F\|_\infty$	secs
continuation	2.88×10^{-15}	12.74	4.30×10^{-15}	42.63	3.85×10^{-15}	153.97
fsolve (t-r-d)	2.32×10^{-10}	12.07	2.49×10^{-10}	57.98	4.63×10^{-12}	278.89
fsolve (t-r-r)	1.00×10^{-09}	12.05	2.70×10^{-14}	57.55	4.60×10^{-14}	443.19
fsolve (l-m)	4.73×10^{-15}	14.06	2.53×10^{-14}	58.10	4.32×10^{-15}	274.27
lsqnonlin (t-r-r)	1.00×10^{-09}	11.84	2.70×10^{-14}	57.36	4.60×10^{-14}	443.44
lsqnonlin (l-m)	4.73×10^{-15}	14.21	2.53×10^{-14}	57.53	4.32×10^{-15}	273.25
fminunc	3.32×10^{-2}	242.55	-	-	-	-
fminsearch	1.58×10^{-1}	266.55	-	-	-	-

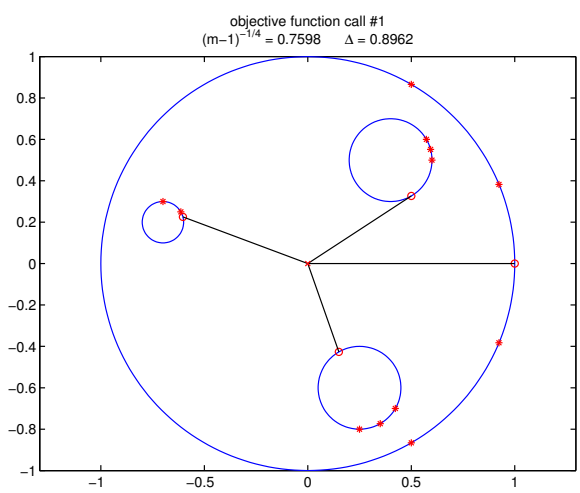

Figure 3.3: A poor initial guess.

Table 3.2: A comparison of the nonlinear solvers which were able to find the map parameters for Figure 3.1, given the initial guess in Figure 3.3.

Solver	$\|F\|_\infty$	secs
continuation	8.160×10^{-15}	135.710
fsolve (l-m)	5.329×10^{-15}	170.573
lsqnonlin (l-m)	5.329×10^{-15}	165.974

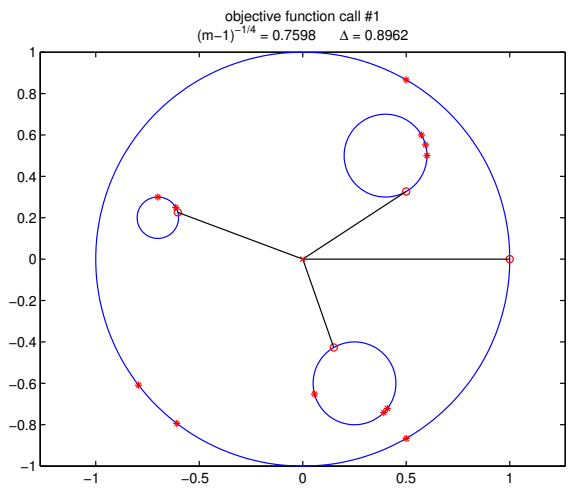

Figure 3.4: A slightly modified, but still poor initial guess.

Table 3.3: A comparison of the nonlinear solvers which were able to find the map parameters for Figure 3.1, given the initial guess in Figure 3.4.

Solver	$\|F\|_\infty$	secs
continuation	8.049×10^{-15}	121.571
fsolve (t-r-r)	3.220×10^{-11}	171.911
lsqnonlin (t-r-r)	3.220×10^{-11}	172.406

3.4 Quadrature

Fast and accurate numerical quadrature is required in order to evaluate the MCSC integrals (2.13) and (2.16). Gauss-Jacobi quadrature, used in [21, 22], is well suited to the evaluation of integrals of the form

$$\int_{-1}^{1} f(t)(1-t)^{\beta}(1+t)^{\gamma}$$

where $f(t)$ is smooth on the interval. The algorithm by Golub and Welsh [25], taken from SC-Toolbox [21], is used to calculate the zeros of the Jacobi polynomials, giving the quadrature weights and nodes.

The Gauss-Jacobi quadrature works well for singularities at the endpoints of integration, but it is also possible that an integration path will be near other singularities of the map. To take care of inaccuracies in the map induced by nearby singularities, we implement compound quadrature with the one-half rule as described in [22, 36], that is,

> **The one-half rule:** No singularity may lie closer to an integration sub-interval than one-half the length of that sub-interval. [22]

The only nearby singularities in the simply connected case were other prevertices. The reflections of prevertices must also be considered in the multiply connected case. This does not change the statement of the one-half rule, only its implementation.

3.5 Integration paths for positioning

In Section 3.1 it was mentioned that the geometric conditions driving the system of equations for the parameter problem was not unique. The discussion in this section, closely following that of [20], gives some examples of this.

As originally formulated, the system of nonlinear equations used to solve the parameter problem relies on integrating from the prevertex $z_{1,1}$ to $z_{1,j}$ for $1 < j \leq m$ to position polygons Γ_2 through Γ_m. If care is not taken this can lead to the difficulties shown in Figure 3.5. There the integration path used to fix polygon position passes too near the

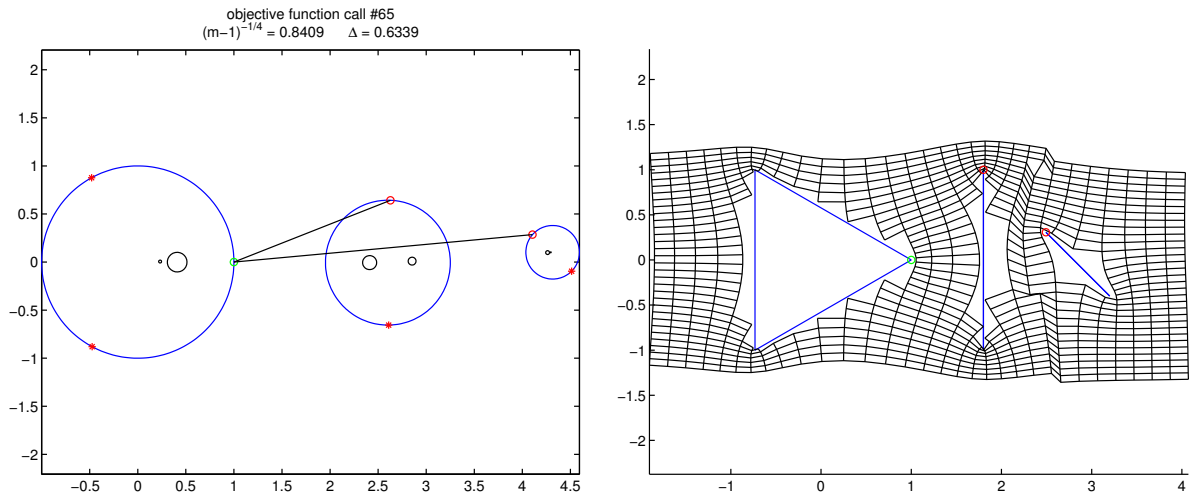

Figure 3.5: By anchoring polygons 2 and 3 to $z_{1,1}$, we create an integration path that passes too close to singularities (reflections of the centers) of the SC product. The resulting grid fails to be orthogonal in some places.

singularities of the Schwarz-Christoffel product—in this case, the reflections of the centers. This problem can be avoided by careful rearrangement of the order of the polygons and the prevertices or by a change of the equations which dictate this positioning. In the current example, we keep the triangle as Γ_1 and change the equation which positions the third polygon (the slit on the right) from

$$f(z_{1,3}) - f(z_{1,1}) = w_{1,3} - w_{1,1} \quad \text{to} \quad f(z_{1,3}) - f(z_{1,2}) = w_{1,3} - w_{1,2},$$

using the position of Γ_2 to dictate that of Γ_3. This result is shown in Figure 3.6.

Table 3.4: Map parameters found for cases shown in Figures 3.5 and 3.6. It should be noted that continuation was successful in the first case, *i.e.*, the algorithm converged but evidently not to a solution to the parameter problem.

Figure	c_2	r_2	c_3	r_3
3.5	2.6015 - 0.0061i	0.6492	4.3150 + 0.1017i	0.2784
3.6	2.6042 - 0.0064i	0.6512	4.2119 - 0.0286i	0.2732

The polygons in Figure 3.7 provide an illustration of a case in which rearranging

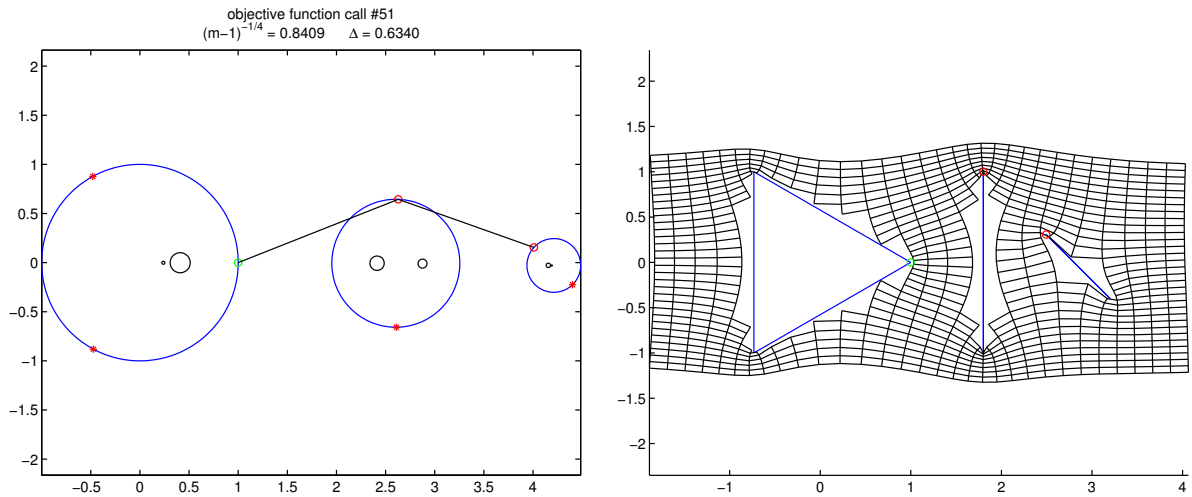

Figure 3.6: The order of the polygons is as in the first example, but for positioning we integrate first from $z_{1,1}$ to $z_{1,2}$ and then from $z_{1,2}$ to $z_{1,3}$.

the order of the polygons and vertices is not likely to produce an integration path which is completely external to the figures and thus does not come near to possible singularities. For instance, the path from $z_{1,1}$ and $z_{1,4}$ would pass inside of C_1 (Γ_4 is the figure in the upper-left corner). In this case, we integrate from $z_{3,1}$ to $z_{1,4}$ instead and the equations which fix the polygon positions are

$$f(z_{1,2}) - f(z_{4,1}) = w_{1,2} - w_{4,1},$$

$$f(z_{1,3}) - f(z_{1,1}) = w_{1,3} - w_{1,1},$$

and

$$f(z_{1,4}) - f(z_{3,1}) = w_{1,4} - w_{3,1}.$$

The requirement that the integration path for positioning be to the first vertex of the polygon being positioned is imposed by the constrained-unconstrained transformation, equations (3.4) and (3.5); recall that the transformation relies on knowledge of the angle of the first prevertex on a circle to recover the remaining angles. This could likely be changed, but the definition of the first vertex on each polygon is flexible which effectively removes this concern. As an

extension of the previous example, we add a fifth polygon; see Figure 3.8. The addition to the positioning equations above is

$$f(z_{1,5}) - f(z_{3,2}) = w_{1,5} - w_{3,2}.$$

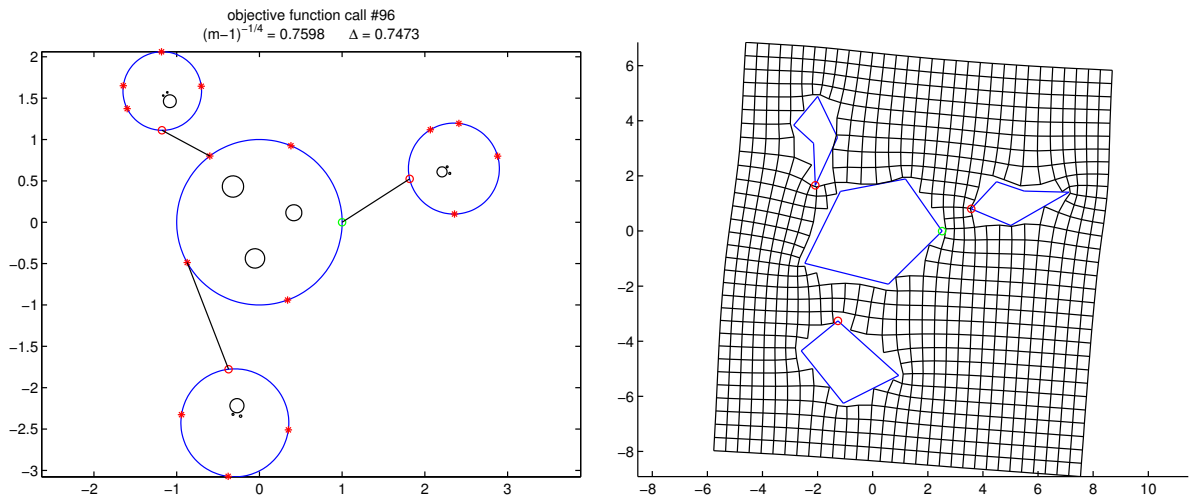

Figure 3.7: Integration paths for positioning only need connect the first prevertex on the target polygon with another known prevertex, *i.e.*, from $z_{3,1}$ to $z_{1,4}$. Note the center polygon is Γ_1 with the others, counter-clockwise from the bottom, being Γ_2, Γ_3, and Γ_4.

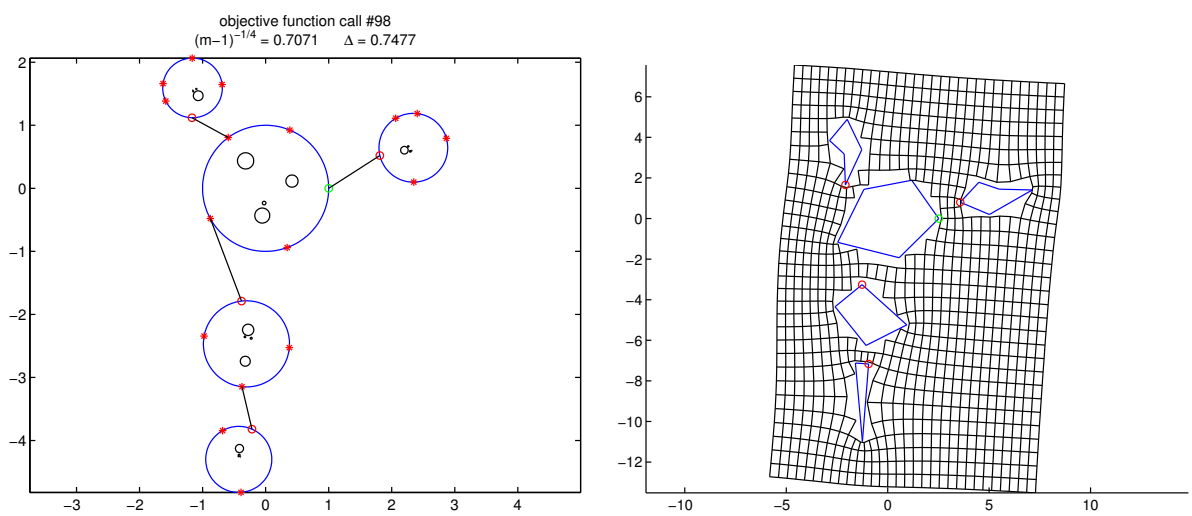

Figure 3.8: Integrating from the first polygon and between polygons may also be combined.

This change to the system of equations for positioning polygons holds for the bounded

case as well. In Figure 3.9 we surround a previous example with a rectangular boundary. The system of equations to position the polygons in this case is

$$f(z_{1,1}) - f(z_0) = w_{1,1} - w_0,$$

$$f(z_{1,2}) - f(z_0) = w_{1,2} - w_0,$$

$$f(z_{1,3}) - f(z_{4,2}) = w_{1,3} - w_{4,2},$$

$$f(z_{1,4}) - f(z_0) = w_{1,4} - w_0,$$

and

$$f(z_{1,5}) - f(z_{3,2}) = w_{1,5} - w_{3,2}.$$

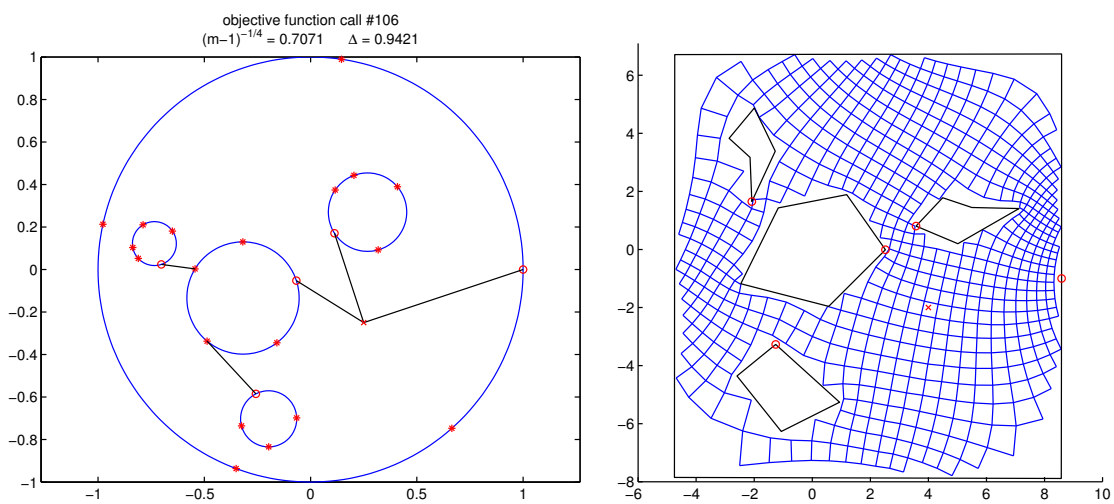

Figure 3.9: A choice of integration paths for positioning in the bounded case. (Γ_2 is the largest inner polygon.)

Note that the map normalization serves as the polygon positioning anchor in both the bounded and unbounded cases. The requirement that $f(z) = A + Bz + O(1/z)$ for $z \to \infty$ in the unbounded domain makes the prevertex $z_{1,1}$ an anchor point. In the bounded domain the requirement that $f(z_0) = w_0$ makes z_0 an anchor. Rewriting the positioning equations requires attention to this condition, as any positioning equation which does not directly or

indirectly make use of this information will result in a system for which, in our experience, a search algorithm will fail to find a valid set of map parameters.

3.6 Error model based on reflected radii

An idea of the error in the mapping function is of importance. The sum of the reflected radii $\sum r_{\nu j}$ of the reflected circles at some level of reflection n, as given in the proof of Lemma 2.14 in the unbounded case or equation 2.18 in the bounded case, gives a useful estimate. Note that the radii $r_{\nu j}$ for the reflected circles can be computed by the reflection routine (see Algorithm A.1 on page 98) and, therefore, provide a built-in method for estimating truncation error provided the reflection formula is used in the calculation of the map.

The errors in the (constrained) parameters (centers, radii, and prevertex angles $\theta_{k,j}$ at the Nth level of reflection are denoted by a vector X_N) are measured by $\|X_N - X_{N-1}\|_\infty$. Given a constant c and a level of reflection N, the estimate $e^{-c}\sum r_{\nu j}$ fits the data very well. This error estimate is first illustrated with the exterior map to three symmetric radial slits displayed in Figure 3.10. The errors and error estimates are given in Figure 3.11. The values for the constant c used in Figures 3.11 and 3.12 were calculated by

$$c = \log\left(\sum_{j=1}^{m}\sum_{\nu\in\sigma_3(j)} r_{\nu j}\right) - \log\left(\|X_3 - X_2\|\right),$$

where $N = 3$ represents the lowest level of reflections shown. The radial slit maps used in this example can also be computed "exactly" by infinite product formulas discussed in Section 2.2.1, and comparisons of the Schwarz-Christoffel map with that of equation (2.5) yield nearly identical errors. Figure 3.13 displays the error and the estimate for the polygonal domain given in Figure 3.12.

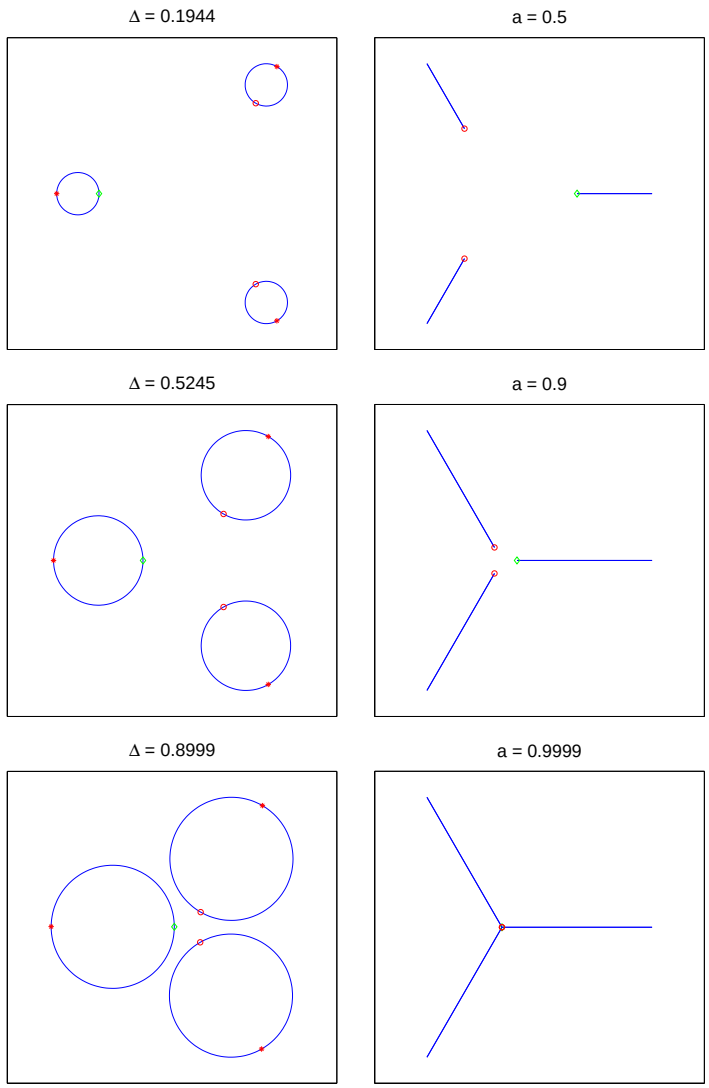

Figure 3.10: Geometry used to test the error estimate based on the sum of the reflected radii.

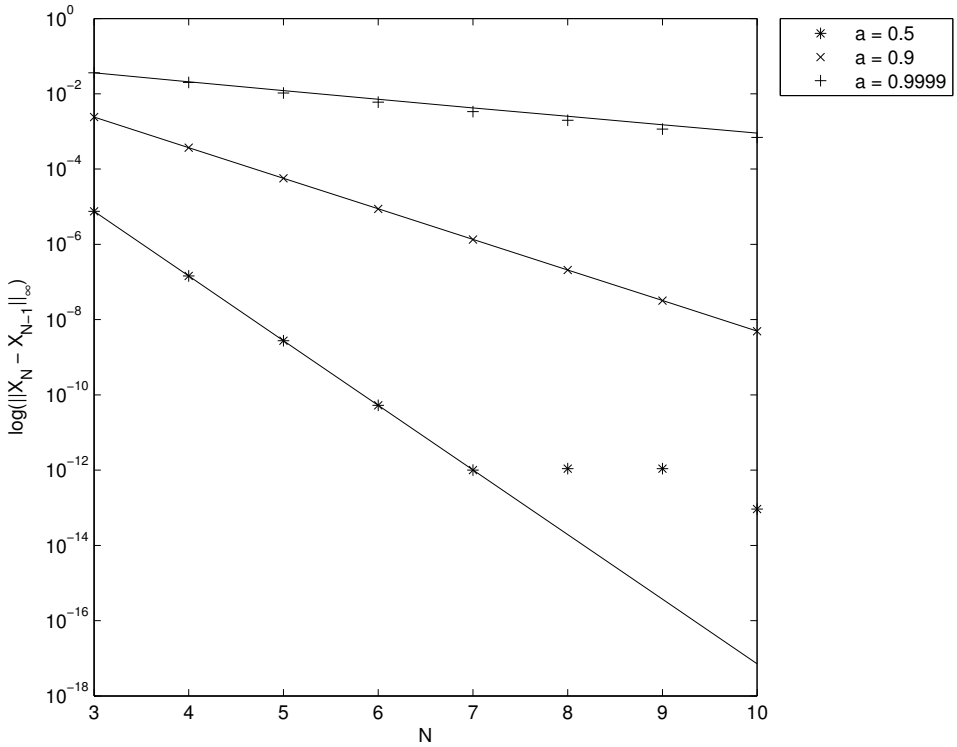

Figure 3.11: The log of error vs. levels of reflection N for three examples of maps to the exterior of three symmetric slits, Figure 3.10. The solid line fits to the log of the errors are $\log\left(\sum r_{\nu j}\right) - c$, where $c = 0.45, 0.64, 1.26$, respectively. Note that the case $a = 0.9999$ violates the separation condition, since $\Delta = 0.8999 > (m-1)^{-1/4} = 2^{-1/4} \approx 0.8409$, and the errors nonetheless decrease, though quite slowly, as one would expect. The errors for the case $a = .5$ level off at about 10^{-12} due to the tolerance setting in the continuation algorithm, which is set here at 10^{-15}, it's smallest feasible setting.

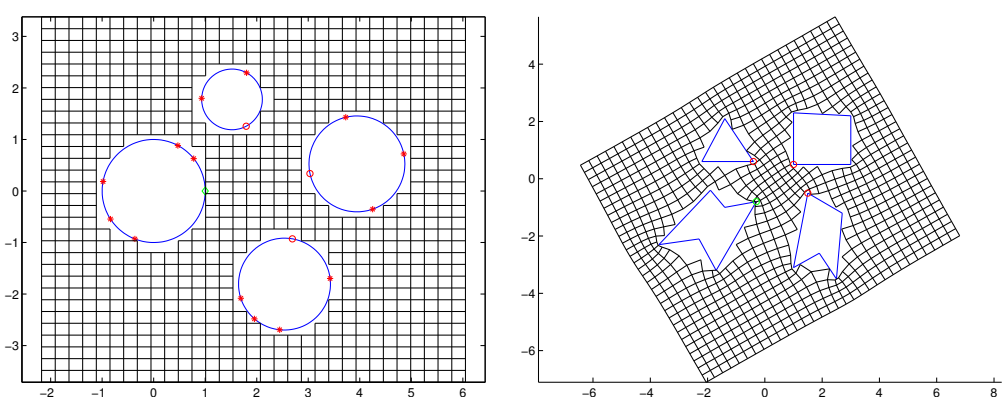

Figure 3.12: An example map to the exterior of 4 polygons used in the graph of the error estimate, Figure 3.13.

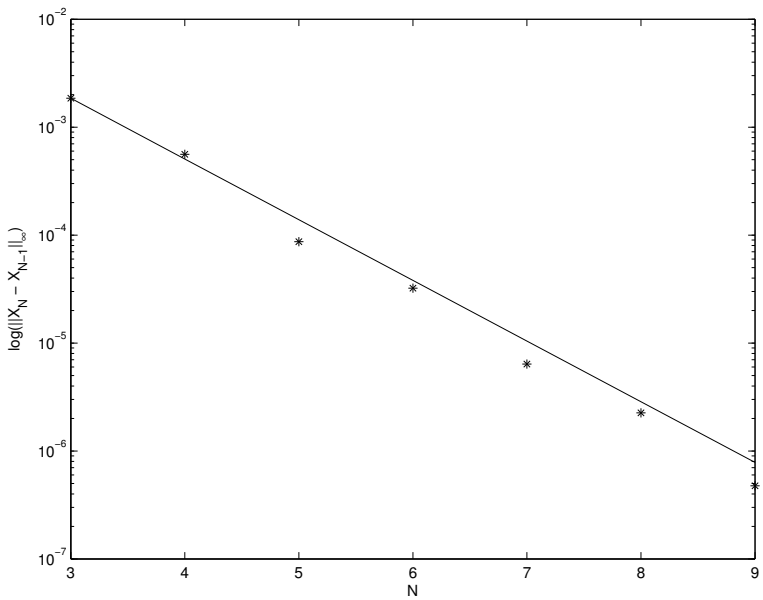

Figure 3.13: Error for Figure 3.12 fit with $\log \sum r_{\nu i} - c$.

3.7 Apparent accuracy

Although sums of the reflected radii give a useful estimate of the error in the MCSC maps, the method in Chapter 4 does not use reflections to calculate these maps. An estimate of the accuracy of the map, inspired by [21], is therefore given. In essence, the images of the prevertices from the solution process are calculated using the appropriate formulas, and this result is compared with known vertex values. The largest deviation from known values is then called the accuracy error, E_{acc}, or apparent (vertex) accuracy. That is,

$$E_{acc} = \max_{j,k} \left| \left(A \int_{z_{k,j}}^{z_{k+1,j}} p(z)\, dz + w_{k,j} \right) - w_{k+1,j} \right|,$$

where $p(z)$ represents equation (3.1) or equation (3.2) as appropriate. The integration path should be through the domain and away from the boundaries. In the simply connected circle map a similar calculation is done [21], but the integration path is simply a line from one prevertex to the origin, and then from the origin to the other prevertex. In the multiply connected case there is no convenient single point through which to integrate each of these (one might integrate through a singularity).

A simple solution to this consists of expanding the radius of each circle (or reducing the radius of the outer circle in the bounded case) by adding (subtracting) one-half the distance to the closest circle. The integration path is then outward (inward) radially from a prevertex on the boundary to the associated point on the expanded (reduced) circle, along the arc of the expanded (reduced) circle to the point associated with the next prevertex, and then radially inward (outward) from the associated point, to the prevertex on the boundary. In other words let c_j, r_j, $z_{k,j}$ and $z_{k+1,j}$ be the center and radius and two prevertices of a circle in question with $\theta_{k,j}$ and $\theta_{k+1,j}$ the angle of the prevertices. Set

$$\tilde{r}_j = r_j \pm \frac{1}{2} \min_{p \neq j} \{ |c_j - c_p| - r_j - r_p \} \quad \text{for} \quad j, p \in \{1, \ldots . m\}.$$

Now set $\tilde{z}_{k,j} = c_j + \tilde{r}_j e^{i\theta_{k,j}}$ and $\tilde{z}_{k+1,j} = c_j + \tilde{r}_j e^{i\theta_{k+1,j}}$. Compute

$$\int_{z_{k,j}}^{z_{k+1,j}} p(z)\, dz = \left(\int_{z_{k,j}}^{\tilde{z}_{k,j}} p(z)\, dz + \int_{\tilde{z}_{k,j}}^{\tilde{z}_{k+1,j}} p(z)\, dz + \int_{\tilde{z}_{k+1,j}}^{z_{k+1,j}} p(z)\, dz \right)$$

where on the right-hand side of the equation, the first and last integrals are along radial lines, and the middle integral is along the arc of the expanded (reduced) circle.

Note that even though one-half the distance between the closest circles is used, the method described here is not the one-half rule for compound quadrature mentioned in Section 3.4.

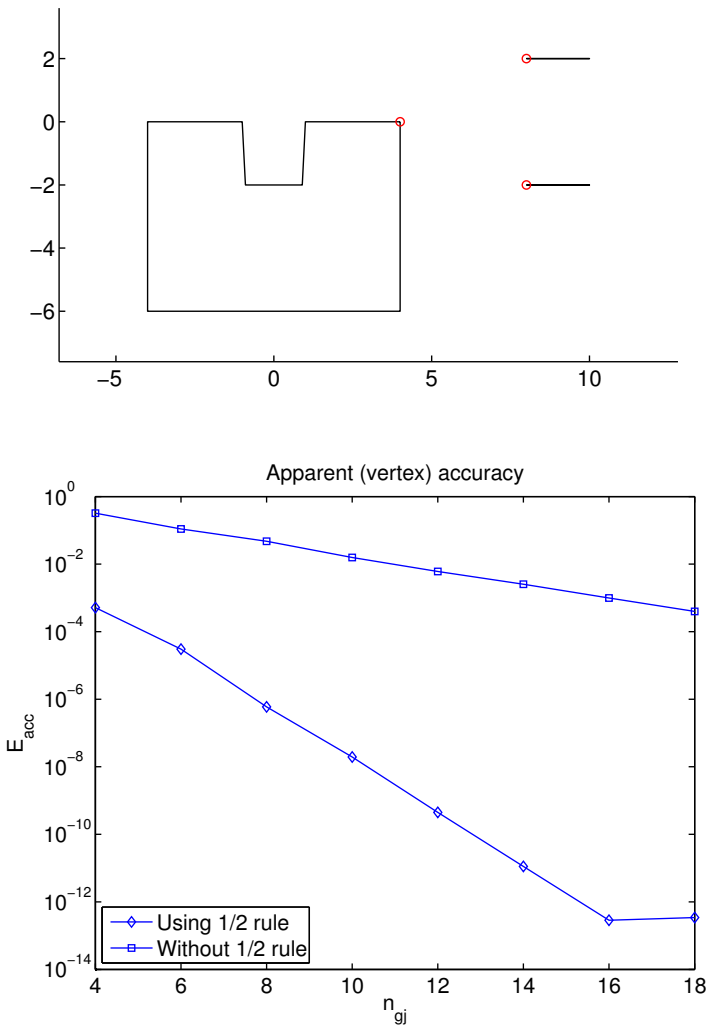

Figure 3.14: Apparent (vertex) accuracy E_{acc} as a function of the number of quadrature points n_{gj}, along with the geometry used to test this. The test was done both with and without the one-half rule for compound quadrature. The truncation level N for the map was held constant while n_{gj} was varied.

Figure 3.14 gives the relationship between E_{acc} and n_{gj}, the number of quadrature

points in each compound integration interval, for the geometry shown. The re-entrant corners on the polygon were chosen to create singularities in equation (2.13) to ensure the one-half rule for compound quadrature is necessary for accurate computation; the slits were chosen to ensure the separation condition, $\Delta < (m-1)^{-1/4}$, was satisfied.

3.8 Inverted slit maps for grid generation

An orthogonal grid under a conformal transformation is of course still an orthogonal grid. While not always necessary the images of these orthogonal grids can assist in visually understanding the conformal transformation in question. The selection of the appropriate grid depends on the problem at hand. This Section discusses the orthogonal grids chosen for the MCSC maps in this work and, briefly, their method of computation.

In early versions of the MCSC numerical work, rectangular grids of dots were chosen in the circle domain, and these dots were simply put through the calculated map and plotted in the polygonal domain, often with lines drawn to emphasize the grid. See Figure 3.12 on page 44 for an example. These grids were unfortunately only a very crude representation of the preservation of angles, although they were very easy to compute.

Conceptually, given a circle domain, an easy grid could be given by taking concentric circles and radial lines from a conformally equivalent circular, radial, or combined circular and radial slit domain and mapping these onto the circle domain. It is only a small difficulty that we have the maps from the circle to the slit domain, but not their inverses. It is possible to use a Newton iteration to calculate the inverse of such maps, since the calculation of their derivatives is not complicated. For example the derivative of the log of the unbounded map to a slit radial domain, given by equation (2.7), is

$$\frac{d}{dz}\left(\log f(z)\right) = \frac{f'(z)}{f(z)} = \frac{1}{z-a} + \sum_{j=1}^{m} \sum_{\substack{n=0 \\ \nu\in\sigma_n(j)}}^{\infty} \left(\frac{1}{z-a_{\nu j}} - \frac{1}{z-s_{\nu j}}\right)$$

so that multiplication by f gives f'. Adapting the idea given in [22], the following strategy is used to invert the map. The point $a \in \mathbb{D}$ such that $f(a) = 0$ is given, so this is used as the starting point for inversion. The radial lines starting at the origin are treated first;

a rough estimate of the preimage of the points next to the origin are given by solving the initial value problem

$$\frac{dw}{dz} = \frac{1}{f'(z)} \quad \text{with} \quad f^{-1}(0) = a$$

by one of MATLAB's built in ODE solvers. The result of this is used as the initial guess for Newton's method to find the preimage points to a desired accuracy. Once the first set of points has been inverted, these points are used as the initial guess to Newton's method to find the next set of points along the radial lines. Each complete set of points is then used as the initial guess for the next round of iterations to find the next set of points until the radial lines are complete. One of the radial lines is then selected to determine the initial guess for inverting points along the circular lines; again Newton's method and adjacent points are used to complete the circular grid line preimages.

The difficulty in this method comes when a grid line must cross a slit, since the preimage of a grid line in the circle domain will have to jump a circle, so to speak. This can be overcome once the prevertices of the slit tips are known, which can be found by noting that the radial slit tips occur at the maximum and minimum of $|f(C_j)|$ for circles which map to radial slits, and the circular slit tips occur at the maximum and minimum of $\arg f(C_j)$ for the circles which map to circular slits. The derivatives of these functions along the slits with respect to the angle around the preimage circle change sign on either side of the slit tips, and so a simple bisection method may be employed. It is then noted that the preimage of a grid line will meet a circle boundary at an angle on the circle with respect to one of the slit tip preimages; the corresponding angle on the other side of the tip preimage is then used as an initial guess to an ODE solver, whose result is then put into the Newton iteration to continue inverting the grid line.

At the time of this writing, only the code for inverting lines from a radial slit domain is complete, but there are no foreseen difficulties with extending this to the circular and mixed circular and radial slit domains. See Figure 2.8 on page 20 and Figure 2.10 on page 23 for examples of this grid.

Two other types of canonical domain used for orthogonal grid generation are applied in Chapter 5. The first is the slit rectangular domain: Once the bounded circle domain $\mathbb{D}$ for a given bounded polygonal domain $\mathbb{P}$ is determined, a modified parameter problem is used to find a conformally equivalent rectangular domain with four marked arcs on the outer boundary of the circle going to the four sides of a rectangle and the interior circles going to horizontal slits. A rectangular grid is then imposed on this rectangular domain, and then inverted to the circle domain in a fashion similar to that of the slit domains above. Again the inverse of the map is calculated using a Newton iteration, and the derivative of the map used is simply the integrand of the bounded MCSC formula. See Figures 5.1 and 5.2 on pages 83 and 84 for examples.

The last type is the slit annular domain as given in Section 2.2.2. Here the grid is a polar grid as in the slit domains above with the exception of the spacing of the circular grid lines which use a log-linear spacing. The points which make the radial grid lines are not linearly spaced but log-linearly spaced from the inner ring to the outer. Were this log-linear spacing not implemented, the grid lines would be clustered around the circle which maps to the outer ring of the annulus. See Figures 5.5 and 5.6 on pages 87 and 89 for examples.

CHAPTER 4

MAPS BY LAURENT SERIES

The maps in this Chapter take a selection of those presented in Chapter 2 and evaluate all or parts of the infinite product expressions using truncated Laurent series. Coefficients of the series are found by solving a linear system of equations derived from the boundary conditions of the given map. The linear systems are then solved numerically in the least squares sense. It is shown this method is much more efficient than the reflection method.

4.1 Slit maps

This section concerns a method of computation for unbounded and bounded radial, circular, and mixed radial and circular slit maps given by equation (2.11) which bypasses the use of the reflection formula. A linear system for the Laurent coefficients is derived from the boundary conditions of the map. The map from the bounded circle domain to a radial slit half-plane (see equation (2.12)) is similarly treated. We will continue to use $\mathbb{D}$ to denote the m-connected circle domain with $\partial\mathbb{D} = \bigcup_{j=1}^{m} C_j$ and $\mathbb{P}$ to denote the conformally equivalent slit domain with $\partial\mathbb{P} = \bigcup_{j=1}^{m} \Gamma_j$.

4.1.1 Unbounded case

Let $f(z)$ be the mixed slit map such that $f(a) = 0$ and $f(z) = O(z)$ as $z \to \infty$, and start by noticing that the argument of $f(C_j)$ is constant if f maps C_j to a radial slit, and the modulus of $f(C_j)$ is constant if f maps C_j to a circular slit. That is,

$$\operatorname{Im}\{\log f(z)\} = \text{const.}, \quad \text{for } z \in C_j \text{ where } \Gamma_j \text{ is a radial slit, and} \tag{4.1}$$

$$\operatorname{Re}\{\log f(z)\} = \text{const.}, \quad \text{for } z \in C_j \text{ where } \Gamma_j \text{ is a circular slit.} \tag{4.2}$$

Write $f(z) = (z-a)e^{g(z)}$, where $g(z)$ is analytic in $\mathbb{D}$ and $g(z) = O(1/z)$ as $z \to \infty$ and is given by a sum of Laurent series expansions around the centers of the C_j,

$$g(z) = \sum_{j=1}^{m} \sum_{n=1}^{\infty} \frac{d_{n,j} r_j^n}{(z-c_j)^n} \tag{4.3}$$

(the r_j^n are factored out of the coefficients for numerical stability). This gives $\log f(z) = \log(z-a) + g(z)$, and the boundary conditions in terms of $g(z)$ become

$$\operatorname{Im}\{g(z)\} = \text{const.} - \arg(z-a), \quad \text{for } z \in C_j \to \text{ radial slit, and} \tag{4.4}$$

$$\operatorname{Re}\{g(z)\} = \text{const.} - \log|z-a|, \quad \text{for } z \in C_j \to \text{ circular slit.} \tag{4.5}$$

Discretize by limiting the Laurent expansion around each circle to N terms, and select M collocation points z on each C_j. Define the column vector $x = [d_{n,j}]_{mN\times 1}$ and the matrix

$$F_j = \left[r_j^n (z-c_j)^{-n}\right]_{M\times mN}, \quad \text{for } z \in C_j, \tag{4.6}$$

where the rows are determined by the collocation points and the columns by the terms in g. Writing $x = x_R + ix_I$ and $F = F_{R_j} + iF_{I_j}$ gives the approximations

$$\operatorname{Re}\{g(z)\} \approx F_{R_j}x_R - F_{I_j}x_I \quad \text{and} \quad \operatorname{Im}\{g(z)\} \approx F_{I_j}x_R + F_{R_j}x_I.$$

as appropriate for $z \in C_j$. Define the larger matrix

$$A = \begin{bmatrix} A_1 \\ \vdots \\ A_m \end{bmatrix}_{mM\times 2mN} \quad \text{where} \quad A_j = \begin{cases} \begin{bmatrix} F_{I_j} & F_{R_j} \end{bmatrix}_{M\times 2mN}, & C_j \to \text{ radial slit} \\ \begin{bmatrix} F_{R_j} & -F_{I_j} \end{bmatrix}_{M\times 2mN}, & C_j \to \text{ circular slit.} \end{cases}$$

Note that the pairwise difference of $\operatorname{Im}\{\log f\}$ and $\operatorname{Re}\{\log f\}$ for points on any C_j are zero, so define the matrices

$$P = \begin{bmatrix} -1 & 1 & & & \\ & -1 & 1 & & \\ & & \ddots & \ddots & \\ & & & -1 & 1 \end{bmatrix}_{(M-1)\times M} \quad \text{and} \quad E = \begin{bmatrix} P & & & \\ & P & & \\ & & \ddots & \\ & & & P \end{bmatrix}_{m(M-1)\times mM},$$

and set

$$y = \begin{bmatrix} y_1 \\ \vdots \\ y_m \end{bmatrix}_{mM\times 1} \quad \text{where} \quad y_j = \begin{cases} [-\arg(z-a)]_{M\times 1}, & z \in C_j \to \text{ radial slit} \\ [-\log|z-a|]_{M\times 1}, & z \in C_j \to \text{ circular slit.} \end{cases}$$

This gives at last the linear system

$$EA \begin{bmatrix} x_R \\ x_I \end{bmatrix} = Ey, \tag{4.7}$$

whose solution in the least squares sense using the MATLAB backslash operator gives the coefficients of g. The system given by equation (4.7) can be made square if $M = 2N$, but it was found in all experimental cases that the overdetermined system, given when $M = 2N+1$, has a smaller condition number, and so the overdetermined system is used in practice.

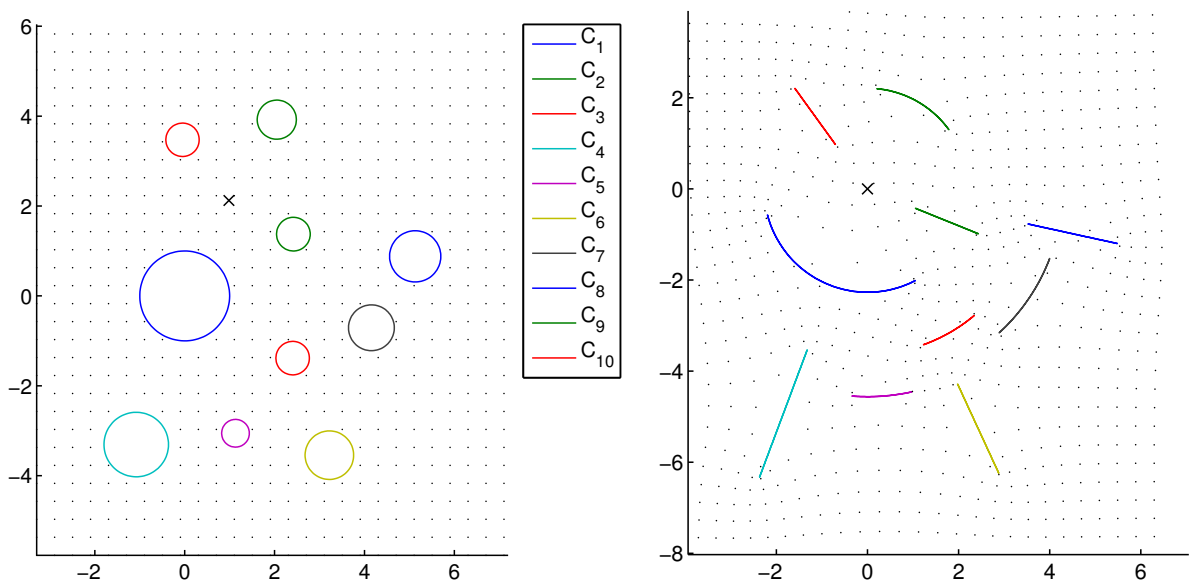

Figure 4.1: An example of the unbounded combined radial and circular slit map with $m = 10$ and $N = 25$.

Remark 4.1. It is also possible to state boundary conditions using the derivatives of equations (4.1) and (4.2) with respect to the argument of z on each C_j parametrized by $z = c_j + r_j e^{i\theta}$, that is

$$\frac{\partial}{\partial\theta} \operatorname{Im}\{\log f(z)\} = \operatorname{Re}\left\{\frac{z - c_j}{z - a} + (z - c_j)g'(z)\right\} = 0, \quad z \in C_j \to \text{ radial slit}$$
$$\frac{\partial}{\partial\theta} \operatorname{Re}\{\log f(z)\} = -\operatorname{Im}\left\{\frac{z - c_j}{z - a} + (z - c_j)g'(z)\right\} = 0, \quad z \in C_j \to \text{ circular slit.}$$

Note these conditions are exactly those used in the proofs of Theorems 2.7 and 2.10. The condition for the radial slit was stated in this work as Lemma 2.8; the condition for the circular slit follows a similar calculation and was not stated here, but is given in [15]. Rearranging the terms in the above conditions leads to

$$\operatorname{Re}\{(z-c_j)g'(z)\} = -\operatorname{Re}\left\{\frac{z-c_j}{z-a}\right\}, \quad z \in C_j \to \text{ radial slit} \tag{4.8}$$

$$\operatorname{Im}\{(z-c_j)g'(z)\} = -\operatorname{Im}\left\{\frac{z-c_j}{z-a}\right\}, \quad z \in C_j \to \text{ circular slit.} \tag{4.9}$$

These boundary conditions, now in terms of g' instead of g, give a linear system which does not need the difference matrix E. Numerically, the condition number of the matrix based on equations (4.8) and (4.9) for an overdetermined system is slightly larger than that of the condition number for the matrix an overdetermined system based on equations (4.1) and (4.2). Although the system given by equations (4.1) and (4.2) involves a matrix-matrix multiplication, the matrix E is sparse, and taking advantage of this results in little increase in computation time over that of the method given by equations (4.8) and (4.9).

4.1.2 Bounded case

Combined slit map

The reflection formula for the bounded mixed radial and circular slit map is the same as the unbounded case, equation (2.11). It makes sense then to use the same boundary condition linearization as in the unbounded case. The map is written

$$f(z) = (z-a)e^{g(z)}$$

as above, but in the bounded case we have

$$g(z) := \sum_{n=1}^{\infty} d_{n,1} z^n + \sum_{j=2}^{m} \sum_{n=1}^{\infty} \frac{d_{n,j} r_j^n}{(z-c_j)^n},$$

the Taylor expansion inside C_1 and Laurent series expansions external to $C_2, \ldots, C_j$. The boundary conditions (4.1) and (4.2) are applied with the exception that C_1 always maps to a circle (its image will have constant modulus). The result is shown in Figure 4.2.

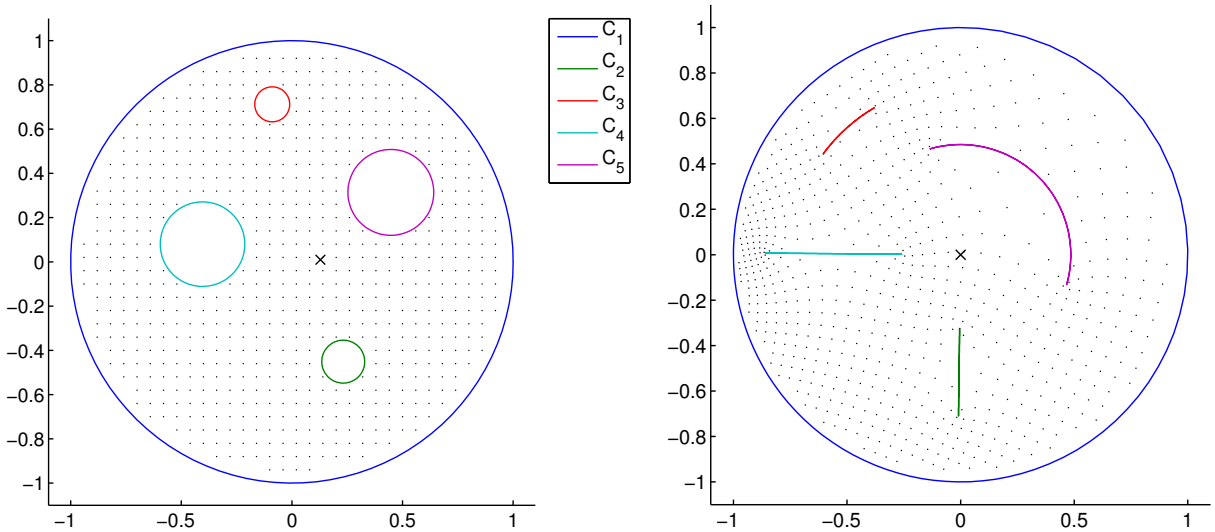

Figure 4.2: An example of the bounded combined radial and circular slit map with $m = 5$ and $N = 25$.

Half-plane radial slit map

As in the case of the mixed slit maps, we consider the approximation of the log of the reflection map, equation (2.12), that is

$$\log f(z) = \log(z - b) - \log(z - a) + g(z) \tag{4.10}$$

where $g(z)$ is analytic in $\mathbb{D}$ and given as the sum of the Taylor expansion inside the outer boundary with the Laurent expansions outside the inner boundaries,

$$g(z) = \sum_{n=1}^{\infty} d_{1,n} z^n + \sum_{j=2}^{m} \sum_{n=1}^{\infty} \frac{d_{j,n} r_j^n}{(z - c_j)^n},$$

and again the r_j^n are factored out of the $d_{j,n}$ for numerical stability. Every boundary component $C_j \in \partial\mathbb{D}$ maps to a boundary $\Gamma_j \in \partial\mathbb{P}$ with constant argument, and the boundary condition would simply be

$$\operatorname{Im}\{g(z)\} = \text{const.} - \arg \frac{z - b}{z - a} \quad \text{for } z \in C_j,\ j = 1, \ldots, m, \tag{4.11}$$

but recall that a and b are points on a circle $C_p \in \mathbb{D}$ such that $f(a) = \infty$ and $f(b) = 0$, and it is clear that there is a singularity at a. On circle C_p we then use the derivative of the

argument of f with respect to the angle on C_p, which gives the boundary conditions used in this map,

$$\operatorname{Im}\{g(z)\} = \text{const.} - \arg\frac{z-b}{z-a} \quad \text{for } z \in C_j,\ j = 1,\dots,m,\ j \neq p \tag{4.12}$$

$$\operatorname{Re}\{(z-c_p)g'(z)\} = 0 \quad \text{for } z \in C_p. \tag{4.13}$$

The implementation of the system of equations to find the coefficients for the Laurent expansion of g is similar to that of the MCSC factor maps described in Section 4.2.1 below, and will not be given here; see [19] for details. See Figure 4.3 for an example.

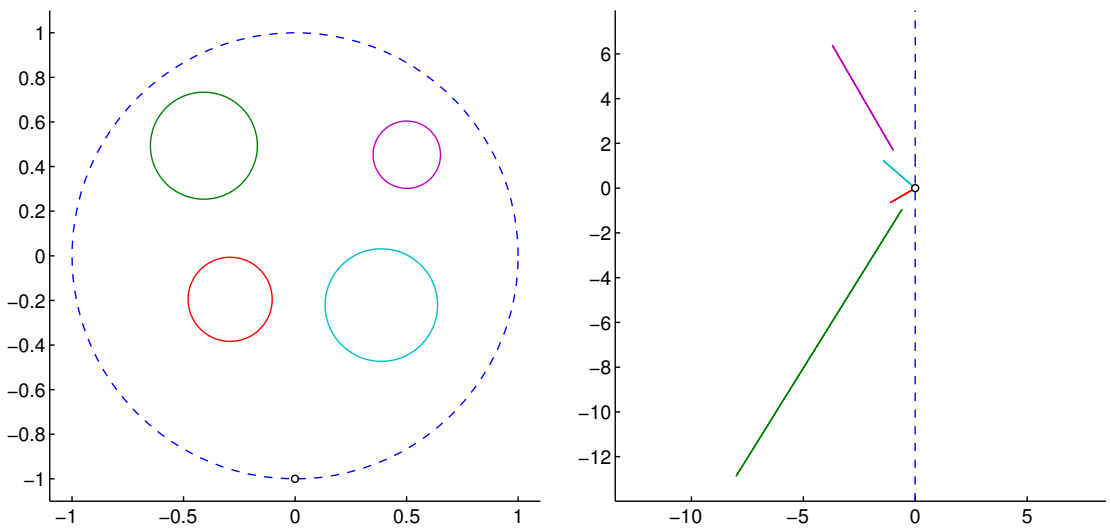

Figure 4.3: An example of a map to a radial slit half-plane using the Laurent approximation.

4.2 Unbounded Schwarz-Christoffel maps

Consider the inner infinite products for the unbounded Schwarz-Christoffel formula given in equation (2.13), which will be written here

$$f_{z_{k,j}}(z) := \prod_{\substack{n=0\\ \nu\in\sigma_n(j)}}^{\infty} \frac{z - z_{k,\nu j}}{z - s_{\nu j}}. \tag{4.14}$$

This means (2.13) can be viewed as

$$f(z) = A\int^{z} \prod_{j=1}^{m}\prod_{k=1}^{K_j} \left(f_{z_{k,j}}(\zeta)\right)^{\beta_{k,j}}\, d\zeta + B, \tag{4.15}$$

This finite product formula is more in line with the framework proposed in [22] where the factors ensure the derivative of the map is piecewise continuous on the boundary with given jumps at the corners.

Temporarily, for notational convenience, let a_j be any point on the boundary of $\mathbb{D}$, that is $a_j \in C_j$ for some $j = 1, \ldots, m$, so that we now consider

$$f_{a_j}(z) := \prod_{\substack{n=0 \\ \nu \in \sigma_n(j)}}^{\infty} \frac{z - a_{\nu j}}{z - s_{\nu j}}. \tag{4.16}$$

Note that $f_{a_j}(a_j) = 0$ and $f_{a_j}(\infty) = 1$. Numerical computation of this function using reflections shows that it maps boundary circles C_p, $p \neq j$, to radial slits with respect to the origin. These slits are contained in a region, the image of $\mathbb{D}$, which is bounded by the image of C_j, $f_{a_j}(C_j)$. It also appears that the image of $\mathbb{D}$, ignoring the radial slits, is star-like with respect to the origin. See Figures 4.4 and 4.5 for some examples of this map.

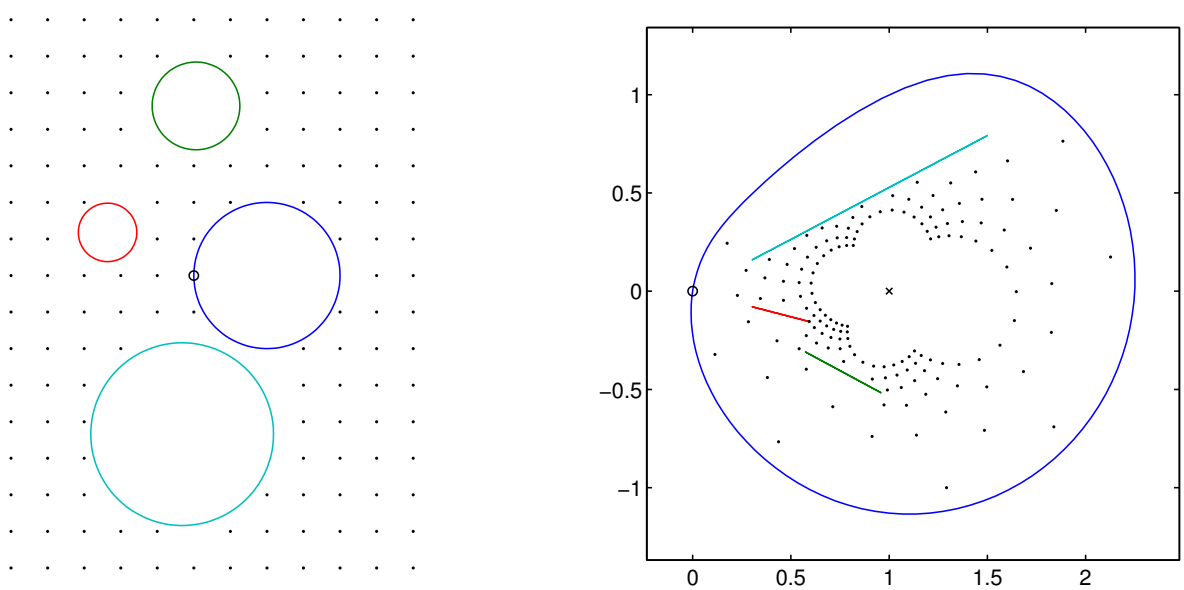

Figure 4.4: One example of the effect of f_{a_j} on $\mathbb{D}$ with connectivity $m = 4$ and $N = 5$ levels of reflection.

Under the assumption the boundary components C_p, $p \neq j$, map to radial slits, the following theorem may be given.

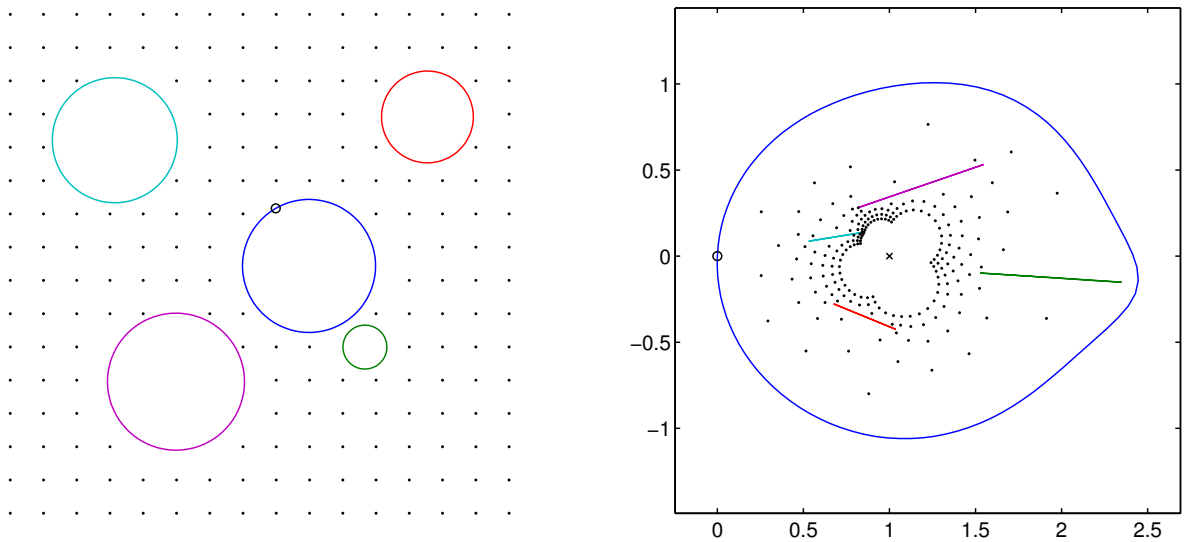

Figure 4.5: Another example of f_{a_j} with $m = 5$ at $N = 5$ levels of reflection.

Theorem 4.2. *The function f_{a_j} satisfies*

$$\arg f_{a_j}(z) = \text{const.} \quad \textit{for} \quad z \in C_p,\ p \neq j.$$

That is, f_{a_j} maps the circles C_p, $p \neq j$, to radial slits with respect to the origin if and only if

$$\operatorname{Re}\left\{(z - c_p)\frac{f'_{a_j}(z)}{f_{a_j}(z)}\right\} = 0 \quad \textit{for} \quad z \in C_p.$$

Proof. Consider the parametrization $z = c_p + r_p e^{i\theta}$. If f_{a_j} maps the C_p, $p \neq j$, to radial slits, then

$$0 = \frac{d}{d\theta}\arg f_{a_j} = \frac{d}{d\theta}\operatorname{Im}\left\{\log f_{a_j}\right\} = \operatorname{Im}\left\{ir_p e^{i\theta}\frac{f'_{a_j}}{f_{a_j}}\right\} = \operatorname{Re}\left\{r_p e^{i\theta}\frac{f'_{a_j}(c_p + r_p e^{i\theta})}{f_{a_j}(c_p + r_p e^{i\theta})}\right\}. \qquad \square$$

Define a singularity function $S_{a_j}(z)$ for $f_{a_j}(z)$ on $\mathbb{D}$ by

$$S_{a_j}(z) := \frac{f'_{a_j}(z)}{f_{a_j}(z)} = \frac{d}{dz}\log f_{a_j}(z) = \sum_{\substack{n=0 \\ \nu\in\sigma_n(j)}}^{\infty}\left(\frac{1}{z - a_{\nu j}} - \frac{1}{z - s_{\nu j}}\right). \tag{4.17}$$

This definition only makes sense if S_{a_j} is the uniform limit of a sequence of functions with derivatives on $\mathbb{D}$. As has been the theme, define a sequence of functions by

$$S_{a_j,N}(z) := \sum_{n=0}^{N} \sum_{\nu \in \sigma_n(j)} \left(\frac{1}{z - a_{\nu j}} - \frac{1}{z - s_{\nu j}} \right). \tag{4.18}$$

Lemma 4.3. *For m-connected regions $\mathbb{D}$, $m > 1$, satisfying the separation condition $\Delta < (m-1)^{-1/4}$, the sequence $S_{a_j,N}$ converges uniformly to S_{a_j} on $\overline{\mathbb{D}}$ such that*

$$|S_{a_j}(z) - S_{a_j,N}(z)| = O\left(\left(\Delta^2 \sqrt{m-1} \right)^{N+1} \right).$$

Proof. The proof is similar to that of the convergence of the singularity function given in the proof of Theorem 2.7. □

It is now possible to state two theorems describing the boundary behavior of S_{a_j}, and thus of f_{a_j}. However, first note that given $w = e^{i\theta}$,

$$\operatorname{Re}\left\{ \frac{w}{w-1} \right\} = \frac{1}{2} \tag{4.19}$$

since

$$\frac{w}{w-1} = \frac{e^{i\theta/2}}{e^{i\theta/2} - e^{-i\theta/2}} = \frac{\cos(\theta/2) + i\sin(\theta/2)}{i2\sin(\theta/2)} = \frac{1}{2} - i\cot\frac{\theta}{2}.$$

Theorem 4.4. *Suppose $z \in C_p$, $j \neq p$ for $j, p \in \{1, \ldots, m\}$. If $\Delta < (m-1)^{-1/4}$, then*

$$\operatorname{Re}\left\{ (z - s_p) S_{a_j,N}(z) \right\} = O\left(\left(\Delta^2 \sqrt{m-1} \right)^{N} \right)$$

and

$$\operatorname{Re}\left\{ (z - s_p) S_{a_j}(z) \right\} = 0. \tag{4.20}$$

Proof. The proof of this is similar to that of Lemma 2.9; here, however, the sums over the circles $1, \ldots, m$ are missing. □

Theorem 4.5. *Suppose $z \in C_j$ and $\Delta < (m-1)^{-1/4}$. Then*

$$\mathrm{Re}\left\{(z-s_j)S_{a_j,N}(z)\right\} = -\frac{1}{2} + O\left(\left(\Delta^2\sqrt{m-1}\right)^N\right)$$

and

$$\mathrm{Re}\left\{(z-s_j)S_{a_j}(z)\right\} = -\frac{1}{2}. \tag{4.21}$$

Proof. With the parametrization $z = s_j + r_j e^{i\theta}$ one may write

$$\begin{aligned}
(z-s_j)S_{a_j,N}(z) &= (z-s_j)\left[\frac{1}{z-a_j} - \frac{1}{z-s_j} + \cdots \right.\\
&\qquad \left. + \left(\frac{1}{z-a_{\nu j}} + \frac{1}{z-a_{j\nu j}}\right) - \left(\frac{1}{z-s_{\nu j}} + \frac{1}{z-s_{j\nu j}}\right) + \cdots\right]\\
&= -1 + \frac{z-s_j}{z-a_j} + \cdots\\
&\qquad + \left(\frac{(z-s_j)/(a_{\nu j}-s_j)}{(z-s_j)/(a_{\nu j}-s_j)-1} + \frac{(z-s_j)/(a_{j\nu j}-s_j)}{(z-s_j)/(a_{j\nu j}-s_j)-1}\right)\\
&\qquad - \left(\frac{(z-s_j)/(s_j-s_{\nu j})}{(z-s_j)/(s_{\nu j}-s_j)-1} + \frac{(z-s_j)/(s_{j\nu j}-s_j)}{(z-s_j)/(s_{j\nu j}-s_j)-1}\right)\\
&\qquad + \cdots .
\end{aligned}$$

Then, with $a_j = s_j + r_j e^{i\theta_j}$ in conjunction with equations (2.8) and (4.19),

$$\begin{aligned}
\mathrm{Re}\left\{(z-s_j)S_{a_j,N}(z)\right\} &= -1 + \mathrm{Re}\left\{\frac{e^{i\theta}}{e^{i\theta}-e^{i\theta_j}}\right\} + (1-1) + (1-1) + \cdots\\
&= -1 + \mathrm{Re}\left\{\frac{e^{i(\theta-\theta_j)}}{e^{i(\theta-\theta_j)}-1}\right\} = -\frac{1}{2}.
\end{aligned}$$

□

A difficulty at this point is the lack of an existence theorem for f_{a_j} as described. The following is given as conjecture, but at the time of this writing is unproven.

Conjecture 4.6. *If f_{a_j} is an analytic function on an unbounded, multiply connected domain $\mathbb{D}$ such that $f_{a_j}(0) = 0$ and $f_{a_j}(\infty) = 1$ with the boundary conditions*

$$\arg f_{a_j}(z) = \text{const. } \textit{for } z \in C_p,\ p \neq j \textit{ and} \tag{4.22}$$

$$\partial \arg f_{a_j}(z)/\partial\theta = -1/2 \textit{ for } z = c_j + r_j e^{i\theta} \in C_j, \tag{4.23}$$

then f_{a_j} is a uniquely determined conformal map from the circle domain to the interior of a domain bounded by a curve $\Gamma_j = f_{a_j}(C_j)$ through the origin, and star-like with respect to the origin, with interior radial slits $\Gamma_p = f_{a_j}(C_p)$ for $p \neq j$.

In terms of singularity functions $S_{z_{k,j}}(z)$ given by equation (4.17), where we have substituted using prevertices $z_{k,j}$ in place of a_j, the function given by equation (4.15) satisfies the same boundary conditions as the map defined in terms of reflections, equation (2.13). To see this define

$$S(z) := \sum_{j=1}^{m} \sum_{k=1}^{K_j} \beta_{k,j} S_{z_{k,j}}(z).$$

Recall that $\sum \beta_{k,j} = 2$ for a given j. Then, applying Theorems 4.4 and 4.5,

$$\begin{aligned}
\operatorname{Re}\{(z-c_j)S(z)\} &= \sum_{p=1}^{m} \sum_{k=1}^{K_p} \beta_{k,p} \operatorname{Re}\left\{(z-c_j)S_{z_{k,p}}(z)\right\} \\
&= \sum_{k=1}^{K_j} \beta_{k,j} \operatorname{Re}\left\{(z-c_j)S_{z_{k,j}}(z)\right\} \\
&= \left(-\frac{1}{2}\right) \sum_{k=1}^{K_j} \beta_{k,j} \\
&= -1.
\end{aligned}$$

Compare this to Lemma 2.16 for the boundary condition given for the singularity function from the MCSC formula in terms of reflections.

4.2.1 Linear system for a map factor as a series

The factors $f_{z_{k,j}}$ of equation (4.15) are now computed numerically assuming Conjecture 4.6 holds by using these conditions to build a linear system of equations describing the coefficients of a Laurent expansion for the function. This is a modification of the method given above in Section 4.1 used to compute slit maps.

For brevity we again use f_{a_j} in place of $f_{z_{k,j}}$. Begin by writing the function f_{a_j} in the form

$$f_{a_j}(z) = \frac{z-a_j}{z-c_j} e^{g(z)},$$

where g is analytic in the domain and $g(z) \to 0$ as $z \to \infty$. Then $f_{a_j}(a_j) = 0$ and $f_{a_j}(\infty) = 1$, as required. The function g is given as the sum of the Laurent series expansions on the exterior of each boundary circle,

$$g(z) = \sum_{p=1}^{m} \sum_{\ell=1}^{\infty} \frac{d_{\ell,p} r_p^{\ell}}{(z - s_p)^{\ell}}.$$

Since $\operatorname{Im}\left\{\log f_{a_j}\right\} = \arg f_{a_j}$, the boundary conditions (4.22) and (4.23) above are now

$$\operatorname{Im}\left\{\log f_{a_j}\right\} \equiv \text{const.}, \quad \text{for all } z \in C_p, \quad p \neq j$$

and

$$\frac{\partial}{\partial \theta} \operatorname{Im}\left\{\log f_{a_j}\right\} = -\frac{1}{2}, \quad \text{for all } z \in C_j.$$

Note for $z = c_j + r_j e^{i\theta}$,

$$\frac{\partial}{\partial \theta} \operatorname{Im}\left\{\log f_{a_j}(z)\right\} = \operatorname{Im}\left\{ i r_j e^{i\theta} \frac{f'_{a_j}(z)}{f_{a_j}(z)} \right\} = \operatorname{Re}\left\{ (z - c_j) \frac{f'_{a_j}(z)}{f_{a_j}(z)} \right\}$$

where

$$\frac{f'_{a_j}(z)}{f_{a_j}(z)} = \frac{d}{dz} \log f_{a_j}(z) = \frac{1}{z - a_j} - \frac{1}{z - c_j} + g'(z)$$

which gives

$$\operatorname{Re}\left\{ (z - c_j) \frac{f'_{a_j}(z)}{f_{a_j}(z)} \right\} = \operatorname{Re}\left\{ \frac{z - c_j}{z - a_j} - 1 + (z - c_j) g'(z) \right\} = -\frac{1}{2}.$$

Using equation (4.19) we have also

$$\operatorname{Re}\left\{ \frac{z - c_j}{z - a_j} \right\} = \operatorname{Re}\left\{ \frac{e^{i\theta}}{e^{i\theta} - e^{i\theta_j}} \right\} = \frac{1}{2}.$$

The boundary conditions may thus be restated in terms of g by

$$\operatorname{Im}\{g(z)\} = \text{const.} - \arg \frac{z - a_j}{z - c_j}, \quad \text{for all } z \in C_p, \quad p \neq j; \tag{4.24}$$

$$\operatorname{Re}\left\{(z - c_j) g'(z)\right\} = 0, \quad \text{for all } z \in C_j. \tag{4.25}$$

The coefficients $d_{\ell,p}$ of g are found by solving a linear system of equations based on these conditions.

For computation we discretize by limiting the index ℓ in g to N terms, and choose M points z on each boundary circle. Let $x = [d_{\ell,p}]$ be the $(mN \times 1)$ column vector of coefficients. Define for $p = 1, \ldots, m$ the matrices

$$F_p = \left[r_p^\ell (z - s_p)^{-\ell} \right]_{M \times mN} \quad \text{for} \quad z \in C_p,\ p \neq j.$$

Based on

$$g'(z) = \sum_{p=1}^{m} \sum_{\ell=1}^{\infty} \frac{-\ell d_{\ell,p} r_p^\ell}{(z - s_p)^{\ell+1}}$$

define

$$G = \left[-\ell (z - c_j) r_p^\ell (z - s_p)^{-\ell-1)} \right]_{M \times mN} \quad \text{for} \quad z \in C_j.$$

With $F_p = F_{R_p} + iF_{I_p}$, $G = G_R + iG_I$, and $x = x_R + ix_I$ a calculation shows

$$\mathrm{Im}\{g(z)\} \approx F_{I_p} x_R + F_{R_p} x_I \quad \text{on any} \quad C_p,\ p \neq j$$

and

$$\mathrm{Re}\left\{(z - c_j) g'(z)\right\} \approx G_R x_R - G_I x_I \quad \text{on} \quad C_j.$$

The values of $\mathrm{Im}(f_{a_j})$ may not be known in advance, but the difference of $\mathrm{Im}(f_{a_j})$ for any pair of points on a circle C_p, $p \neq j$, is zero. Then define

$$P = \begin{bmatrix} -1 & 1 & & & \\ & -1 & 1 & & \\ & & \ddots & \ddots & \\ & & & -1 & 1 \end{bmatrix}_{M-1 \times M}$$

so that for $z \in C_p$ we have

$$P \begin{bmatrix} F_{I_p} & F_{R_p} \end{bmatrix} \begin{bmatrix} x_R \\ x_I \end{bmatrix} = -P \left[\arg \tfrac{z - a_j}{z - c_j} \right]_{M \times 1}$$

by the boundary condition (4.24). By the boundary condition (4.25) it is also the case

$$\begin{bmatrix} G_R & -G_I \end{bmatrix} \begin{bmatrix} x_R \\ x_I \end{bmatrix} = \begin{bmatrix} 0 \end{bmatrix}.$$

For the sake of exposition suppose $j \notin \{1, m\}$. Define the block matrices

$$B_1 = \begin{bmatrix} F_{I_1} \\ \vdots \\ F_{I_{j-1}} \\ G_R \\ F_{I_{j+1}} \\ \vdots \\ F_{I_m} \end{bmatrix}_{mM \times mN} \quad \text{and} \quad B_2 = \begin{bmatrix} F_{R_1} \\ \vdots \\ F_{R_{j-1}} \\ -G_I \\ F_{R_{j+1}} \\ \vdots \\ F_{R_m} \end{bmatrix}_{mM \times mN},$$

where the matrices G_R and $-G_I$ occupy the jth block-row, and the block diagonal difference matrix

$$E = \begin{bmatrix} P & & & & \\ & \ddots & & & \\ & & I & & \\ & & & \ddots & \\ & & & & P \end{bmatrix}_{m(M-1)+1 \times mM},$$

where the $(M \times M)$ identity matrix occupies the jth block-row. A solution to the linear system

$$E \begin{bmatrix} B_1 & B_2 \end{bmatrix} \begin{bmatrix} x_R \\ x_I \end{bmatrix} = -E \begin{bmatrix} \arg \frac{z-a_j}{z-c_j} \\ \vdots \\ 0 \\ \vdots \\ \arg \frac{z-a_j}{z-c_j} \end{bmatrix}_{mM \times 1} \tag{4.26}$$

in the least squares sense by the use of the MATLAB backslash operator gives the coefficients for approximating g.

To choose the number of collocation points M, consider that for the system given by equation (4.26) to be square a calculation shows that M must satisfy

$$M = \frac{2mN + m - 1}{m}.$$

The ceiling function could be employed to allow for any truncation level N without regard to m, which would make the system overdetermined in the case M is not an integer. For

consistency we just require that the system always be overdetermined by the inequality

$$M > \frac{2mN + m - 1}{m},$$

where

$$M = 2N + 1 = \frac{2mN + m}{m} > \frac{2mN + m - 1}{m}$$

satisfies this condition.

4.2.2 Numerical examples

Here numerical examples of the finite product computations using least squares, as well as comparisons with the reflection method are given. The examples below use these representations to evaluate the derivative of the MCSC transformation in solving the parameter problem as outlined in Chapter 3.

Example 4.7. The first example is shown in Figure 4.6. It is clear from Figures 4.8, 4.9, and 4.10 that the finite product method performs much better than the reflection method; one gets better convergence and accuracy for less computation time. The vectors $X(N)$ are the MCSC parameters after the solution process has finished at N levels of reflection or a series truncation level of N terms appropriately. We compare $\|X(N) - X(N-1)\|_\infty$ in the case of reflections and $\|X(N) - X(N-3)\|_\infty$ for the series. Figure 4.7 shows one of the slit maps in the finite product representation.

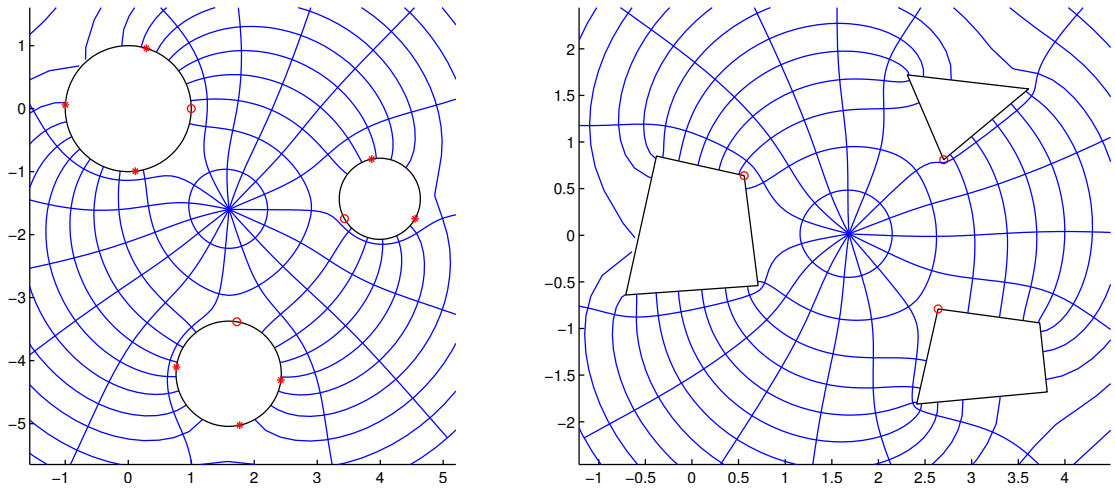

Figure 4.6: Simple exterior map with $m = 3$. See Example 4.7. In terms of separation, $\Delta \approx 0.8409$ and $(m-1)^{-1/4} \approx 0.4078$.

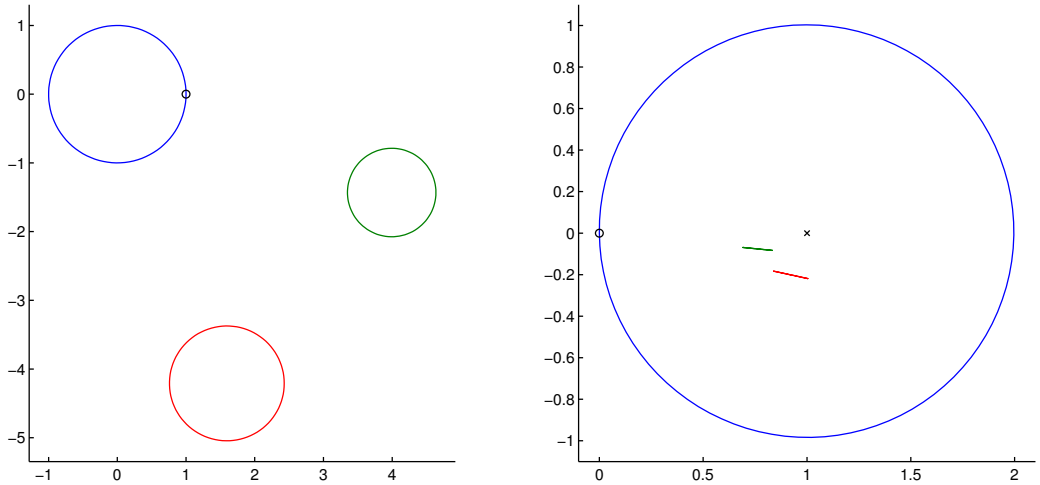

Figure 4.7: The map $f_{z_{1,1}}$ for Example 4.7; *i.e.*, the MCSC factor with $k = 1$, $j = 1$.

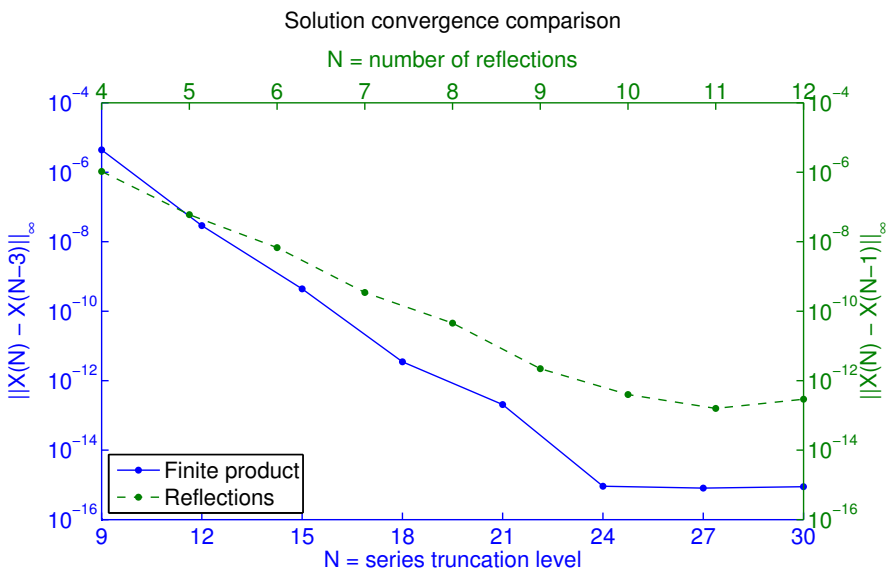

Figure 4.8: Comparison of convergence of the solution to the parameter problem for both methods for Example 4.7.

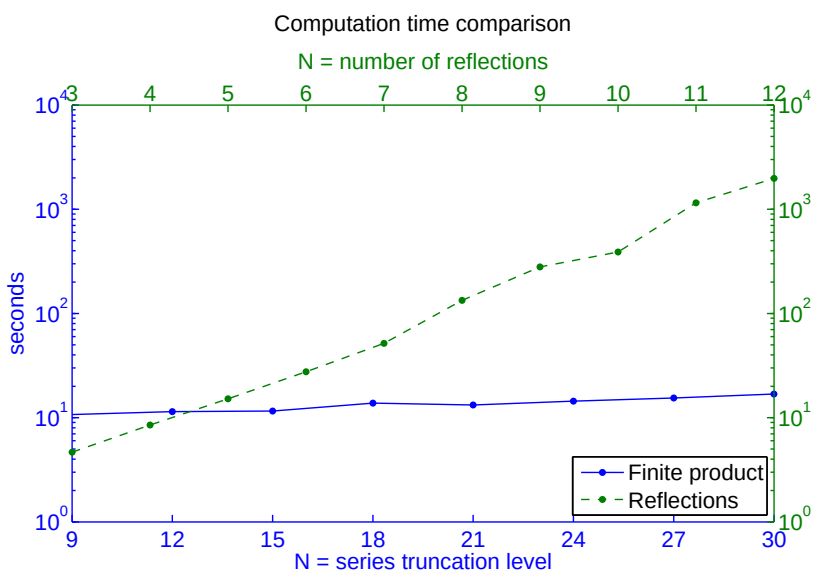

Figure 4.9: Comparison of computation time to find solution of the parameter problem for Example 4.7. Each method was started with the same initial guess.

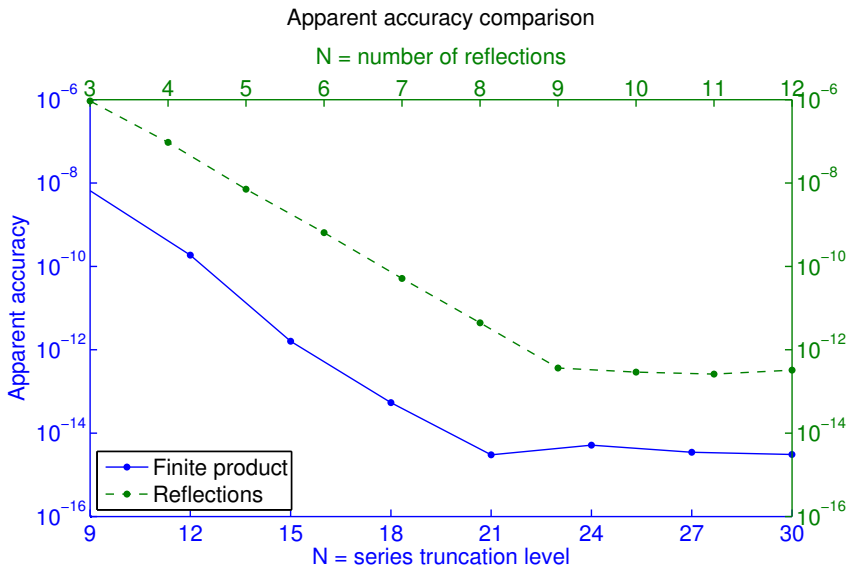

Figure 4.10: Comparison of apparent accuracy for Example 4.7.

Example 4.8. The next example, see Figure 4.11, is only slightly more complicated with 4 unbounded polygons ($m = 4$), but shows a more extreme example of the difference in computation time between the two methods. This is due to the higher connectivity and higher vertex count. Note for this example the separation condition is not satisfied, *i.e.*, $\Delta > (m-1)^{-1/4}$.

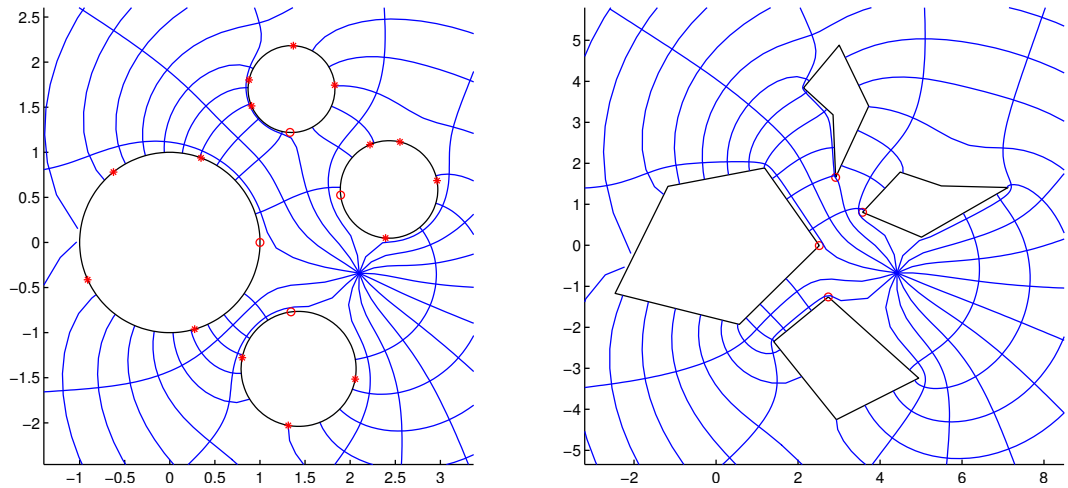

Figure 4.11: Example 4.8 with $m = 4$ and higher vertex count.

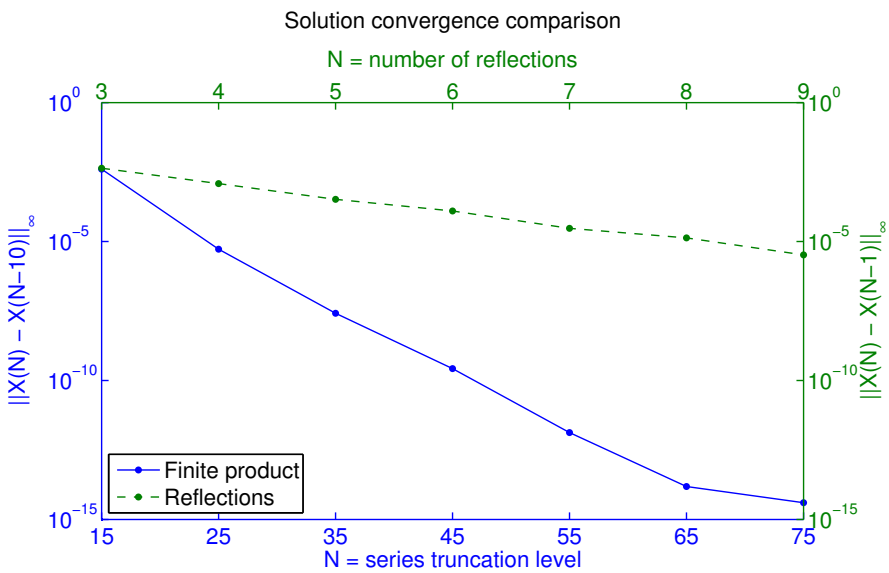

Figure 4.12: Convergence comparison for the solution to the parameter problem for the 4-connected domain in Example 4.8. Note the slow convergence of the reflection method, since in this example we have $\Delta \approx 0.8164$ with $(m-1)^{-1/4} \approx 0.7598$.

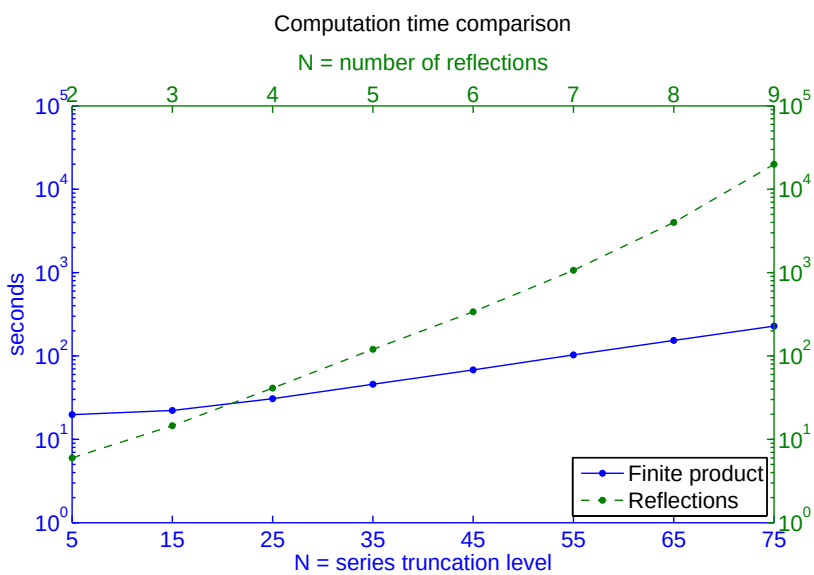

Figure 4.13: Comparison of computation times for Example 4.8.

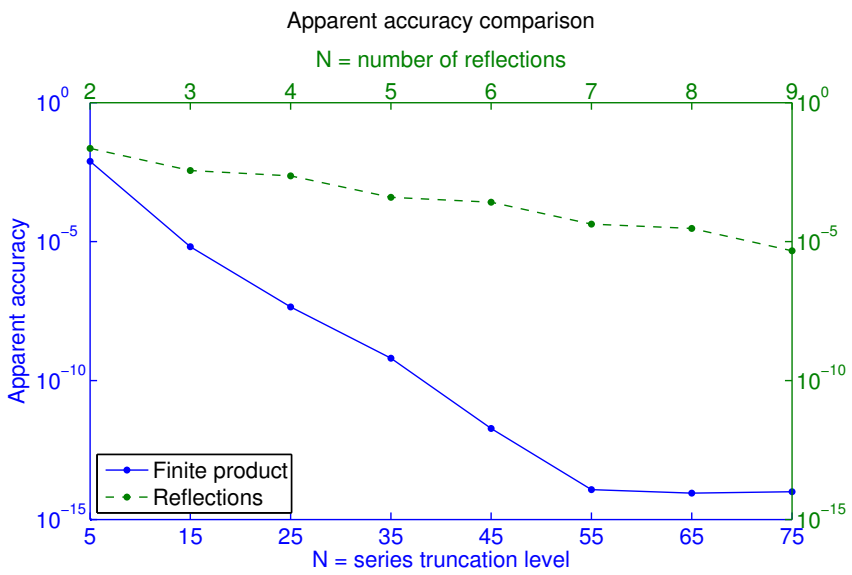

Figure 4.14: Comparison of apparent accuracy for Example 4.8.

Example 4.9. This example compares performance of the two methods in a domain with close to touching circles. See Figure 4.15. Figures 4.17 and 4.18 show the finite product method achieves better accuracy for approximately the same computation time. Even with $\Delta \approx 0.9474$ ($(m-1)^{-1/4} \approx 0.8409$) it is clear that, as in the reflection case, the separation condition is a sufficient, not necessary condition for the convergence of the infinite series. To of the factor maps are also given for two of the prevertices on C_1 (the largest circle), $z_{1,1}$ and $z_{6,1}$; see Figures 4.19 and 4.20.

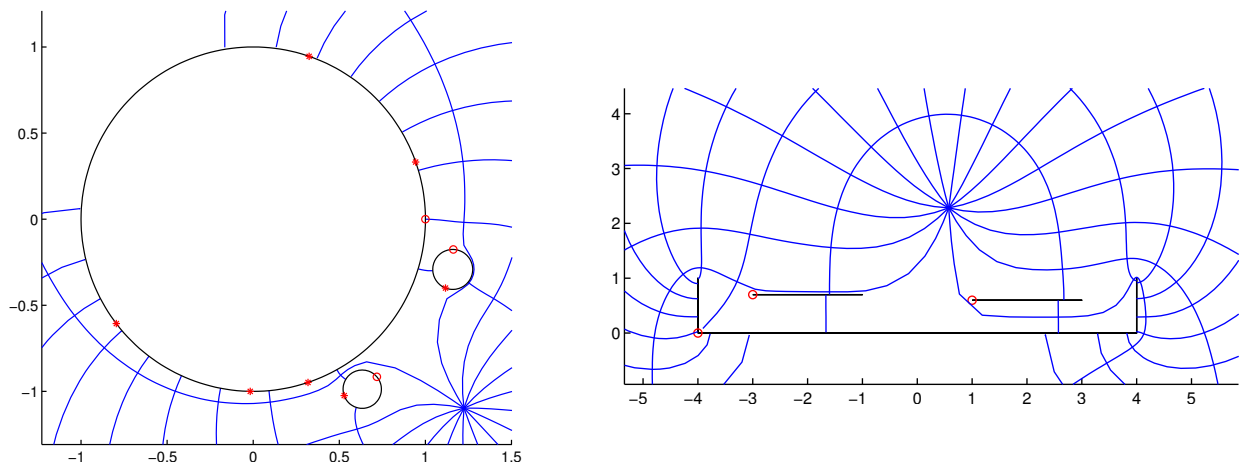

Figure 4.15: For Example 4.9, the circles in the domain are very close to touching: $\Delta \approx 0.9474$ with $(m-1)^{-1/4} \approx 0.8409$.

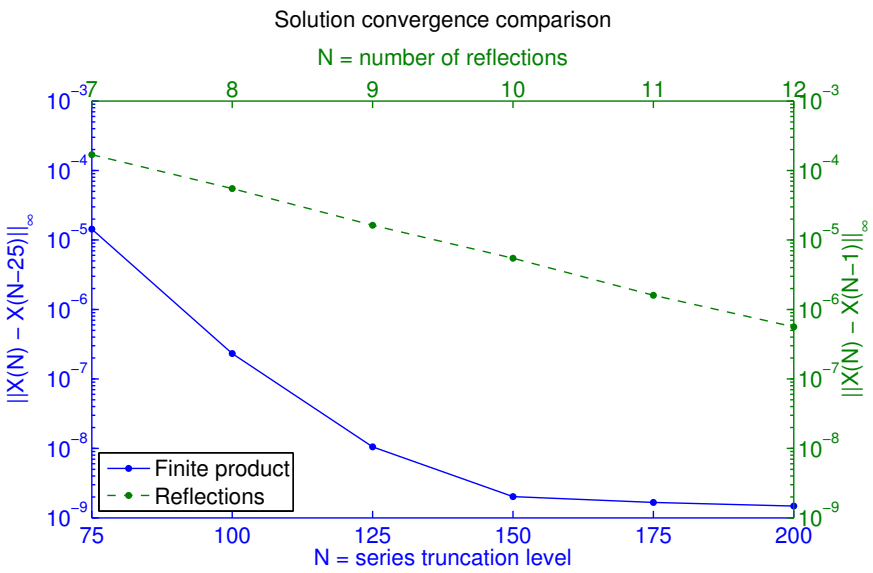

Figure 4.16: Convergence for Example 4.9.

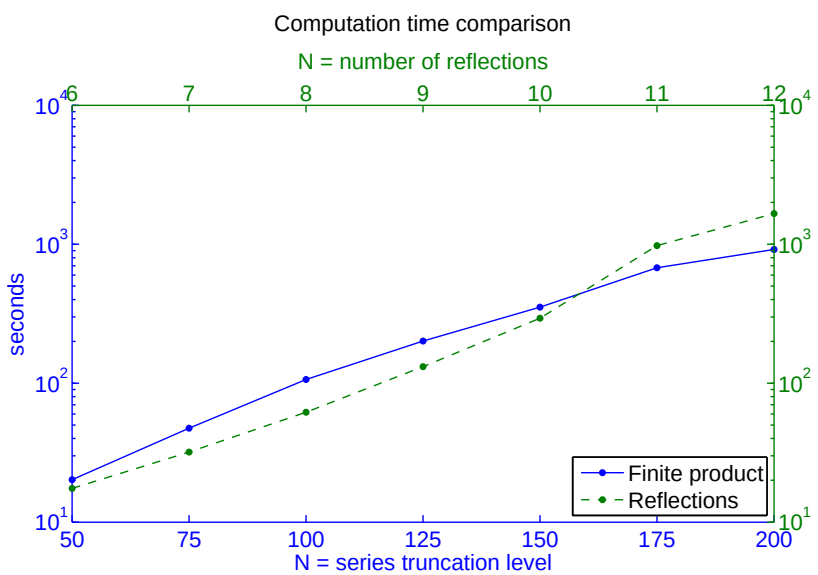

Figure 4.17: Time comparison for Example 4.9.

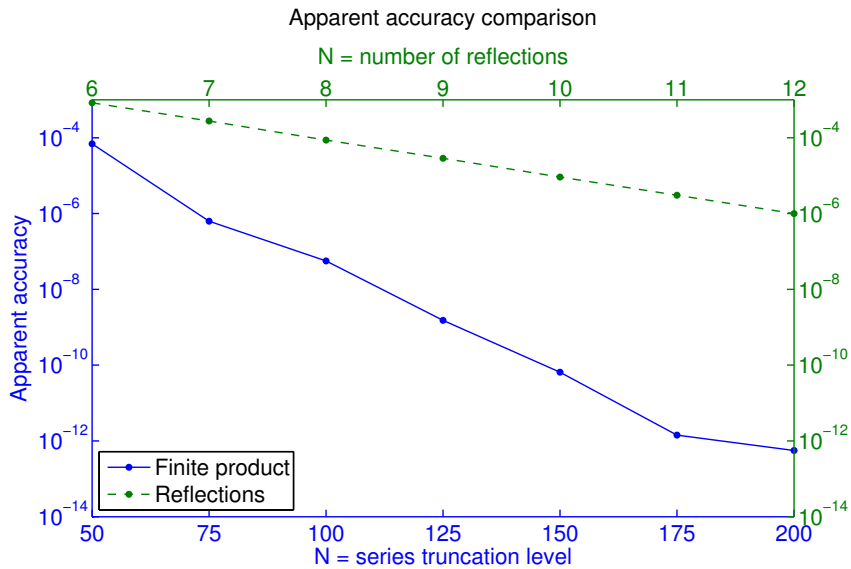

Figure 4.18: Accuracy comparison for Example 4.9.

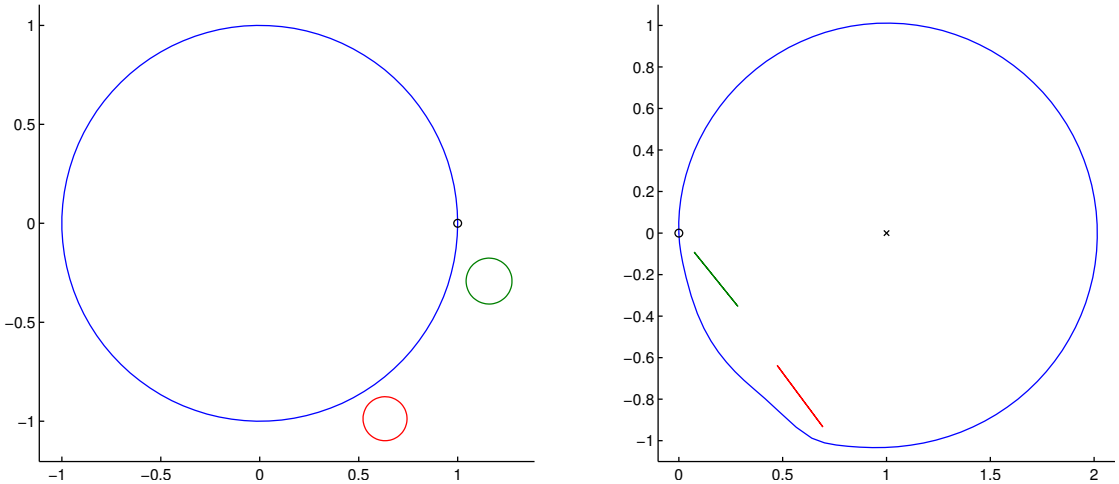

Figure 4.19: The MCSC factor map $f_{z_{1,1}}$ for Example 4.9.

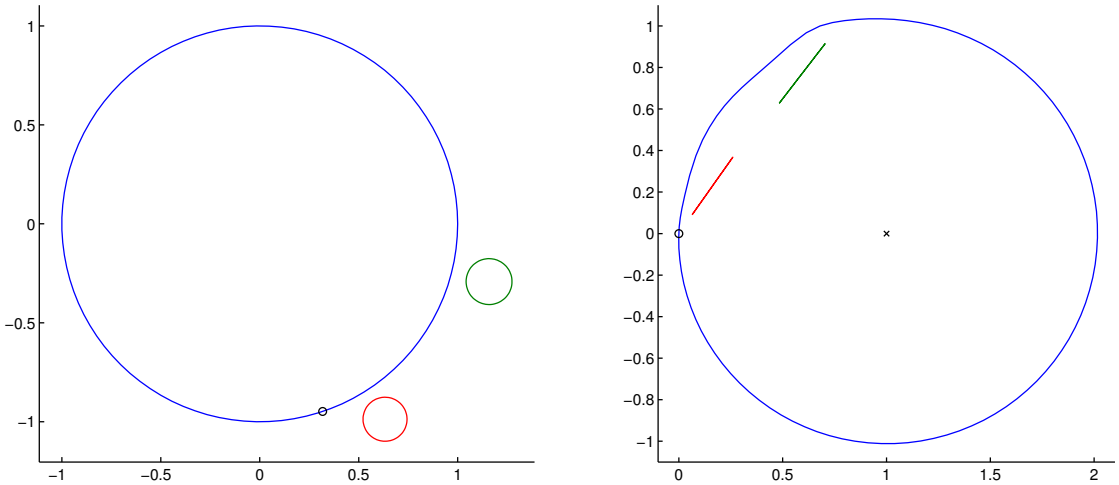

Figure 4.20: The MCSC factor map $f_{z_{6,1}}$ for Example 4.9.

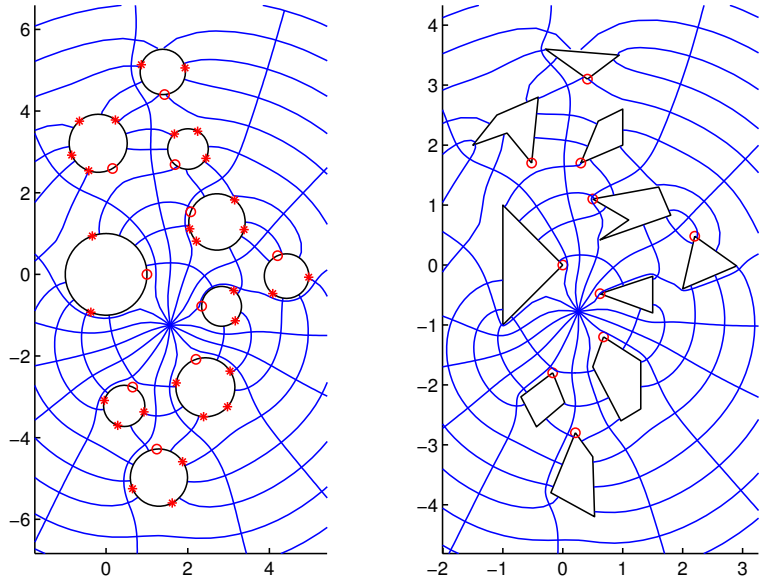

Figure 4.21: An example of high connectivity, $m = 10$. This took around 5 hours to solve the parameter problem with the reflection method, and around 5 minutes using the finite product method.

Example 4.10. The last example involves high connectivity, $m = 10$; see Figure 4.21. On the same hardware, the reflection method took just a little over 5 hours to solve the parameter problem, while the finite product method took around 5 minutes to solve the same problem.

CHAPTER 5

AN APPLICATION

In this Chapter the polygonal domains $\mathbb{P}$ represent infinitely thin plates of uniform electrical resistance. This exposition closely follows [16]. Two parts of the boundary, the so-called "marked sides", are assumed to be perfect conductors and the remainder of the boundary is insulated. The values of the resistance are invariant under conformal mapping (see [26, Sec. 16.11] and [32, Sec. 2.2] for an introduction) and mapping to an appropriate canonical domain gives those values as ratios of simple geometric quantities. In the calculations below, maps from the circle domains to two types of canonical or model domains are used: rectangles with horizontal slits and annuli with radial slits. The maps to the rectangles with horizontal slits are computed as a special case of the more general mapping problem using techniques adapted from Section 2.3.2. The maps to radial slit annuli just require the application of the method discussed in Section 2.2.2. Therefore, the maps between the polygonal resistors and the model domains are known implicitly via maps from the circle domains. This is all that is needed to find the values of the resistance. Conformal mapping has been applied often to such calculations. For instance, the recent book [32] considers applications of conformal mapping to the calculation of resistance of integrated circuit networks. Most of the applications in the literature so far have considered only simply or doubly connected domains. The methods developed here can be used for polygonal domains of arbitrary finite connectivity.

There are a number of possibilities for the choice of a canonical domain in conformal mapping of multiply connected domains [31]. The choice can be made on the basis of geometric appeal or by convenience for a set of applications. In this Chapter canonical domains where either a rectangle with horizontal slits or an annulus with radial slits are used. We first consider the rectangle with horizontal slits. If the domain, $\mathbb{D}$, under consideration is bounded and its outer boundary is a contour $\mathbb{C}_1$, then, with the specification of an ordered

set of four points on $\mathbb{C}_1$, one may think of $\mathbb{D}$ as a "generalized marked quadrilateral". There is a conformal map of this configuration onto a rectangle in which the four marked points are taken to the corners of the rectangle with the marked sides mapped to the vertical ends and the interior boundary components, Γ_2, $\Gamma_3, \ldots, \Gamma_m$, mapped to horizontal slits. This map and the rectangle are uniquely determined by the aspect ratio of the rectangle and the specification of the images of two of the marked points.

These facts follow from a variational principle due to Rengel. An exposition can be found in Pflüger [33]; see also [27], [31, Chap. VII], and [35]. This idea, together with a Schwarz-Christoffel transformation for finitely connected polygonal domains, are used to compute resistances of multiply connected resistors. The resistance can be given in terms of the Dirichlet integral of the electrical potential with voltages applied to the marked sides (conductors) and normal derivatives set to zero on the insulated sides. The Dirichlet integral is invariant under conformal mapping. This potential is easily found for a rectangle. The resistance is just the ratio of the adjacent sides of the conformally equivalent rectangle to the marked sides which represent the electrical contacts. The inclusion of horizontal slits, which are parallel to the direction of the current, does not change the resistance, so that once the map to this model domain is known, the resistance calculation is trivial. An important precursor of this work is that of Trefethen [37] in which simply connected resistors were analyzed using simply connected Schwarz-Christoffel transformations. The Schwarz-Christoffel methodology was also a natural choice there for the problem of designing resistors of specified resistance by "trimming", that is, varying the resistance by cutting slits into the domain from the boundary in order to change the initial resistance to the specified value. These of ideas of resistor analysis are extended here to arbitrary finite connectivity. The design problem follows as in [37], since the resistance of a multiply connected "quadrilateral" has the same monotonicity properties that justified the resistor trimming calculation there. We will discuss the trimming problem in future work.

In addition to polygonal resistors with exterior electrical contacts, resistances with interior contacts are also computed. For such configurations another model domain is appropriate, namely, a circular ring (or annulus) with radial slits. The domain $\mathbb{D}$ can be mapped to an annulus with radial slits where two chosen interior boundary components are mapped to the inner and outer circular boundaries and the remaining boundary components are mapped to the radial slits. The ratio of the inner and outer radii are then uniquely determined and the lengths and locations of the radial slits are determined up to a rotation of the annulus. The resistance is then given by the logarithm of the ratio of the radii of the outer and inner circular boundaries.

The problem of crack detection in which unknown slits are determined via "generalized Schwarz-Christoffel parameter problems" [37] is likely to yield to similar analysis to that in the simply and doubly connected cases, [23, 24], but this problem is left to future work.

5.1 Maps to rectangles with $m-1$ parallel slits

In this section it is shown how to adapt the map from Section 2.3.2 to compute maps from the circle domain $\mathbb{D}$ to rectangles with horizontal slits, thus, implicitly giving the maps between the polygonal resistors and the conformally equivalent horizontally slit rectangles. This is a special parameter problem where $\mathbb{D}$ and the prevertices of the corners of the rectangles are known. Rectangles with $m-1$ parallel slits are shown to be canonical domains in [33] using Schwarz reflection and mapping to circular slit annuli. As explained above, the ratio of the length to the height of a conformally equivalent rectangle with horizontal slits is the resistance of the previously described polygonal resistor. In the examples below, maps to radial slit annuli will be used, but those maps do not require the solution of a parameter problem.

The Schwarz-Christoffel map from the circle domain $\mathbb{D}$ to the rectangle with horizontal

slits is given (up to a scaling by A and a translation) by

$$f'(z) = A\left(\prod_{k=1}^{4}(z-\zeta_{k,1})^{-1/2}\right)\prod_{j=2}^{m}\prod_{\substack{n=0\\ \nu\in\sigma_n(j)}}^{\infty}\left(\prod_{k=1}^{4}(z-\zeta_{k,\nu j1})^{-1/2}\prod_{k=1}^{2}(z-\gamma_{k,\nu j})\right). \tag{5.1}$$

The $\zeta_{k,1} \in C_1, k = 1, \ldots, 4$, are given and map to the four vertices of the rectangle, $f(\zeta_{k,1})$. Set $f(\zeta_{1,1}) = i$ and $f(\zeta_{2,1}) = 0$ to fix A and the translation. (Note, that in the examples the $\zeta_{k,1}$ are prevertices of Γ_1 of the polygonal resistor corresponding to the endpoints of the marked sides, as indicated in the figures. However, this need not be the case. The endpoints of marked sides can be chosen anywhere on Γ_1. If the $\zeta_{k,1}$ are preimages of other specified points on Γ_1, then the map to the resistor must be inverted to find the $\zeta_{k,1}$'s. This will not be done here.) The circle centers, c_j, and radii, r_j, for $j = 2, \ldots, m$ are also given. Therefore, one only need solve for the preimages $z_{k,j}$, $k = 1, 2$, $j = 2, \ldots, m$, of the tips of the horizontal slits, $w_{k,j} = f(z_{k,j})$. This requires $2m - 2$ real equations that force the slits to be horizontal and the length of the top of the slit to equal the length of the bottom of the slit, *i.e.*, the top and bottom slits form closed curves. The equations are

$$\sin\left(\arg(f(z_{1,j}) - f(z_{2,j}))\right) = 0,$$

and

$$\left|\int_{C_j^t} f'(z)dz\right| = \left|\int_{C_j^b} f'(z)dz\right|$$

for $j = 2, \ldots, m$, where, for the second set of equations, C_j^t denotes the arc of C_j from $z_{1,j}$ to $z_{2,j}$ and C_j^b denotes the arc of C_j from $z_{2,j}$ to $z_{1,j}$, both traversed in the counterclockwise direction. Again a change to unconstrained coordinates is used to find the prevertex angles, $\theta_{k,j}$, for the prevertices $z_{k,j}$.

5.2 Resistance examples

Examples of two types of resistance calculations are given. The first computes resistances for multiply connected polygonal "quadrilaterals", that is, domains – here, polygonal – with two marked sides on their (outer) boundaries, representing electrical contacts where

voltages are given and indicated by thick lines in the figures. The marked sides are separated by two unmarked sides, indicated by thin lines. The unmarked sides and the interior boundaries are insulated. The second type of example computes resistances for circuits with voltages given on two interior boundaries with the remaining boundaries insulated. (Note this second case with interior contacts would also be an appropriate problem for the Schwarz-Christoffel transformation for unbounded domains, developed in [18] and computed in [14] and [19]. However, this will not be pursued here.) These problems, like many applications of conformal mapping, can be solved easily using maps to the appropriate "model" domain. The model domains are, basically, the canonical slit domains, first cataloged by Koebe [27]. Many of these domains are rigorously treated in such texts as [33, 31].

5.2.1 Computation of resistances for quadrilaterals

In this case, the model domain is a rectangle with horizontal slits as in Section 5.1. When constructing the rectangle domain, vertices $f(z_{1,1}) = i$ and $f(z_{2,1}) = 0$ are fixed. Resistances are calculated by computing the real parts of the third and fourth vertices, $f(z_{3,1})$ and $f(z_{4,1})$, which are just the lengths of the bottom R_b and the top R_t of the rectangles. These lengths should be equal and their difference gives an estimate of the error; see Table 5.1. The Schwarz-Christoffel map is again evaluated using a truncated product, and so the accuracy of the calculations are dependent on the number of levels of reflection N chosen to do the computation. An example of a resistor with $m = 3$ is given in Figure 5.1, and a table of calculated resistance values with the associated levels of reflection used is given in Table 5.1. In the tables and the error plots in the figures, it is found that the sum of the radii at the Nth level, $\sum_{|\nu|=N} r_\nu$, as discussed in Section 3.6, gives a practical estimate of the error. This quantity can be computed easily from the reflections of the circles. For instance, the bottom plot in Figure 5.1 illustrates that the error estimates $|R_b(N) - R_b(N-1)|$, $|R_t(N) - R_t(N-1)|$, and $\|X_N - X_{N-1}\|_\infty$ given by the computations with successive levels of reflection $N-1$ and N are well-approximated by $\sum_{|\nu|=N} r_\nu$. In addition the values of Δ

Table 5.1: Accuracy of resistance calculations for Figure 5.1 with $m = 2$ and $\Delta \approx 0.8080$. Sample computational times are given. The times roughly double with each increase in N, as expected.

N	resistance (bottom)	resistance (top)	$\sum_{\lvert\nu\rvert=N} r_\nu$	sec
3	1.8330969110	1.8328044088	$1.6 \cdot 10^{-2}$	2.0
4	1.8328657973	1.8328484817	$3.3 \cdot 10^{-3}$	3.1
5	1.8328713577	1.8328427644	$7.3 \cdot 10^{-4}$	5.6
6	1.8328410576	1.8328392515	$1.6 \cdot 10^{-4}$	12.0
7	1.8328408268	1.8328390036	$3.4 \cdot 10^{-5}$	19.3
8	1.8328388750	1.8328387543	$7.3 \cdot 10^{-6}$	37.7
9	1.8328388440	1.8328387436	$1.6 \cdot 10^{-6}$	72.8
10	1.8328387363	1.8328387293	$3.5 \cdot 10^{-7}$	155.4
11	1.8328387340	1.8328387289	$7.6 \cdot 10^{-8}$	372.9
12	1.8328387285	1.8328387281	$1.6 \cdot 10^{-8}$	1069.7

and $(m-1)^{-1/4}$ are given in the figures. The number of evaluations of the objective function is also given and provides some measure of the difficulty of the nonlinear problem.

See Figures 5.2, 5.3, and 5.4 for other examples. Computation time for the multiply-connected Schwarz-Christoffel map is exponential in the level of reflections. As a consequence, the N's chosen for the resistance measurements in these examples were based arbitrarily on the increasing amount of time required to perform these calculations on the author's computer. Note that high accuracy with a large number of reflections is feasible for the doubly connected example in Figure 5.2.

5.2.2 Computation of resistances for interior contacts

In this case, the model domain is an annulus with radial slits. This is the canonical domain given in 2.2.2. Given this domain, the resistance R is then given by the log of the

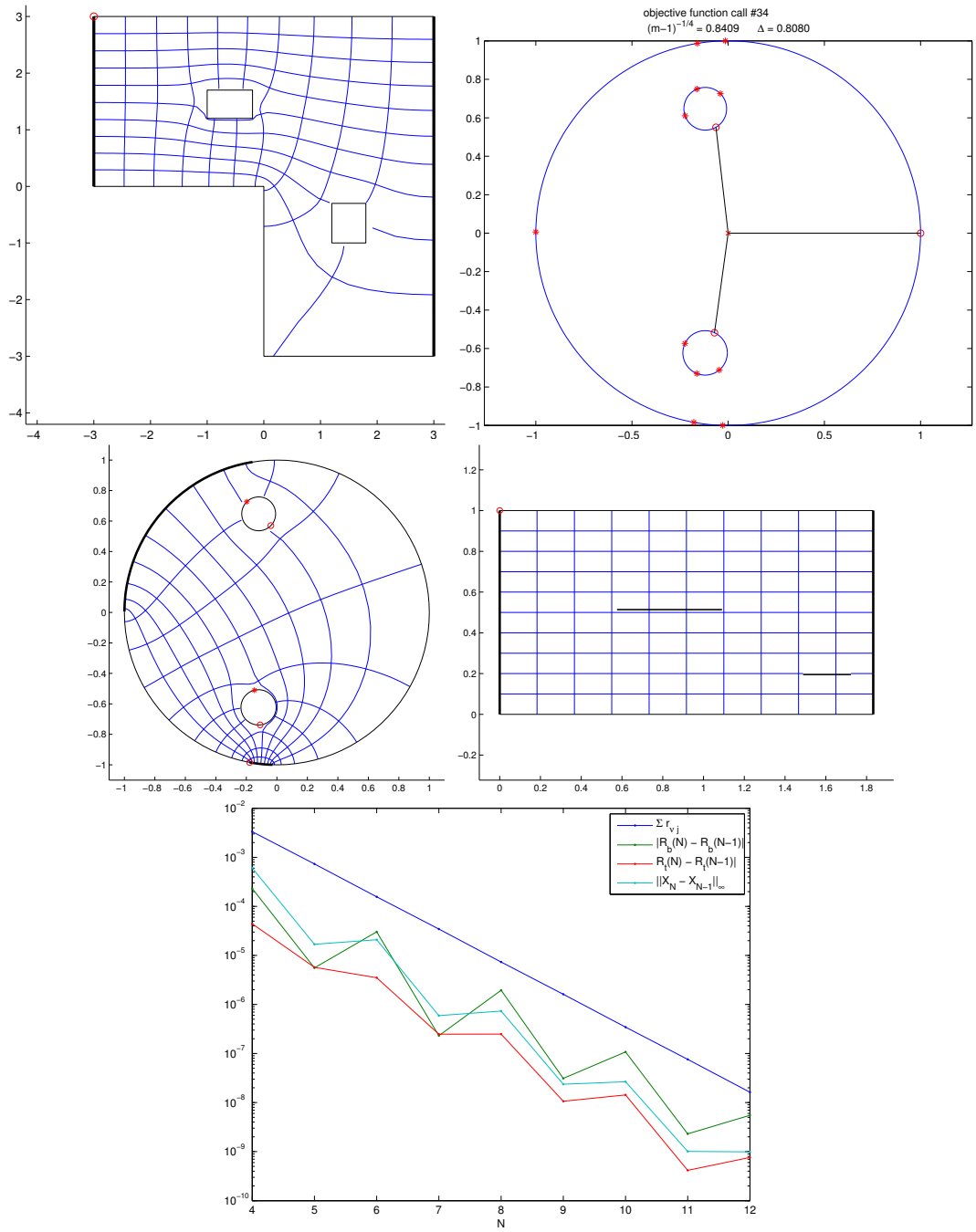

Figure 5.1: A resistor with $m = 3$. Resistance $= 1.832838728$. The errors in the resistance and the parameters X_N are well-estimated by the sum of the radii at the Nth level $\sum_{|\nu|=N} r_\nu$.

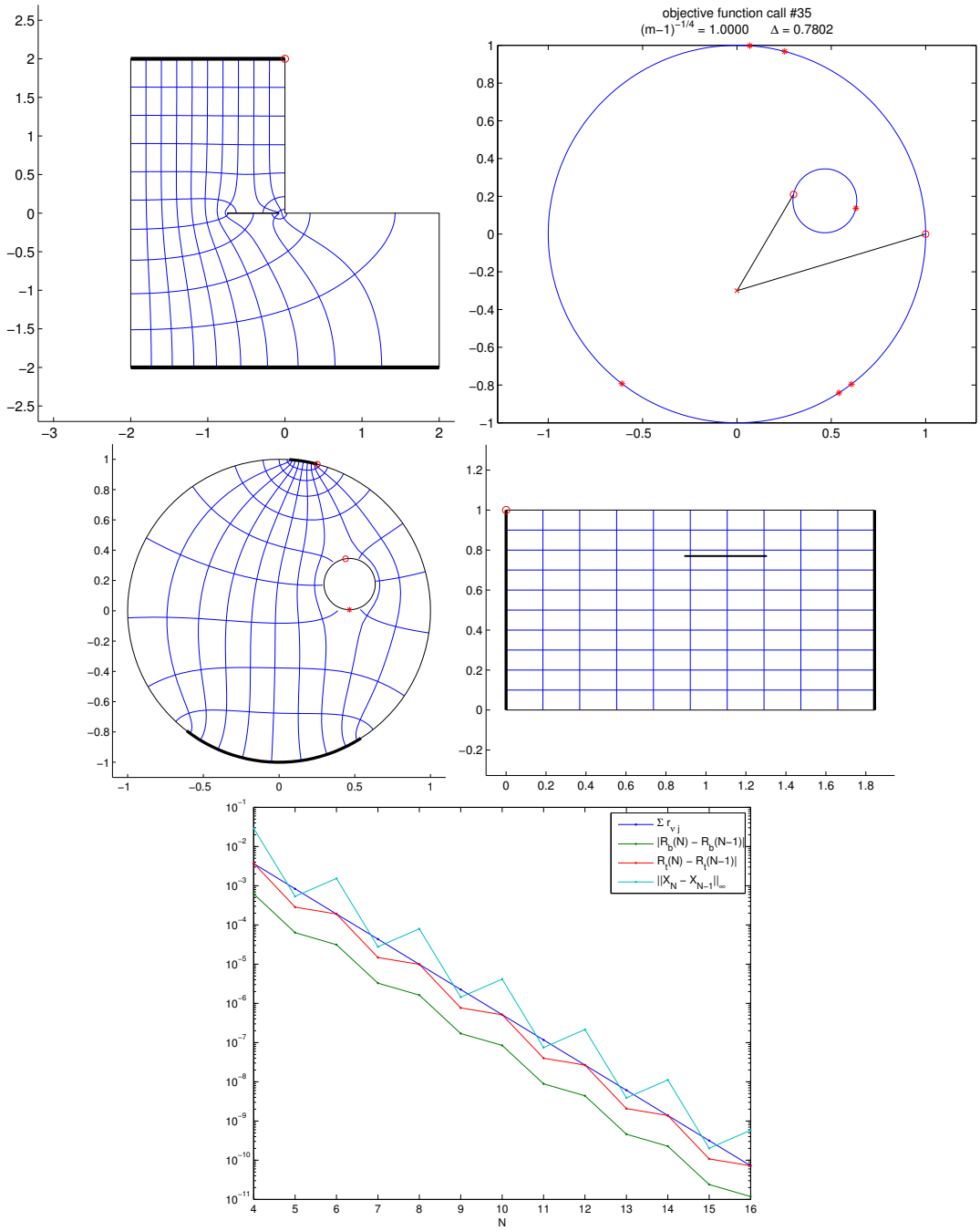

Figure 5.2: A doubly connected resistor. Resistance measurements for $N = 16$ are $R_b = 1.84354823853007$ and $R_t = 1.84354823853003$ (bottom and top measurements). The time was only 0.81 seconds, since the number of reflections does not increase geometrically with N in the doubly connected case.

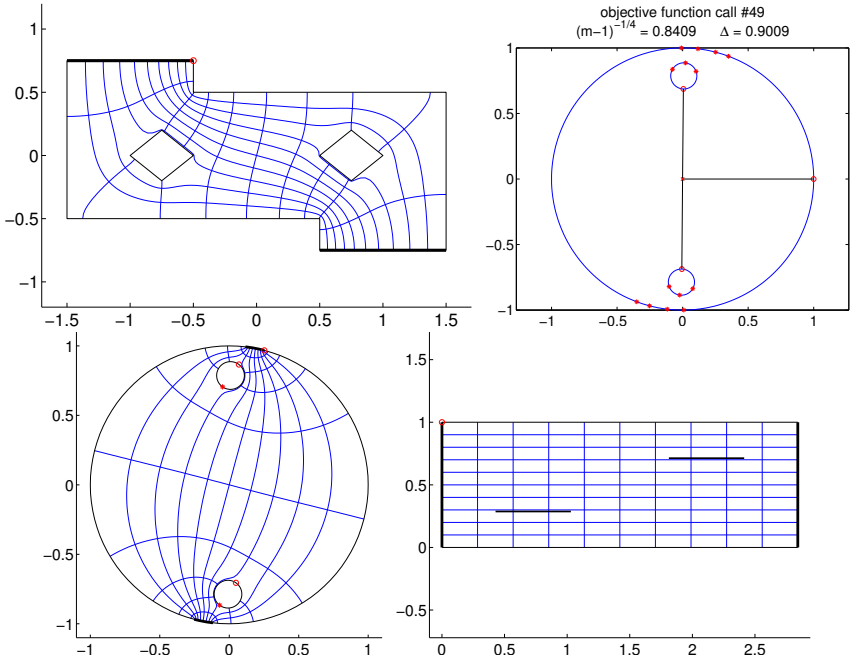

Figure 5.3: A resistor with $m = 3$. Resistance measurements for $N = 11$ are $R_b = 2.8419984 = R_t$.

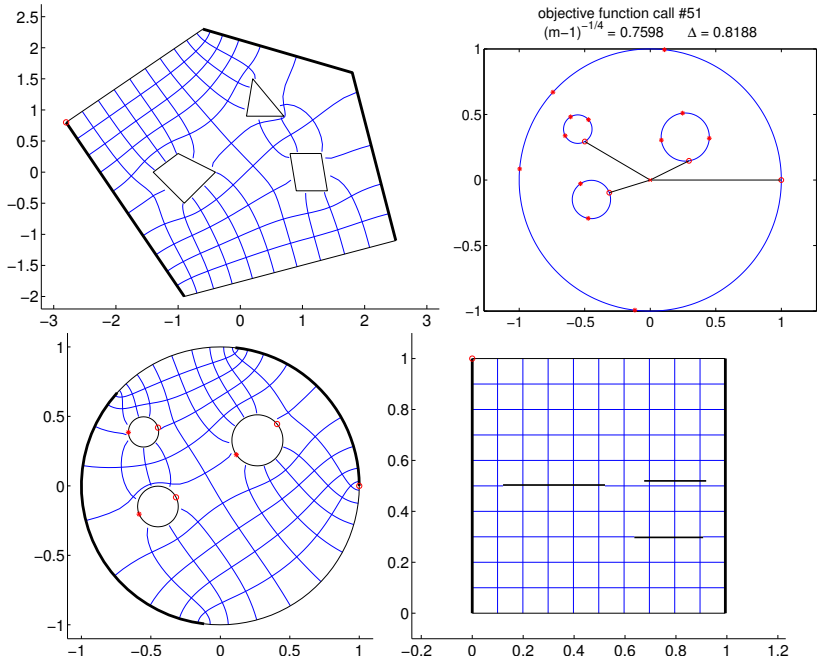

Figure 5.4: A resistor with $m = 4$. Resistance measurements for $N = 6$ are $R_b = 0.9940 = R_t$.

ratio of the radii of the inner and outer circles,

$$R = \frac{1}{2\pi} \log \frac{r_{outer}}{r_{inner}},$$

where $r_{outer} = |f_{ji}(z)|, z \in C_j$, and $r_{inner} = |f_{ji}(z)|, z \in C_i$.

The first example, shown in Figure 5.5, is a symmetric triply connected bar. Voltages are given on the interior square boundaries. The exterior boundary is insulated. This example is computed in [37] with simply connected Schwarz-Christoffel transformations by exploiting the symmetry to subdivide the domain into four simply connected domains. For the calculations done here, symmetry is not exploited. The bottom right graph in Figure 5.5 is a plot of accuracy at reflection levels N=3 to N=12. In the accuracy graph, the value R_T is the resistance given in [37] to several digits and is listed here in Table 5.2 as the exact value. The R_{median} and R_{mean} values in the error plot come from the fact that 100 points on each circle are mapped to the slit-ring domain. The other three pictures are plotted with $N = 8$. This is a difficult example for this method. The inner circular boundary of the annulus is not visible to the eye in the figure and the radial slit very nearly touches the inner circle. The inner circles of the conformally equivalent circle domain which map to the inner and outer annulus boundaries are also barely visible and nearly touch the unit circle, as indicated by the fact that the separation parameter is $\Delta = 0.9968$.

The second example, shown in Figure 5.6, is an asymmetric polygon with interior contacts. The resistance cannot be calculated by subdividing the domain and using simply connected conformal maps. The inner circular annulus boundary is visible here, but the radial slit still appears to be touching the inner circle.

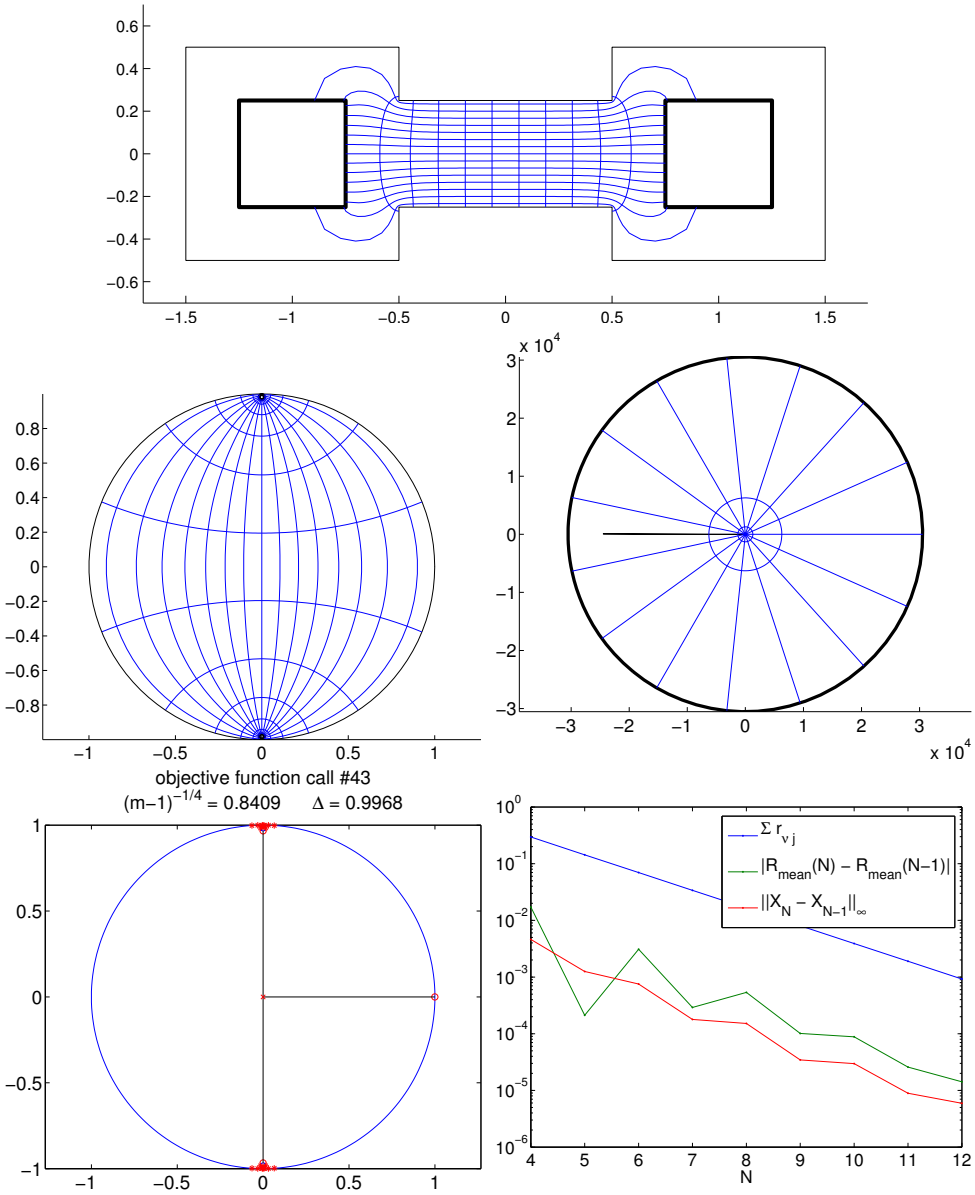

Figure 5.5: An interior contact with $m = 3$ from [37, Fig. 2d].

Table 5.2: Accuracy of resistance calculations for Figure 5.5 with $m = 3$ and $\Delta = 0.9968$.

N	R_{mean}	$\sum_{\lvert\nu\rvert=N} r_\nu$
3	2.81475482267	0.0095309
4	2.75464368554	0.0049531
5	2.75699777668	0.0025849
6	2.77062007508	0.0013568
7	2.77137596289	0.0007121
8	2.76784836631	0.0003741
9	2.76801923981	0.0001965
10	2.76899878312	0.0001032
11	2.76905554016	0.0000542
12	2.76879077906	0.0000285
exact value	2.76886750270	

Table 5.3: Accuracy of resistance calculations for Figure 5.6 with $m = 3$ and $\Delta = 0.9540$.

N	R_{mean}	$\sum_{\lvert\nu\rvert=N} r_\nu$
3	0.381664	0.60637
4	0.364481	0.29556
5	0.364269	0.14338
6	0.367363	0.06984
7	0.367653	0.03391
8	0.367116	0.01651
9	0.367015	0.00802
10	0.367103	0.00390
11	0.367129	0.00189
12	0.367115	0.00092

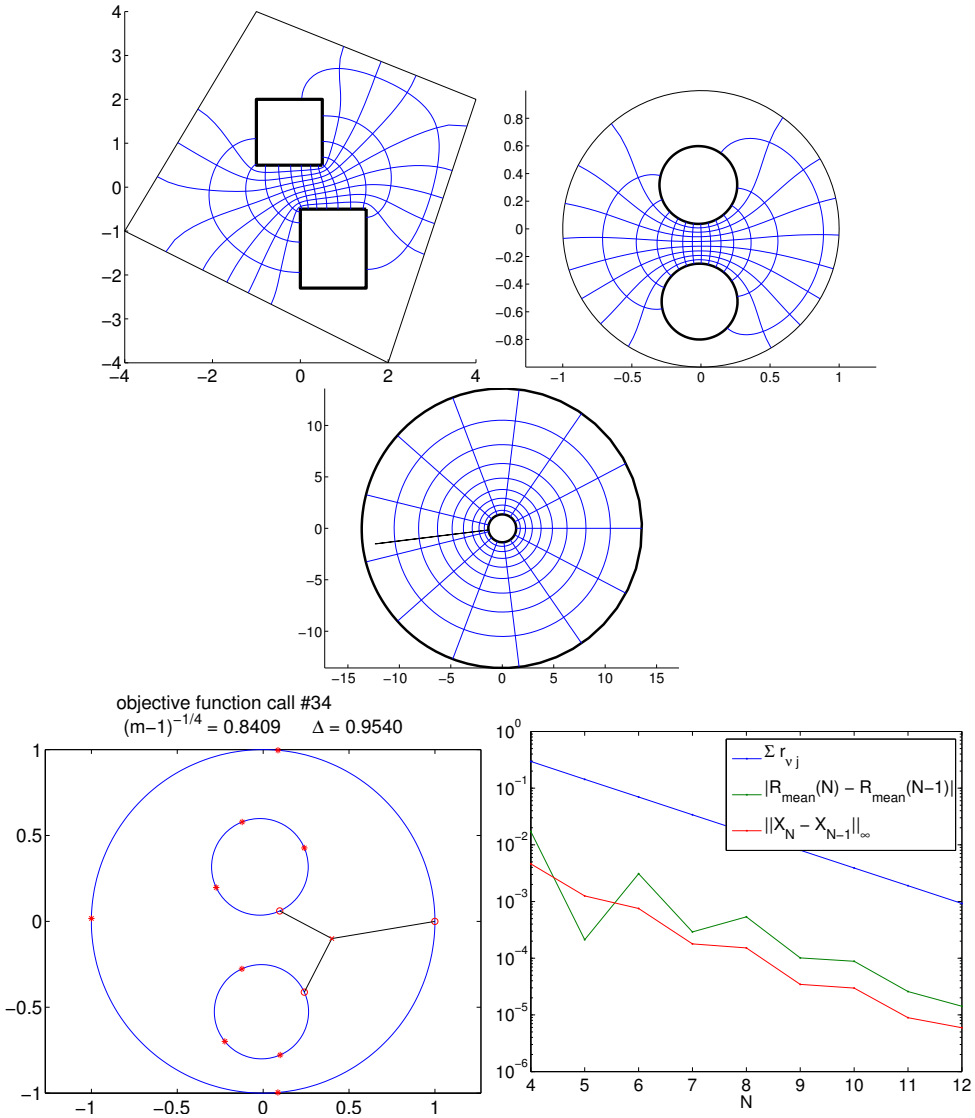

Figure 5.6: An asymmetric interior contact with $m = 3$ and $\Delta = 0.9540$.

CHAPTER 6

CONCLUSION

6.1 Concluding remarks

The main goal of this project was the numerical computation of the multiply connected Schwarz-Christoffel map, unbounded and bounded, originally given in [18, 13]. This was accomplished as presented in this dissertation using the reflection method for both bounded and unbounded maps. In addition a Laurent series method was presented for the unbounded case which showed a great reduction in computational complexity of the problem. An application for bounded maps was presented. Several slit map canonical domains given in terms of reflection formulas were also cataloged. Laurent series methods for calculating some of these slit maps were given.

6.2 Future work

Although the main goal of this work was accomplished, there is more work to be done. A method for the computing the integrand of the unbounded MCSC map was given in terms of finite products of Laurent series estimates in terms of slit maps; the development of an equivalent method for the bounded case is in progress. Part of the difficulty with the bounded case is the determination of the correct pairing of an extra level of reflection of the first circle with the other reflections. As of this writing, no factor map similar to that shown by Figures 4.4 and 4.5 have been determined for the bounded case.

The expression of the integrands of the MCSC maps as factors of slit maps was discussed in [19], along with attempts to connect these formulas to those of Crowdy [8, 9]. Crowdy's formulas for mapping to bounded and unbounded polygonal domains from a conformally equivalent circle domain are expressed in terms of Schottky-Klein prime functions, and software has been developed [10] to calculate the prime functions from an efficient solu-

tion to a boundary value problem. It would be of interest to see the numerical behavior of the MCSC maps where the integrands are calculated by this algorithm.

Instead of creating an estimate for each factor of a product as presented in this dissertation, it would be even more efficient to create one single estimate for the entire MCSC integrand. One method under investigation is to make a Laurent series approximation to the singularity function, $S(z) = f''(z)/f'(z)$, of the bounded or unbounded map based on the boundary values of $S(z)$. In fact a better understanding of the Riemann-Hilbert boundary problem given by the condition on $S(z)$, *e.g.*, Lemma 2.16, might also lead to more efficient methods for solutions to these problems by, for example, an adaptation of the methods in [38]. A recent paper by Mityushev [30] discusses the map from the circle domain to the circular slit domain in terms of a Riemann-Hilbert problem.

Large geometric distortions inherent in many conformal maps also create problems numerically. The case of crowding, where prevertices corresponding to the ends of long channels become exponentially close in the aspect ratio of the channel, is a well known problem in the simply connected case and has been largely solved; see [3, 22]. In the multiply connected case, elongated channels between boundary components can cause circles to nearly touch; see Figure 4.15 and [5] for examples. In the case of crowding, an adaptation of the ideas given in [3] to multiply connected domains is necessary. When circles are close to touching, it is expected that the Laurent series will converge slowly, *e.g.*, Example 4.9, and some combination of reflections and Laurent series expansions as in [7] may be useful.

Domains of very high connectivity will involve very large numbers of unknowns. Here it might be possible to adapt ideas from [4] in order to compute maps of simply connected polygons with thousands of vertices. In [4] the fast multipole method is used to speed up the evaluations of $f'(z)$, and a side length iteration is used to solve the parameter problem with fewer computations per step than quasi-Newton iterations.

Finally, we desire to polish the experimental code and release it to the public. There

are some issues that should be dealt with before this happens. One is the automatic selection of an initial guess for the iterative solution of the parameter problem.

Another is the selection of integration paths for circle positioning; this was discussed in part in Section 3.5. Automatic selection of these paths would be best, but it is not clear how this might be implemented. Allowing the user to select these paths, for domains of up to at least a moderate connectivity, might work. It would also be useful to add a procedure which keeps integration paths inside of the computational domain in order to avoid rare failures of convergence; such a procedure is investigated in [28].

REFERENCES

LIST OF REFERENCES

[1] E. Allgower and K. Georg. *Numerical Continuation Methods: An Introduction*. Springer-Verlag, New York, 1990.

[2] V. Andreev and T. McNicholl. A potential-theoretic construction of the Schwarz-Christoffel map for finitely connected domains. *Complex Variables and Elliptic Equations*, pages 1–21, 2011.

[3] L. Banjai. Revisiting the crowding phenomenon in Schwarz-Christoffel mapping. *SIAM Journal on Scientific Computing*, 30:618–636, 2008.

[4] L. Banjai and L. Trefethen. A multipole method for Schwarz-Christoffel mapping of polygons with thousands of sides. *SIAM Journal on Scientific Computing*, 25:1042–1065, 2003.

[5] N. Benchama, T. DeLillo, T. Hrycak, and L. Wang. A simplified Fornberg-like method for conformal mapping of multiply connected regions – comparisons and crowding. *Journal of Computational and Applied Mathematics*, (209):1–21, 2007.

[6] J. Case. Breakthrough in conformal mapping. *SIAM News*, 41, January 2008.

[7] H. Cheng and L. Greengard. A method of images fo rthe evaluation of electrostatic fields in systems of closely spaced conducting cylinders. *SIAM Journal on Applied Mathematics*, 58:122–141, 1998.

[8] D. Crowdy. The Schwarz-Christoffel mapping to bounded multiply connected polygonal domains. *Proceedings of the Royal Society A*, 461:2653–2678, 2005.

[9] D. Crowdy. Schwarz-Christoffel mapping to unbounded multiply connected polygonal regions. *Mathematical Proceedings of the Cambridge Philisophical Society*, 142:319–339, 2007.

[10] D. Crowdy and C. Green. The Schottky-Klein prime function. http://www2.imperial.ac.uk/~dgcrowdy/SKPrime.

[11] D. Crowdy and J. Marshall. Conformal mapping between canonical multiply connected domains. *Computational Methods and Function Theory*, 6:59–76, 2006.

[12] D. Crowdy and J. Marshall. Green's functions for Laplace's equation in multiply connected domains. *IMA Journal of Applied Mathematics*, 72:278–301, 2007.

[13] T. DeLillo. Schwarz-Christoffel mapping of bounded, multiply connected domains. *Computational Methods and Function Theory*, 6(2):275–300, 2006.

[14] T. DeLillo, T. Driscoll, A. Elcrat, and J. Pfaltzgraff. Computation of multiply connected Schwarz-Christoffel maps for exterior domains. *Computational Methods and Function Theory*, 6(2):301–315, 2006.

[15] T. DeLillo, T. Driscoll, A. Elcrat, and J. Pfaltzgraff. Radial and circular slit maps of unbounded multiply connected circle domains. *Proceedings of the Royal Society A*, 464:1719–1737, 2008.

[16] T. DeLillo, A. Elcrat, and E. Kropf. Calculation of resistances for multiply connected domains using Schwarz-Christoffel transformations. *Computational Methods and Function Theory*, 11(2):725–745, 2011.

[17] T. DeLillo, A. Elcrat, and J. Pfaltzgraff. Schwarz-Christoffel mapping of the annulus. *SIAM Review*, 43:469–477, 2001.

[18] T. DeLillo, A. Elcrat, and J. Pfaltzgraff. Schwarz-Christoffel mapping of multiply connected domains. *Journal d'Analyse Mathématique*, 94(1):17–47, 2004.

[19] T. DeLillo and E. Kropf. Slit maps and Schwarz-Christoffel maps for multiply connected domains. *Electronic Transactions on Numerical Analysis*, 36:195–223, 2010.

[20] T. DeLillo and E. Kropf. Numerical computation of the Schwarz-Christoffel transformation for multiply connected domains. *SIAM Journal on Scientific Computing*, 33(3):1369–1394, 2011.

[21] T. Driscoll. A MATLAB toolbox for Schwarz-Cristoffel mapping. *ACM Transactions of Mathematical Software*, 22:168–186, 1996.

[22] T. Driscoll and L. Trefethen. *Schwarz-Christoffel Mapping*, volume 8 of *Cambridge Monographs on Applied and Computational Mathematics*. Cambridge, 2002.

[23] A. Elcrat and C. Hu. Determination of surface and interior cracks from electrostatic measurements using Schwarz-Christoffel transformations. *International Joural of Engineering Science*, 34:1165–1181, 1996.

[24] A. Elcrat, V. Isakov, and O. Neculoiu. On finding a surface crack from boundary measurements. *Inverse Problems*, 11:343–351, 1995.

[25] G. Golub and J. Welsch. Calculation of Gauss quadrature rules. *Mathematics of Computation*, 23:221–30, 1969.

[26] P. Henrici. *Applied and Computational Complex Analysis*, volume 3. John Wiley, NY, 1986.

[27] P. Koebe. Abhandlungen zur Theorie der Konformen Abbildung, IV: Abbildung Merfach Zusammenhangender Schlichter Bereiche auf Schlitzbereiche. *Acta Mathematica*, 41(1):305–344, December 1916.

[28] M. Landstorfer. Schwarz-Christoffel mapping of multiply connected domains – proof, discussion, and elaboration, MATLAB implementation and search algorithms for integration paths. Diplomarbeit, Department of Mathematics. Fachhochschule Regensburg, 2007. http://www.mathematik.uni-ulm.de/numerik/staff/mlandsto/.

[29] The MathWorks, Inc. *Optimization Toolbox User's Guide*, 2008.

[30] V. Mityushev. Riemann-hilbert problems for multiply connected domains and circular slit maps. *Computational Methods and Function Theory*, 11(2):575–590, 2011.

[31] Z. Nehari. *Conformal Mapping*. Dover, 1975.

[32] N. Papmichael and N. Stylianopoulus. *Numerical Conformal Mapping – Domain Decomposition and the Mapping of Quadralaterals*. World Scientific, Singapore, 2010.

[33] A. Pflüger. Lectures on Conformal Mapping. Department of Mathematics, Indiana University. Bloomington, 1969.

[34] K. Reppe. Calculation of magnetic fields by the means of conformal mapping through numerical integration of the Schwarz-Christoffel mapping function. *Siemens Forschungs und Entwicklungsberichte*, 8:190–195, 1979.

[35] M. Schiffer. *Some recent developments in the theory of conformal mapping*, chapter Appendix to: R. Courant, Dirichlet's Principal, Conformal Mapping, and Minimal Surfaces. Interscience, New York, 1950.

[36] L. Trefethen. Numerical computation of the Schwarz-Christoffel transformation. *SIAM Journal of Scientific and Statistical Computing*, 1(1):82–102, March 1980.

[37] L. Trefethen. Analysis and design of polygonal resistors by conformal mapping. *Zeitschrift für Angewandte Mathematik und Physik*, 35:692–703, 1984.

[38] R. Wegmann. Constructive solution of a certain class of riemann–hilbert problems on multiply connected circular regions. *Journal of computational and applied mathematics*, 130(1):139–161, 2001.

[39] R. Wegmann. Methods for numerical conformal mapping. In R. Kunau, editor, *Handbook of Complex Analysis, Geometric Function Theory*, volume 2, pages 351–477. Elsevier, 2005.

APPENDIX

APPENDIX A

CODE EXAMPLES

This Appendix gives MATLAB implementation examples of some of the algorithms described in previous Chapters.

Program A.1. The reflection algorithm was discussed in Section 2.1.

```
function [zn,cn,rn,sn,jlr,rsum] = reflect_alg(zin,cn,rn,sn,vc,N)
  % preallocate
  m = numel(rn); % connectivity by radius count
  zrows = zeros(sum((m-1).^(1:N)),m);
  cn = [cn; zrows]; % centers
  rn = [rn; zrows]; % radii
  sn = [sn; zrows]; % reflected centers
  zn = zeros(max(vc),sum((m-1).^(0:N)),m); % prevertices
  zn(:,1,:) = zin;
  sumrl = zeros(N,m); % for summing reflected radii

  % initialize (nu = 1 is level 0 - original circles)
  % jlr(nu,j) = leading index = index of circle of last reflection
  jlr = [1:m; zrows];

  % outer j loop over m circles
  for j=1:m
    % track reflections from circle j down to level N
    num = 0;
    for level = 1:N
      sumrl(level,j)=0;
      nul = num+1;
      if m ~= 2
        num = ((m-1)^level - 1)/(m-2);
      elseif m == 2
        num = nul;
      end
      nuj = num;
      for nu = nul:num
        for j1 = 1:m
```

```
          if j1 ~= jlr(nu,j)
            nuj = nuj+1;
            jlr(nuj,j) = j1;
            [cn(nuj,j) rn(nuj,j)] = ...
              centrad(cn(1,j1),rn(1,j1),cn(nu,j),rn(nu,j));
            zn(1:vc(j),nuj,j) = ...
              reflect(cn(1,j1),rn(1,j1),zn(1:vc(j),nu,j));
            sn(nuj,j) = ...
              reflect(cn(1,j1),rn(1,j1),sn(nu,j));
            sumrl(level,j) = sumrl(level,j) + rn(nuj,j);
          end
        end
      end
    end
  end

  % calculate the sum of reflected radii at each reflection level
  rsum = zeros(1,N+1);
  rsum(1) = sum(rn(1,:));
  for level = 1:N
    rsum(level+1) = 0;
    for j = 1:m
      rsum(level+1) = rsum(level+1) + sumrl(level,j);
    end
  end
end
```

Program A.2. This function gives centers and radii of reflected circles, used in Program A.1.

```
function [co ro] = centrad(c,r,ci,ri)
  % reflects circle with center ci, radius ri through circle with
  % center c, radius r, to get circle with center co, radius ro
  co = c + r^2*(ci - c)/(abs(ci - c)^2 - ri^2);
  ro = r^2*ri/abs(abs(ci - c)^2 - ri^2);
end
```

Program A.3. This function reflects through circles, used in Program A.1.

```
function zo = reflect(c,r,zi)
  % reflects zi through circle with center c, radius r to get zo
  zo = c + r^2./conj(zi - c);
end
```

Program A.4. This function calculates the coefficients of the series representation for the radial and circular slit maps discussed in 4.1.

```
function x = calc_coefficients(a0,c,r,N,rcs)
  m = numel(c); % connectivity by number of centers

  %% sample points
  M = 2*N + 1; % makes system just overdetermined
  z = repmat(c,M,1) + repmat(exp(2i*pi*(0:M-1)'/M),1,m)*diag(r);
  z = z(:);

  %% Laurent basis matrices and RHS
  F = zeros(m*M,2*m*N);
  Fp = zeros(M,m*N);
  rh = zeros(m*M,1);
  za0 = z - a0;

  for p = 1:m
    blk = (p-1)*M+1:p*M;

    for j = 1:m
      zcj = r(j)./(z(blk)-c(j));
      Fp(:,(j-1)*N+1) = zcj;
      for ell = 2:N
        Fp(:,(j-1)*N+ell) = Fp(:,(j-1)*N+ell-1) .* zcj;
      end
    end

    if rcs(p)
      % circular slit
      F(blk,:) = [ real(Fp) -imag(Fp) ];
      rh(blk) = -log(abs(za0(blk)));
    else
      % radial slit
      F(blk,:) = [ imag(Fp) real(Fp) ];
      rh(blk) = -angle(za0(blk));
      if any(diff(rh(blk)) > pi)
        rh(blk) = mod(rh(blk),2*pi);
      end
    end
  end
```

```
  % difference block matrix
  E = sparse(kron(eye(m),toeplitz([-1 zeros(1,M-2)],[-1 1 zeros(1,M-2)])));

  % matrix-matrix multiplication is less than O(n^3) since E is sparse
  x = (E*F)\(E*rh);
  x = complex(x(1:numel(x)/2),x(numel(x)/2+1:end));
end
```

Program A.5. This function calculates the coefficients of the series part of $\log f_{a_j}(z)$ described in Section 4.2.

```
function x = calc_coefficients(c,r,aj,N)
  sj = c(j);

  %% sample points
  M = 2*N+1; % makes system overdetermined
  z = repmat(exp(1i*(2*pi*(1:M)'/M)),1,m);
  z = z*diag(r);
  z = repmat(c(:).',M,1) + z;
  z = z(:);

  %% setup B1 and B2
  A = Amatrix(I,z);
  B1 = imag(A); B2 = real(A);

  jrows = (j-1)*M+1:j*M;
  zG = z(jrows);
  G = zeros(M,m*N);
  for p = 1:m
    G(:,(p-1)*N+1:p*N) = ...
      A(jrows,(p-1)*N+1:p*N) .* (-(zG-sj)./(zG-c(p))*(1:N));
  end
  GR = real(G); GI = imag(G);

  B1(jrows,:) = GR;
  B2(jrows,:) = -GI;

  %% the E matrix
  D = toeplitz([-1 zeros(1,M-2)],[-1 1 zeros(1,M-2)]);
  arg = cell(1,m);
```

```
  for p = 1:m
    if p == j
      arg{p} = eye(M);
    else
      arg{p} = D;
    end
  end
  E = sparse(blkdiag(arg{:}));

  %% right-hand side
  argas = (z-aj)./(z-sj);
  argas(jrows) = 0;
  argas = angle(argas);
  rhs = -E*argas;

  %% solve linear system
  B = E*[B1 B2];
  x = B\rhs;

  x = complex(x(1:end/2),x(end/2+1:end));
end
```

Program A.6. Returns the matrix of basis functions for the series part of $\log f_{a_j}(z)$ from Section 4.2. Used in Program A.5.

```
function A = matrix_A(z,c,r,N)
  % return matrix of basis functions for g
  m = numel(r);

  A = zeros(length(z),m*N);
  for j = 1:m
    zcn = r(j)./(z-c(j));
    A(:,(j-1)*N+1) = zcn;
    for n = 2:N
      A(:,(j-1)*N+n) = A(:,(j-1)*N+n-1) .* zcn;
    end
  end
end
```